Analysis and Performance Evaluation of Reception Schemes for Correlated MIMO System

A thesis submitted in partial fulfillment of the requirements for the award of degree of

Doctor of Philosophy

Submitted by

Simranjit Singh

Under the guidance of

Dr. Manjeet Singh Patterh,
Professor, ECED,
Punjabi University

Dr. Rajesh Khanna,
Professor, ECED,
Thapar University

Department of Electronics & Communication Engineering
Thapar University, Patiala-147004, Punjab, India
August 2014

Certificate

This is to certify that the thesis entitled "**Analysis and Performance Evaluation of Reception Schemes for Correlated MIMO System** " being submitted by Mr. Simranjit Singh, to the Department of Electronics and Communication Engineering, Thapar University, Patiala, Punjab for the award of Doctor of Philosophy in Electronics and Communication Engineering, is a bonafide research work carried out by him under the supervision and guidance of the undersigned. The matter presented in this thesis has not been submitted to any other university or institute for the award of any degree.

Dr. Manjeet Singh Patterh,
Professor and Head,
ECED, Punjabi University,
Patiala, Punjab,
India.

Dr. Rajesh Khanna,
Professor and Head,
ECED, Thapar University,
Patiala, Punjab,
India.

Abstract

The rapid advancement in wireless communications has led to an increasing demand on the data rates for applications such as seamless high definition video streaming, video conferencing etc. As the bandwidth/frequency spectrum available for wireless systems is limited, all the demands have to be fulfilled within this spectrum only. This entails the development of bandwidth efficient wireless systems which can deliver higher data rates without requiring additional bandwidth. A very promising solution to this problem is the use of Multiple-Input Multiple-Output (MIMO) systems incorporating multiple antennas at the transmitter and receiver. MIMO systems effectively enable the use of spatial dimension in order to increase the data rate without imposing any bandwidth penalty on the system. Transmitting different data streams from different antennas enables the use of same spectrum for transmitting different data, i.e. the number of antennas is directly proportional to the data rate that can be achieved. This technique of increasing the data rate is called Spatial Multiplexing (SM) because it exploits the multiplexing gain. To achieve this, variety of receivers such as Zero Forcing (ZF), Minimum Mean Squared Error (MMSE), Vertical Bell Labs Layered Space Time (VBLAST) etc. have been developed for spatial multiplexing. The increase in capacity is true for a channel with rich scattering and antennas with sufficient spacing amongst them. However, with the size of wireless devices becoming smaller by the day, it is becoming difficult for the system designers to incorporate independent multiple antennas on the same device. This leads to correlation between different antennas, taking away the advantage of spatial dimension. Spatial correlation may significantly degrade the performance of a MIMO system.

Firstly, the existing spatial multiplexing techniques are studied in detail. The error performance of these techniques is evaluated in uncorrelated and correlated fading channels. To complete the study, a brief analysis of computational complexity of various receivers is also done. Based on the error rate performance and complexity parameters, the MMSE receiver is selected.

Secondly, a Fractional Fourier Transform (FRFT) based generic MMSE receiver is proposed for multiple antenna systems. Based on a recently proposed novel method for filtering signals in the fractional Fourier domains, the proposed receiver gives a lower mean square error (MSE) as

compared to the conventional MMSE receiver. The proposed receiver is generic in the sense that it can be used with all systems irrespective of the antenna configuration. Since this dissertation is focused on the receiver side of wireless systems, first a receiver is proposed for Single-Input Multiple-Output (SIMO) systems as a fractional optimum combining diversity technique. Then a generalized receiver is proposed for MIMO systems as a fractional MMSE receiver. The bit error rate performance of the proposed receiver is studied in uncorrelated and correlated fading channels.

Based on fractional domain filtering, improved channel estimation schemes are proposed for rapidly fading channels and block fading channels. To estimate a rapidly fading channel, an interpolation technique is used where pilot symbols are transmitted at equally spaced intervals. With the channel estimate known at pilot positions, the rest of the channel is estimated using interpolation. For block fading channels, pilot symbols are prefixed to the transmitted block. The channel estimated using prefixed pilots remains constant throughout the transmission block. Both the proposed techniques are shown to give better quality channel estimates than their respective conventional counterparts.

In the last part of the dissertation, the error rate performance of the proposed fractional MMSE receiver is considered with Low Density Parity Check Coding (LDPC). Channel coding is often viewed as a smart way to reduce the errors in transmission and improving the link reliability. The reason for selecting LDPC codes is that they are powerful channel codes with excellent error performance but a low decoding complexity. There have been simulations that perform within 0.0045 dB of the Shannon limit using LDPC codes for an Additive White Gaussian Noise (AWGN) channel. The use of LDPC codes along with fractional MMSE improves the error performance of the fractional MMSE considerably.

List of Publications

Journal Publications: 8

Simranjit Singh, Rajesh Khanna, Manjeet Singh Patterh, "Analysis of FRFT based MMSE Receiver for MIMO Systems," **Wireless Personal Communication** (Springer), Published Online on 3rd July 2013, DOI: 10.1007/s11277-013-1202-0 **(SCI Indexed, I.F.=0.428)**

Simranjit Singh, Rajesh Khanna, Manjeet Singh Patterh, "Optimum Combining in Fractional Domain," **International Journal of Electronics**, vol. 99, no. 11, pp. 1589-1602, 2012 **(SCI Indexed, I.F=0.509)**

Simranjit Singh, Rajesh Khanna, Manjeet Singh Patterh, "Fractional Channel Estimation and Equalization for MIMO systems," **Elektronika ir Elektrotechnika**, vol. 18, no. 9, pp. 47-50, 2012 **(SCI Indexed, I.F=0.411)**

Simranjit Singh, Rajesh Khanna, Manjeet Singh Patterh, "Improved Fractional Channel Estimation for MIMO systems in the Low SNR Regime," **Elektronika ir Elektrotechnika**, vol. 19, no. 1, pp. 65-68, 2013 **(SCI Indexed, I.F=0.411)**

Simranjit Singh, Rajesh Khanna, Manjeet Singh Patterh, "Fractional Optimum Linear Receiver for quasi-static MIMO systems" International Journal of Physical Sciences, vol. 6, no. 21, 4990-4998, 30 Sep 2011

Simranjit Singh, Rajesh Khanna, Manjeet Singh Patterh, "Fractional Fourier Transform based Pilot Symbol Assisted Modulation" Research Journal of Applied Sciences, Engineering and Technology, vol. 4, no. 1, 59-65, 2012

Simranjit Singh, Rajesh Khanna, Manjeet Singh Patterh, "Performance Analysis of Open and Closed Loop MIMO Systems in Spatially Correlated Channels" International Journal of Information Sciences and Application vol. 2, no. 2, pp. 343-347, 2010

Simranjit Singh, Rajesh Khanna, Manjeet Singh Patterh, "Performance Analysis of MIMO Detectors in Spatially Correlated Fading Channels" International Journal of Applied Engineering Research, Vol. 6, No. 5, pp. 638-642 (2011)

Conference Publications: 2

Simranjit Singh, Rajesh Khanna, Manjeet Singh Patterh, "Performance Analysis of Open and Closed Loop MIMO Systems in Spatially Correlated Channels" International Conference on Technology and Information Systems, DAV College, Amritsar, Nov 20-21, 2010

Simranjit Singh, Rajesh Khanna, Manjeet Singh Patterh, "Sphere Decoder for MIMO Systems: A Review Paper" Proceeding of National conference on communications and networking. NCCN-2010 (SLIET, Longowal), pp. 127-130, 12-13 March 2010

Acknowledgement

I acknowledge with immense gratitude the help and encouragement I have received from many quarters in the course of my doctoral work.

First of all, I am beholden to my supervisor, Prof. (Dr.) Rajesh Khanna, Head of the Department of Electronics and Communication Engineering Department, Thapar University, for providing patient and invaluable guidance and moral support to me at all times. His insightful comments and suggestions helped me overcome every hurdle and every seeming impasse that surfaced during the course of my research work.

My co-supervisor, Prof. (Dr.) Manjeet Singh Patterh, Head of the Department of The Department of Electronics and Communication, Punjabi University, Patiala, was ever ready to offer me help and advice whenever I needed them. I thank him profusely for his generosity. I would also like to thank my Ph.D. committee members for providing valuable suggestions throughout the course of my Ph.D.

My parents, my wife and my friends stood by me during the period of my research and gave me every type of cooperation. My debt to them is too great to be expressed in words.

Contents

List of Figures

List of Tables

Acronyms

3-D	Three Dimensional
AGC	Automatic Gain Control
AoA	Angle of Arrival
AWGN	Additive White Gaussian Noise
BER	Bit Error Rate
BLER	Block Error Rate
BPSK	Binary Phase Shift Keying
CJEE	Conventional Joint Estimation and Equalization
CPSAM	Conventional Pilot Symbol Assisted Modulation
CSI	Channel State Information
CSIT	Channel State Information at the Transmitter
CSIR	Channel State Information at the Receiver
DFT	Discrete Fourier Transform
DFRFT	Discrete Fractional Fourier Transform
DVB	Digital Video Broadcasting
EGC	Equal Gain Combining
FPSAM	FRFT based PSAM
FRFT	Fractional Fourier Transform
FT	Fourier Transform
HT	High Throughput
IDFT	Inverse Discrete Fourier Transform
IEEE	Institute of Electrical and Electronics Engineers
IFRFT	Inverse Fractional Fourier Transform
i.i.d	Independent, Identically Distributed
(I-METRA)	Intelligent Multi-Element Transmit and Receive Antennas
ITU	International Telecommunication Union
IP	Internet Protocol

JCEE	Joint Channel Estimation and Equalization
LDPC	Low Density Parity Check
LOS	Line Of Sight
LS	Least Squares
MIMO	Multiple-Input Multiple-Output
MISO	Multiple-Input Single-Output
ML	Maximum Likelihood
MMSE	Minimum Mean Squared Error
MRC	Maximal Ratio Combining
MSE	Mean Square Error
NLOS	Non Line Of Sight
OC	Optimum Combining
OJEE	Optimum Joint Estimation and Equalization
pdf	Probability Density Function
PSAM	Pilot Symbol Assisted Modulation
QAM	Quadrature Amplitude Modulation
QPSK	Quadrature Phase Shift Keying
Rx	Receiver
SC	Selection Combining
SCM	Spatial Channel Model
SEP	Symbol Error Probability
SIC	Successive Interference Cancellation
SM	Spatial Multiplexing
SINR	Signal to Interference plus Noise Ratio
SIMO	Single-Input Multiple-Output
SISO	Single-Input Single-Output
SNR	Signal to Noise Ratio
SSC	Switch and Stay Combining
STBC	Space-Time Block Coding
STC	Space-Time Coding
STTC	Space-Time Trellis Coding

TC	Threshold Combining
TV	Television
Tx	Transmitter
VBLAST	Vertical Bell Labs Layered Space-Time
ZF	Zero Forcing
ZMCSCG	Zero Mean Circularly Symmetric Complex Gaussian
ZMCSG	Zero Mean Circularly Symmetric Gaussian

Chapter 1
Introduction

The past decade has seen a rapid progress in the field of communication. The first electrical communication system called Telegraphy was proposed by Samuel Morse in 1844. The information was sent using Morse code in the form of dots and dashes. In 1894, Guglilemo Marconi demonstrated the first form of wireless communication when he invented the wireless radio. At the time, no one could predict that Guglilemo Marconi's invention would have such a great impact on the society. Today, a century after his invention, life cannot be imagined without cell phones, radio, satellites, Bluetooth etc. The next generation wireless systems are expected to offer services like remote internet connectivity, Internet Protocol (IP) telephony, online gaming services, high-definition mobile Television (TV), seamless video conferencing and three dimensional (3-D) TV [1-8]. Therefore, the one of the major goals of the next generation wireless systems is to increase the data rate and the capacity. This poses a problem for the system engineers because the available electromagnetic frequency spectrum is limited. Hence, to meet the higher data rate demands, with the constraint of a limited spectrum, the goal should be to improve the spectral efficiency. Along with that, most of the challenges in wireless communication arise from the fact that the signal is transmitted over unconstrained propagation medium and is subjected to many undesirable phenomena [9-10].

An effective way of increasing the spectral efficiency without imposing any bandwidth penalty is the use of multiple antennas at the transmitter and receiver. The system employing multiple antennas at both ends is called a Multiple-Input Multiple-Output (MIMO) system. In, addition to the traditional wireless systems which exploit the time and frequency dimensions, the MIMO systems exploit the space dimension which helps in better utilizing the available spectrum without needing any additional bandwidth. MIMO systems benefit from the rich scattering in the fading channel which is otherwise considered to be an obstacle in conventional wireless systems. A significant advancement in data rates was promised with the studies indicating a linear increase in capacity with the use of antenna arrays at both transmitter and receiver [11-13]. Before the concept of multiple antennas at the transmitter and/or receiver, the traditional wireless systems used a single transmit and a single receive antenna, i.e. they were Single-Input Single-

Output (SISO). When the wireless channel is in a deep fade (channel attenuation is large), the number of transmission errors in a SISO system is large. To combat multipath fading and the large number of errors due to it, the concept of receive diversity was proposed [14]. Receive diversity is achieved by using a Single-Input Multiple-Output (SIMO) system with a single transmit antenna and multiple antennas at the receiver end.

Figure 1.1: Single-input single-output (SISO) system

1.1 Receive Diversity

Although receive diversity can also be achieved using frequency, time and/or polarization, the most commonly used diversity is spatial diversity which is achieved with the help of multiple receive antennas. The advantage of using spatial diversity over other techniques is that it does not require additional power or bandwidth. Spatial diversity is employed to improve the link reliability by using multiple antennas at the receiver side and is based on the concept that the paths between the transmit antenna and different receive antennas cannot be all in a deep fade at the same time. Unless the channels are correlated (the spacing between antennas is less than approximately half of the wavelength), the use of spatial diversity improves the Bit Error Rate (BER) considerably by realization of independent fading paths.

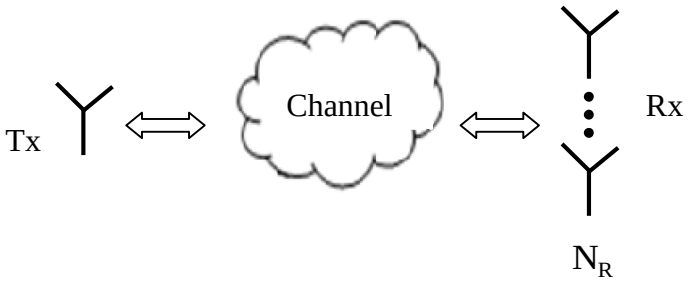

Figure 1.2: Single-input multiple output (SIMO) system

The signal received on N_R antennas can be combined in several different ways to achieve an acceptable Signal to Noise Ratio (SNR). A brief description of the commonly used diversity techniques is given below [15-16]:

Selection Combining (SC): In this technique, the combiner selects the signal with the highest instantaneous SNR and sends it to the demodulator. The output from the SC is the signal with the highest SNR out of all the branches. Since it is hard to find the SNR, the decision can be made by using the total receiver power (signal + noise power) provided the noise power is same on all the branches.

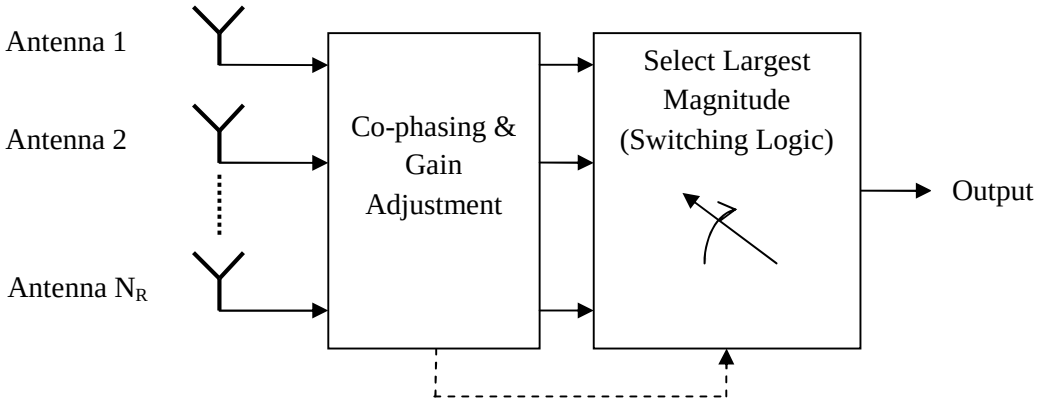

Figure 1.3: Selection combing diversity technique

Threshold Combining (TC): In selection combining, there is a need to continuously monitor SNR on all the branches. For continuously transmitting systems, SC requires a dedicated receiver on each branch for this purpose. Threshold combining eliminates this requirement by sequentially scanning each branch and outputting the first one having SNR above the preset threshold. Once selected, the branch remains connected to the demodulator for as long as its SNR stays above the threshold. Therefore, this technique is sometimes referred to as Switch and Stay combining (SSC).

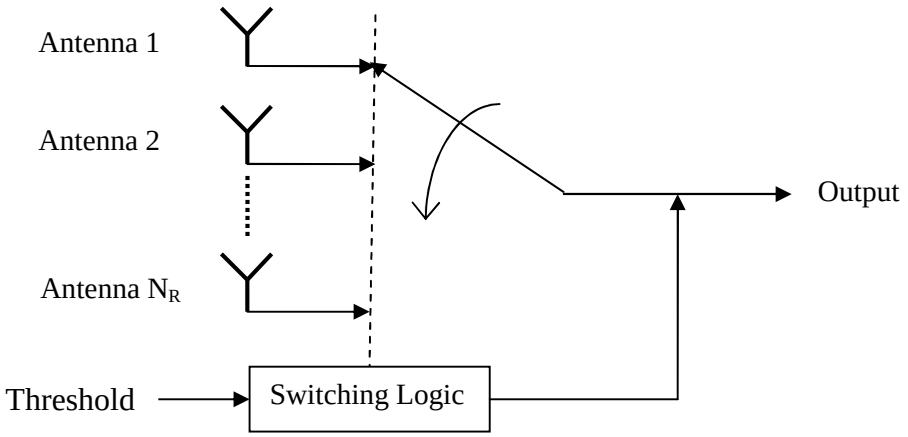

Figure 1.4: Threshold combining diversity technique

Maximal Ratio Combining (MRC): In SC and TC, the output of the combiner is connected to one of the branches, i.e. the output is connected to a single branch. However, in MRC, the output is a weighted sum of signals on all the branches. The advantage of this technique is that if any single branch does not have acceptable SNR, then there is more possibility that the weighted sum of all the branches would result in an acceptable SNR [17]. This technique is the optimal receive diversity technique and is considered to be a special case of Maximum Likelihood (ML) decoding which is discussed in chapter 2.

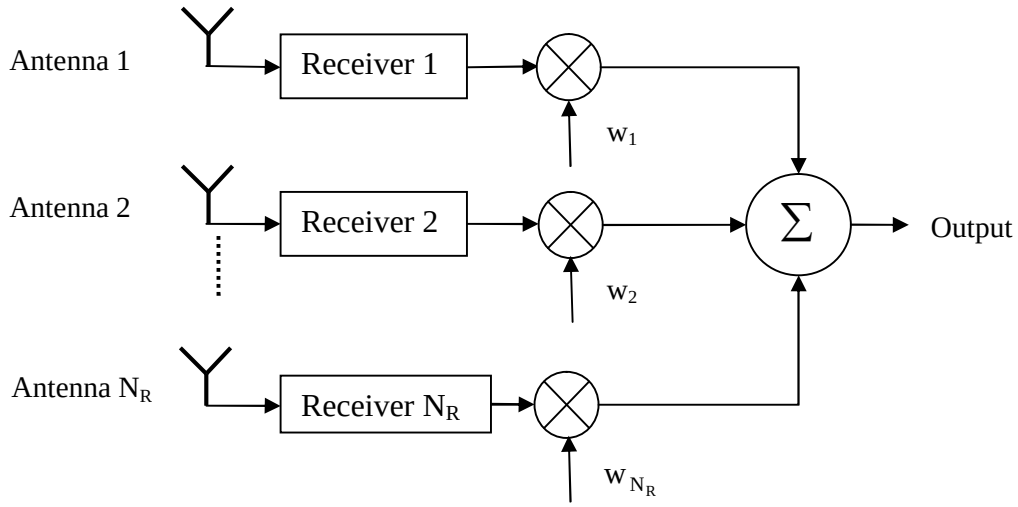

Figure 1.5: Maximal ratio combining/Optimum combining

Equal Gain Combining (EGC): Although MRC is considered to be optimal, it requires knowledge of instantaneous SNR on all the branches. A simpler technique called EGC requires all the weights in MRC to be set to unity. The disadvantage of this technique is that it also requires dedicated receivers on each branch.

Optimum Combining (OC): Optimum combining technique proposed by Winters based on Wiener filtering is the best diversity technique [18]. It is similar to MRC but it focuses on maximizing the Signal to Interference plus Noise Ratio (SINR) rather than SNR. Therefore, in an interference dominated environment, OC performs better than all other diversity techniques and in non-interfering environment; OC reduces to MRC [19].

Recently, a novel method of improving the Wiener filtering based on Fractional Fourier Transform (FRFT) was proposed. In this method, wiener filtering is performed in the optimum

fractional domain rather than time or frequency domain [20-21]. This method has the advantage of reduced BER due to the signal compactness in the optimum fractional domain. Fractional domain Wiener filtering method is discussed in detail in chapter 3.

1.2 Transmit Diversity

The transmit diversity is achieved by the use of multiple antennas at the transmitter with a single antenna at the receiver, known as Multiple Input Single Output (MISO) system. In such a system the transmit power is divided amongst the multiple transmit antennas. This technique requires pre-processing of the signal before transmission. The commonly used techniques with MISO are Space Time Trellis Coding (STTC) proposed by Tarokh et al. [22-25] and Space Time Block Coding (STBC), initially proposed by Almouti [26] and finally generalized by Tarokh [27]. MISO systems are particularly useful in systems where the receiver is not sufficiently large to incorporate multiple antennas, while the transmitter could easily accommodate multiple antennas.

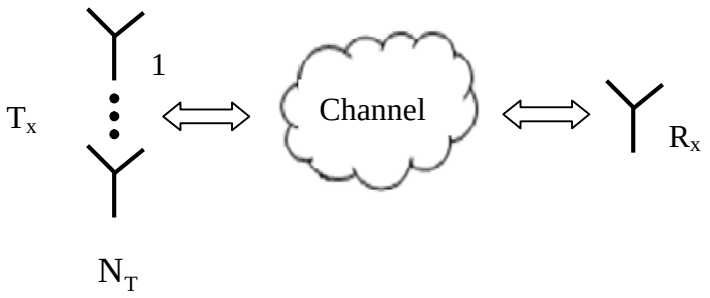

Figure 1.6: Multiple-input single output (MISO) system

1.3 Multiple Input Multiple Output (MIMO)

The use of multiple antennas at the transmitter and receiver enables the use of spatial dimension to improve the bandwidth efficiency. Rich multipath scattering in the wireless channel, which is generally considered to be a hindrance in SISO systems, actually aids the MIMO systems by providing independent channels to different sets of antennas. Theoretically, the capacity of MIMO increases linearly with the number of min (N_T, N_R) antennas. Therefore, without needing any additional bandwidth or power, MIMO systems provide the solution for the increasing data rate demands [28-32]. Various spatial multiplexing techniques for MIMO systems are discussed in detail in chapter 2.

MIMO systems can be used for obtaining variety of gains depending on the way they are set up. If the same data stream is transmitted from all the transmit antennas, multiple antennas improve the link reliability because of the spatial diversity. Such schemes are jointly called Space-Time Coding (STC) schemes. The STTC and STBC schemes initially proposed for MISO systems were extended for MIMO systems to exploit the diversity gain. However, multiple antennas can also be used to improve the spectral efficiency by transmitting different data from different antennas. Assuming the channels between different set of antennas are independent, identically distributed (i.i.d), the multiple antennas increase the spectral efficiency by exploiting the multiplexing gain. Schemes have also been formulated for utilizing the combination of spatial multiplexing and space-time coding; however there is a trade-off relationship limiting the diversity and multiplexing gains [33-37].

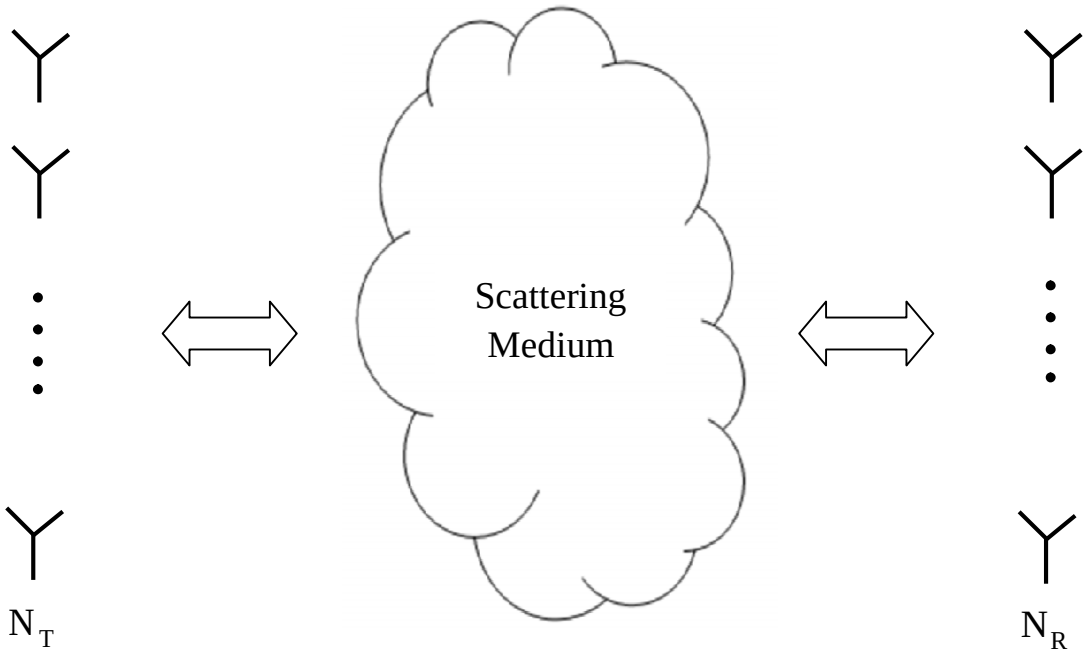

Figure 1.7: Multiple-input multiple-output system (MIMO) system

As the size of all devices tends to decrease, the physical space for system engineers to work with is decreasing constantly. As the MIMO systems depend on the spatial dimension to extract the maximum bandwidth efficiency, the decreasing size of wireless devices makes it difficult. As it is already known in theory, for the channels between two independent sets of antennas to be uncorrelated, the antenna spacing should be approximately 0.5λ (.38 λ to be exact) [15].

Practically, however, this distance is not always achievable and as a consequence the channels between different sets of antennas are correlated. The channel correlation has the effect of decreasing the capacity that can be achieved by using multiple antennas [13, 38].

Different methods for modeling the spatial correlation have been discussed. Two most common methods are correlation based Intelligent Multi-Element Transmit and Receive Antennas (I-METRA) channel model and ray based Spatial Channel Model (SCM) [39-45]. The effect of spatial correlation on MIMO systems has been studied in detail. The most effective way to deal with spatial correlation is to use precoding which requires the Channel State Information at the Transmitter (CSIT) side. In practical situations, it is not always possible to provide channel state information on the transmitter side and the spatial correlation degrades the capacity considerably. The method for modeling spatial correlation for simulations is described in detail in chapter 2.

1.4 Channel Coding

Along with the advent of multiple antenna schemes, another effective way of improving the reliability of a communication system is error control coding/error correction coding. In this method, some redundant bits are added to the information stream. These redundant bits are used for error detection and correction on the receiver side. Channel coding has increasingly become one of the most popular methods to increase the link reliability of multi antenna systems. The idea is to add redundancy to the original signal to make it more immune to channel impairments such as noise and fading. Channel coding adds redundancy in the discrete domain and can be thought of as a medium for accommodating desirable system trade-offs such as error performance vs. bandwidth or power vs. bandwidth. It is possible to get up to 10 dB performance improvement by the use of channel coding. At the receiver end, the decoder uses these redundant bits to efficiently extract the originally transmitted message with lesser number of errors. Basically channel coding is used to minimize the BER at the receiver. Channel codes are of three types:

1. Block codes
2. Turbo codes
3. Convolutional codes

One of the best error correction codes are Low Density Parity Check (LDPC) codes due to their near Shannon limit performance [46]. For very long block length LDPC codes have been shown to achieve the Shannon capacity of an Additive White Gaussian Noise (AWGN) channel within 0.0045dB [47].

Turbo codes, proposed by Berrou et. al. in 1993 are another class of powerful error correcting codes which serve as the main competitors for LDPC codes when being considered for various wireless standards. For frame lengths greater than 10,000 bits, LDPC codes are shown to outperform turbo codes [46, 48]. Another advantage of LDPC codes over turbo codes is that they do not exhibit an error floor. The decoding complexity of LDPC codes is low due to the fact that their decoding algorithm is highly parallelizable. Due to their advantages over other codes, LDPC codes have been selected as the error correction codes in various wireless standards.

LDPC Codes Applications: In 2003, LDPC codes were selected as the error correcting codes for the DVB-S2 standard for satellite transmission of digital television after beating six turbo codes [49]. In 2008, LDPC codes beat convolutional turbo codes for the ITU-T G.hn standard [50]. LDPC codes are also a part of the IEEE 802.11 standard in the High Throughput (HT) PHY specification [51].

1.5 Research Objectives

Keeping in view the tremendous success of MIMO systems, the following research objectives were proposed:

1. To study some of the existing reception schemes for MIMO systems.
2. To propose an improved reception scheme for MIMO systems.
3. To analyze the performance of the proposed scheme with LDPC coding.
4. To analyze the effect of channel correlation on the performance of the proposed receiver.

1.6 Research Contributions

Based on the above objectives, the basic aim of this thesis is to propose an improved reception scheme for multiple antenna systems and analyze it in different wireless environments, i.e. uncorrelated and correlated fading channels. Also the channels are taken to be Line-Of-Sight

(LOS) and Non Line-Of-Sight (NLOS) for a complete study. Different performance evaluation parameters such as bit error rate and mean square error have been used to establish the superiority of the proposed receiver.

Contribution 1: Improved reception scheme of multiple antenna systems

The main contribution of this work is the development of an improved fractional Fourier transform based generic MMSE receiver for multiple antenna systems. This receiver has been shown to outperform the existing MMSE receiver. The proposed MMSE receiver is based on performing the filtering process in the fractional Fourier domain which gives lower MSE as compared to the ordinary MMSE. The performance evaluation of the propose receiver is done in:

1. Uncorrelated fading channels with no spatial correlation
2. Correlated fading channels with low, medium and high correlation coefficient

Finally, the simulation results are compared with the analytical results to verify the correctness of the simulation.

Contribution 2: Improved channel estimation for block and fast fading channels

In this contribution, the proposed receiver has been used for channel estimation of block fading and fast fading channels. For block fading channel estimation, a separate scheme is developed which uses prefixed training symbols at the start of a transmission block. The receiver proposed in contribution 1 is used for channel estimation by extracting the training symbols and using them for obtaining optimum MMSE channel estimates as compared to the ordinary MMSE estimates.

For fast fading channels, however, the prefix training symbols do not work because the channel changes rapidly. Therefore, an interpolation based scheme has to be used where pilot symbols are transmitted at fixed intervals. From the channel response at pilot positions, the rest of the channel response has to be predicted using interpolation. The proposed receiver is used to obtain the channel response at pilot positions and then used for interpolation. The optimum MMSE estimates at pilot positions result in better channel estimation.

Contribution 3: Analysis of the proposed receiver with LDPC coding

Channel coding has become an integral part of today's wireless communication systems due to the development of excellent channel codes. In this contribution, the proposed receiver has been studied with LDPC coding. Using LDPC codes, the BER of the proposed receiver can be reduced due the coding gain provided by LDPC codes resulting in lesser number of errors.

1.7 Dissertation Outline

Chapter 2 of this dissertation gives an overview of the existing MIMO receivers. Different wireless channels used throughout the dissertation have also been presented in this chapter. The spatial correlation model used to model the correlation between different channels has been explained. Performance evaluation of the reviewed MIMO receivers in different fading channels in terms of BER has also been done.

In Chapter 3, an improved fractional Fourier transform based generic MMSE receiver is developed for multiple antenna systems. Firstly, a short description of the fractional Fourier transform and the optimum filtering process is presented. Based on that, an improved MMSE receiver is proposed. Also, the BER of the proposed receiver is analytically derived from MSE using a tight approximation for the Q-function. This MMSE receiver is then simulated in different wireless environments. The performance evaluation of the proposed receiver in spatially correlated fading channels is done in this chapter. Finally, the analytically derived BER and the simulated BER are compared to verify the correctness of the simulation results.

In chapter 4, an improved channel estimation technique is proposed based on the concept developed in chapter 3. Two different types of channel estimation techniques are proposed based on the type of channel, i.e. fast fading or block fading. For block fading channels, a training symbol is sent at the beginning of the block and then channel is estimated using that training symbol. However, for a fast fading channel, sending training symbols at the start is not sufficient because the channel changes rapidly. Therefore, for fast fading channels, an interpolation based technique is proposed in which pilot symbols are time multiplexed with the information at fixed intervals.

Chapter 5 deals with the third objective in which the performance analysis of the proposed reception scheme with LDPC channel coding scheme has been done. Error control coding has become imperative in today's wireless communication standards. Low density parity check codes proposed by Robert Gallager have been proven to be the best error correction codes reaching within 0.0045 dB of the Shannon limit. The data is first channel coded using a parity check matrix, mapped according to the chosen signal constellation and transmitted over different antennas. In this section, the error performance of the proposed receiver is analyzed in different fading channels. It is observed that the receiver with channel coding gives a substantial coding gain as compared to the uncoded scheme.

The thesis is concluded in chapter 6 where the main contributions are highlighted and the scope for further research is described.

Chapter 2
Study of Existing MIMO Receivers

2.1 Introduction

MIMO technology is considered to be a breakthrough in wireless communication because it helps to solve the two major problems of wireless communication: obtaining high capacity from a limited spectrum and multipath fading. In SISO systems, multipath fading is considered to be the major performance limiting factor. Multipath fading is characterized by the reception of multiple replicas of the same signal from different angles and/or at different times. These replicas are called multipath signals and they cause fading by constructively or destructively combining at the receiver and cause signal power at the receiver to fluctuate randomly. While the conventional SISO systems are impaired by multipath fading, MIMO systems actually use it to their advantage. Along with the time and frequency dimensions, MIMO systems exploit the spatial dimension by using multiple antennas at the transmitter and receiver. The additional spatial dimension can be used to obtain array gain, spatial multiplexing gain and/or diversity gain. The data rate increase that can be achieved by using spatially multiplexed MIMO systems is proportional to the number of antennas provided the antennas are uncorrelated.

2.1.1 Array Gain

Array gain is the average increase in the SNR at the detector that arises from the coherent combining effect of multiple antennas at the receiver and/or transmitter. For MIMO systems, the array gain can be obtained if the channel is known perfectly to the transmitter and/or receiver. Array gain (g_a) is characterized by shift of SNR which translates into decrease of BER at a fixed transmit power [52].

$$g_a = \frac{\rho_{out}}{\rho} \tag{2.1}$$

where ρ_{out} is the output SNR and ρ is the single branch average SNR. Array gain is proportional to the number of antennas and improves the power efficiency of wireless systems.

2.1.2 Diversity Gain

In SISO systems, when the fading is severe, the BER increases. The solution to this problem is to provide the receiver with multiple copies of the same signal which can be effectively combined to reduce the impact of fading on BER. This concept is known as diversity and the gain achieved by this process is called diversity gain. The three dimensions to be exploited in wireless communication are time, frequency and space, therefore, the concept of diversity can be applied to any or all these dimensions. MIMO systems, in addition to time and frequency make use of the spatial dimension, so the diversity gain due to space is called spatial diversity. Before the development of MIMO systems, spatial diversity using SIMO systems was seen as a powerful communication technique and was based on the fact that considerable SNR improvement is obtained by combining the multiple copies of the same signal received at different uncorrelated receiver elements. However, in the presence of spatial correlation, the diversity gain advantage is reduced considerably. In MIMO systems, diversity gain can be obtained by sending replicas of the same signal from multiple transmitting antennas. Diversity gain results in improving the quality of communication by increasing the link reliability.

2.1.3 Multiplexing Gain

MIMO systems can also be used to increase the date rate of the wireless system without imposing additional bandwidth or power penalty. This is done by breaking up a high rate signal into lower rate streams. These lower rate streams are then transmitted separately from multiple antennas. This data is then recovered at the receiver and combined to produce the original data. If it is assumed that the channels between different sets of antennas are uncorrelated, the data rate increases proportionally with the number of antennas.

A very interesting analogy of data flow in MIMO systems to water flow in pipes is presented in by M. Jankiraman [53]. The pipes are used to transfer water to a tank or reservoir. Obviously if the number of pipes will be more, the water flow will increase. In the case of fluid mechanics, this hold true no matter what, but, the analogy with MIMO ends here. If the data pipes are independent, i.e. the fading channel is uncorrelated, the data transferred is independent and the increase in capacity is proportional to the increase in the number of data pipes. On the other

hand, if the data pipes are identical (fully correlated/highly correlated), the data transferred will be merely replicas of the same signal and there is no/negligible increase in the capacity.

2.2 System Model

We consider a MIMO system with N_T transmit antennas and N_R receive antennas, where $N_T \leq N_R$ as shown in Fig. 2.1. In the figure, the transmitted signal **x** is a $N_T \times 1$vector, where x_i is the data transmitted by the i^{th} antenna. The covariance matrix of transmitted signal is given by

$$\mathbf{R}_{xx} = E[\mathbf{x}\mathbf{x}^H]. \tag{2.2}$$

H is a $N_R \times N_T$ matrix characterizing the fading (degradation) process between the transmitter and receiver. The transmitted signal is taken to be narrowband; therefore, it experiences flat fading. In this work, two different fading channels, namely, Rayleigh and Rician are considered. The vector **n** ($N_R \times 1$) represents the i.i.d AWGN with zero mean and unit variance ($\sigma_n^2 = 1$). The covariance matrix of noise (R_{nn}) is given by

$$\mathbf{R}_{nn} = E[\mathbf{n}\mathbf{n}^H] \tag{2.3}$$

The noise is considered to be independent of the input signal, i.e. $E[\mathbf{x}\mathbf{n}^H] = \mathbf{0}$. The received signal denoted by **y** is a $N_R \times 1$ matrix given by

$$\mathbf{y} = \mathbf{H}\mathbf{x} + \mathbf{n} \tag{2.4}$$

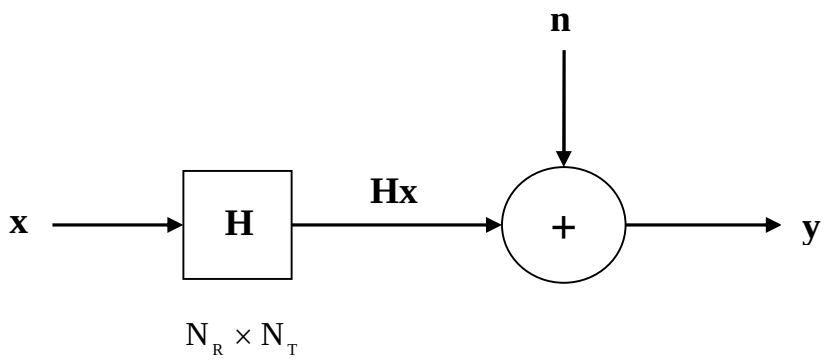

Figure 2.1: System Model

The covariance matrix of the received signal ($\mathbf{R}_{yy}$) is given by:

$$\mathbf{R}_{yy} = E[\mathbf{y}\mathbf{y}^H] \tag{2.5}$$

As already stated, the signal in this dissertation is taken to be narrowband, therefore the fading channels are considered to be frequency flat. A brief explanation of the various fading channels used throughout the course of this dissertation is given below.

2.2.1 Rayleigh Fading

When there is no LOS path between the transmitter and receiver and the number of independent scatterers is sufficiently large, the fading channel can be modeled as Rayleigh fading. The envelope of Rayleigh fading follows the Rayleigh distribution. Rayleigh fading for a MIMO system can be synthesized by constructing a ($N_R \times N_T$) matrix with Zero Mean Circularly Symmetric Complex Gaussian (ZMCSCG) entries with unit variance $\mathcal{CN}$ **(0, 1)**. Furthermore, if the channel is fully uncorrelated, then it is said to be independent and identically distributed and an i.i.d Rayleigh fading channel is denoted by $\mathbf{H}_{iid}$. The received signal power in a typical i.i.d Rayleigh fading channel is shown in Fig. 2.2.

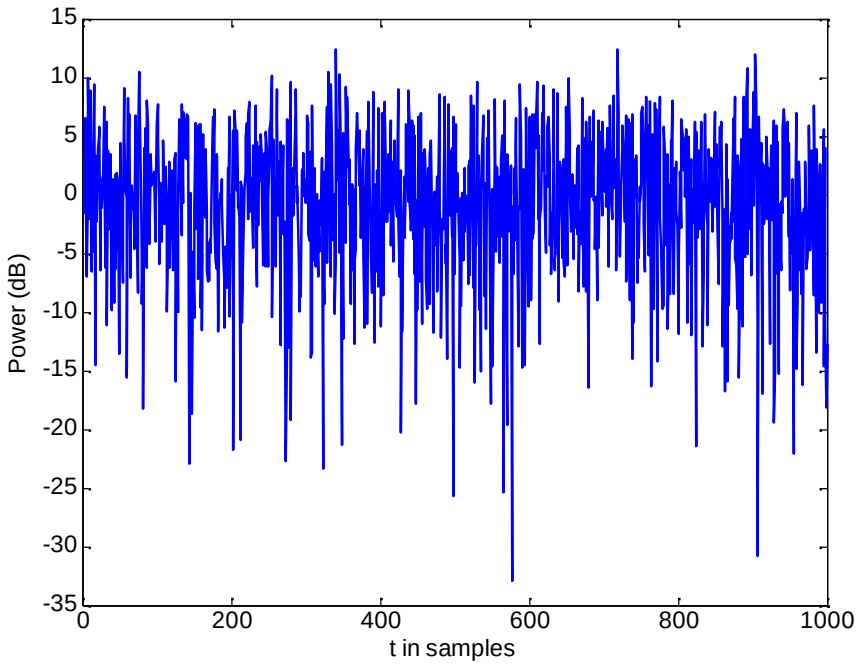

Figure 2.2: A typical Rayleigh fading channel

2.2.2 Rician Fading

In practical situations, the behavior of the fading channel can deviate significantly from $\mathbf{H}_{iid}$ due to the presence of dominant LOS path between the transmitter and receiver. The envelope of the fading channel with a LOS path is assumed to be following Rician distribution. Rician fading can be modeled as the sum of the dominant LOS path ($\mathbf{H}_{LOS}$) and the Gaussian distributed matrix ($\mathbf{H}_{iid}$) and given as

$$\mathbf{H}_{rice} = \sqrt{\frac{K}{K+1}}\mathbf{H}_{LOS} + \sqrt{\frac{1}{K+1}}\mathbf{H}_{iid}, \tag{2.6}$$

where K is the Rician K-factor given by the ratio of the power in the LOS component to the power in the fading component. When K=0, Rician fading reduces to Rayleigh fading, i.e. $\mathbf{H}_{rice}=\mathbf{H}_{iid}$. When $K=\infty$, the channel is assumed to be non-fading. A typical Rician fading channel with K=10 is shown in Fig. 2.3.

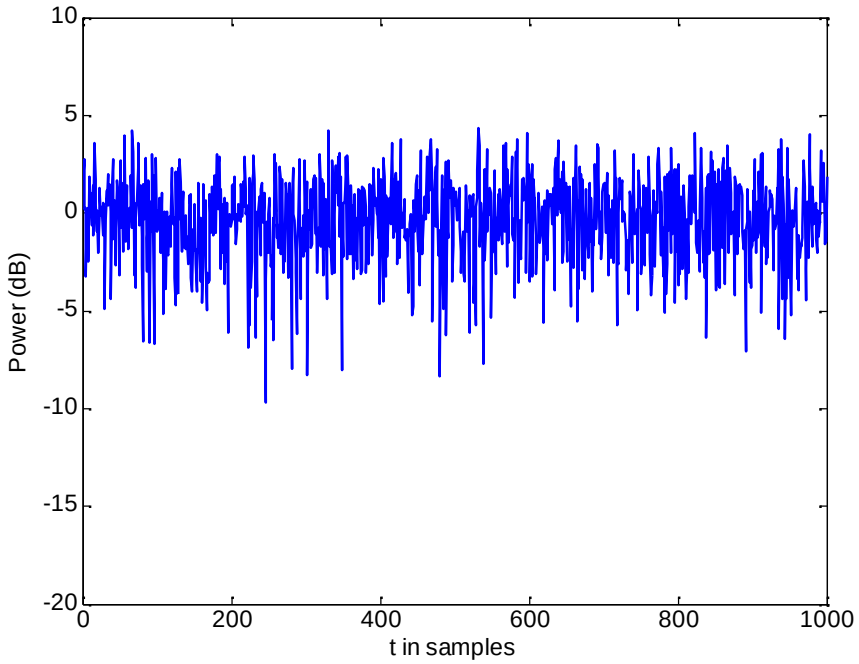

Figure 2.3: A typical Rician fading channel for K-factor=10

As the LOS component of Rician fading becomes stronger, the scattering advantage of the multipath channel is lost and the capacity decreases.

2.3 Spatial Correlation

The classical i.i.d Rayleigh fading model considers the channels between different sets of antennas to be independent. In practical situations, this is rarely the case as the size of all devices tends to decrease; the physical space for system engineers to work with is decreasing constantly. As the advantage of increasing the data rates from MIMO comes from the fact that the additional space dimension in utilized, the decreasing size of wireless devices makes this difficult. As already know in theory, for the channels between two independent sets of antennas to be uncorrelated, the antenna spacing should be greater than 0.5λ [13]. In real life situations, however, this distance is not always achievable and as a consequence the channels between different sets of antennas are correlated. Initially, the spatial correlation was modeled using the full correlation model [38] which is given by

$$\mathbf{R}_{\mathrm{H}} = E[\mathbf{h}\mathbf{h}^{H}], \tag{2.7}$$

where $\mathbf{h} = vec(\mathbf{H})$, which returns a $\mathrm{N_R N_T} \times 1$ vector from a $\mathrm{N_R} \times \mathrm{N_T}$ matrix. $\mathbf{R}_{\mathrm{H}}$ is a $\mathrm{N_R N_T} \times \mathrm{N_R N_T}$ matrix which gives the correlation of all the fading channel matrix elements.

If $\mathbf{h}_{\mathrm{iid}} = vec(\mathbf{H}_{\mathrm{iid}})$ **,** then the correlated fading channel can be generated by

$$\mathbf{H} = \mathbf{R}_{\mathrm{H}}^{1/2}\mathbf{H}_{\mathrm{iid}}. \tag{2.8}$$

However, the use of this model requires a large number of parameters which is undesirable. To, reduce the large number of parameters, a simpler model called the Kronecker model was proposed. This model works on the principle that the transmitter correlation ($\mathbf{R}_{\mathrm{TX}}$) and receiver correlation ($\mathbf{R}_{\mathrm{RX}}$) matrices can be modeled separately. The full correlation matrix can be obtained by the Kronecker product of $\mathbf{R}_{\mathrm{TX}}$ and $\mathbf{R}_{\mathrm{RX}}$ as

$$\mathbf{R}_{\mathrm{H}} = \mathbf{R}_{\mathrm{TX}} \otimes \mathbf{R}_{\mathrm{RX}} \tag{2.9}$$

where $\mathbf{R}_{\mathrm{TX}}=E[\mathbf{H}^{H}\mathbf{H}]$ is a $\mathrm{N_T} \times \mathrm{N_T}$ matrix and $\mathbf{R}_{\mathrm{RX}}=E[\mathbf{H}\mathbf{H}^{H}]$ is a $\mathrm{N_R} \times \mathrm{N_R}$ matrix.

From (2.8) and (2.9), we get:

$$\mathbf{H} = (\mathbf{R}_{\mathrm{TX}} \otimes \mathbf{R}_{\mathrm{RX}})^{1/2}\mathbf{H}_{\mathrm{iid}} \tag{2.10}$$

Eq. (2.10) can be simplified into,

$$\mathbf{H} = \mathbf{R}_{\mathrm{RX}}^{1/2}\mathbf{H}_{\mathrm{iid}}\mathbf{R}_{\mathrm{TX}}^{1/2} \tag{2.11}$$

In this thesis, the correlation matrices $\mathbf{R}_{\mathrm{RX}}$ and $\mathbf{R}_{\mathrm{TX}}$ have been obtained using the method suggested by Van Zelst et al. [54-55] in which these matrices are calculated as a function of the distance between the adjacent antenna elements at the transmitter and receiver. The following transmitter and receiver correlation matrices are of Toeplitz structure and are given by:

$$\mathbf{R}_{\mathrm{TX}} = \begin{bmatrix} 1 & r_{TX} & r_{TX}^4 & \cdots & r_{TX}^{(\mathrm{N_T}-1)^2} \\ r_{TX} & 1 & r_{TX} & \ddots & \vdots \\ r_{TX}^4 & r_{TX} & 1 & \ddots & r_{TX}^4 \\ \vdots & \ddots & \ddots & \ddots & r_{TX} \\ r_{TX}^{(\mathrm{N_T}-1)^2} & \cdots & r_{TX}^4 & r_{TX} & 1 \end{bmatrix}, \tag{2.12}$$

where r_{TX} is the fading correlation between two adjacent transmitter antenna elements and

$$\mathbf{R}_{\mathrm{RX}} = \begin{bmatrix} 1 & r_{RX} & r_{RX}^4 & \cdots & r_{RX}^{(\mathrm{N_R}-1)^2} \\ r_{RX} & 1 & r_{RX} & \ddots & \vdots \\ r_{RX}^4 & r_{RX} & 1 & \ddots & r_{RX}^4 \\ \vdots & \ddots & \ddots & \ddots & r_{RX} \\ r_{RX}^{(\mathrm{N_R}-1)^2} & \cdots & r_{RX}^4 & r_{RX} & 1 \end{bmatrix}, \tag{2.13}$$

where r_{RX} is the fading correlation between two adjacent receiver antenna elements.

If it is assumed that the inter element spacing between adjacent antennas is equal at both transmitter and receiver (as shown in Fig. 2.4), then the model reduces to a single coefficient correlation model given by

$$r_{TX} = r_{RX} = r \approx \exp\left(-23 \cdot \Delta^2 \cdot d^2\right), \tag{2.14}$$

where 'd' is the distance in wavelengths between the antenna elements and Δ is the angular spread. Using the correlation model presented above, the spatial correlation between the antenna elements can be modeled by a single coefficient ranging from zero correlation case to fully correlated case.

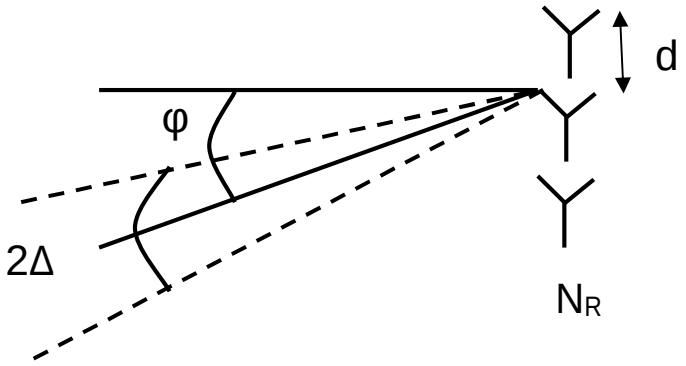

Figure 2.4: The mean Angle of Arrival (AoA) and angle spread of an incoming multipath signal

Also, for small *r*, the higher order terms can be omitted and the resulting correlation matrices are tridiagonal. The model described in this section has been used to implement the spatial correlation throughout this dissertation.

2.4 MIMO Receivers

In the following section, various spatial multiplexing techniques, namely, Zero Forcing (ZF), Minimum Mean Squared Error (MMSE), Vertical Bell Labs Layered Space Time (VBLAST) and maximum likelihood are discussed and compared [53, 56-59]. The system model, fading channels and spatial correlation model discussed in the previous sections are used for simulating the wireless system. The error rate performance of MIMO receivers is compared in correlated and uncorrelated fading channels.

2.4.1 Zero Forcing Receiver

The ZF receiver is a linear MIMO receiver. Linear receiver refers to the receiver using linear processing techniques. It inverts the channel response **H** at the receiver in order to suppress the interference from the other transmitted symbols, i.e. it separates each stream and then decodes it independently. In this case, perfect Channel State Information at the Receiver (CSIR) is considered; otherwise some form of channel estimation has to be used to estimate the Channel State Information (CSI). If it is assumed that the matrix **H** is invertible, the estimated signal $\hat{\mathbf{x}}$ is given by:

$$\hat{\mathbf{x}}_{ZF} = \mathbf{H}^{-1}\mathbf{y} \tag{2.15}$$

$$\hat{\mathbf{x}}_{ZF} = \mathbf{H}^{-1}(\mathbf{Hx} + \mathbf{n}) \tag{2.16}$$

$$\hat{\mathbf{x}}_{ZF} = \mathbf{x} + \mathbf{H}^{-1}\mathbf{n} \tag{2.17}$$

Eq. (2.17) shows that although the ZF receiver removes the spatial interference completely, it has the drawback of *noise enhancement* due to the product of noise with $\mathbf{H}^{-1}$. If **H** matrix is not square, then its inverse is obtained by using the pseudo-inverse ($\mathbf{H}^{\dagger}$).

$$\mathbf{H}^{\dagger} = (\mathbf{H}^{H}\mathbf{H})^{-1}\mathbf{H}^{H} \tag{2.18}$$

Let $\mathbf{W} = \mathbf{H}^{\dagger}$

$$\hat{\mathbf{x}}_{ZF} = \mathbf{Wy} \tag{2.19}$$

$$\hat{\mathbf{x}}_{ZF} = \mathbf{H}^{\dagger}(\mathbf{Hx} + \mathbf{n}) \tag{2.20}$$

$$\hat{\mathbf{x}}_{ZF} = \mathbf{x} + \mathbf{H}^{\dagger}\mathbf{n} \tag{2.21}$$

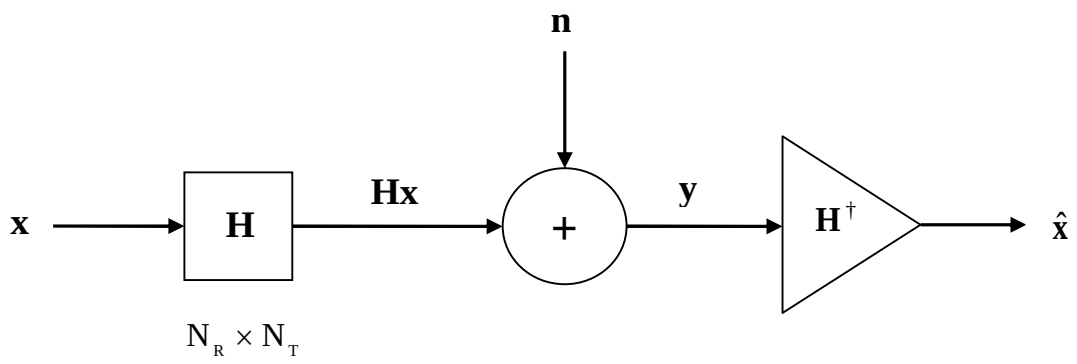

Figure 2.5: Block diagram of the system model with ZF receiver

2.4.2 Minimum Mean Square Error (MMSE) Receiver

As discussed above, the ZF receiver has the problem of noise enhancement, especially at low SNR. MMSE is also a linear MIMO receiver which maximizes the signal to interference plus noise ratio (SINR) by finding a weight matrix **W** which minimizes the Mean Square Error (MSE).

$$\mathbf{W} = \left(\alpha \mathbf{I}_{N_R} + \mathbf{H}^{H}\mathbf{H}\right)^{-1}\mathbf{H}^{H}, \tag{2.22}$$

where $\alpha = N_T / \rho$ and ρ denotes the SNR. When $\alpha = 0$, the MMSE solution reduces to ZF solution.

$$\hat{\mathbf{x}}_{\text{MMSE}} = \mathbf{W}\mathbf{y} \tag{2.23}$$

The MSE is given by

$$\sigma_e^2 = E\left[(\mathbf{x}-\hat{\mathbf{x}})^H(\mathbf{x}-\hat{\mathbf{x}})\right] \tag{2.24}$$

$$\sigma_e^2 = E\left[(\mathbf{x}-\mathbf{W}\mathbf{y})^H(\mathbf{x}-\mathbf{W}\mathbf{y})\right]. \tag{2.25}$$

At low SNR, where the errors are dominated by noise, MMSE receiver acts like a matched filter, and at high SNR, where the errors are dominated by interference, the MMSE receiver acts like ZF receiver. Therefore, MMSE receiver is considered to be the optimum linear receiver [56].

2.4.3 Vertical Bell Labs Layered Space-Time (VBLAST) Receiver

VBLAST is a non linear MIMO detection technique in which the interference from already detected components of **x** is subtracted out of the received signal **y**, therefore, fewer interferers are present. In VBLAST, Successive Interference Cancellation (SIC) is used along with ordering, i.e. the detection of the components of **x** is done according to the optimal detection order. The full MMSE VBLAST detection algorithm is composed of two phases, an initialization and a recursive phase [12, 60]. At the initialization stage, the MMSE estimate ($\mathbf{G}_1$) is obtained.

Initialization:

$$\begin{aligned} &i \leftarrow 1 \\ &\mathbf{G}_1 = \left(\alpha \mathbf{I}_{\mathrm{N_R}} + \mathbf{H}^H\mathbf{H}\right)^{-1}\mathbf{H}^H \\ &k_1 = \arg\min_j \left\|\mathbf{G}_1\right\|^2 \end{aligned} \tag{2.26}$$

Recursion:

$$\begin{aligned} &\mathbf{W}_{k_i} = \left(\mathbf{G}_i\right)_{k_i} \\ &\mathrm{z}_{k_i} = \mathbf{W}_{k_i}{}^T\mathbf{y}_{k_i} \\ &\hat{\mathrm{x}}_{k_i} = Q(\mathrm{z}_{k_i}) \\ &\mathbf{y}_{i+1} = \mathbf{y}_i - \hat{\mathrm{x}}_{k_i}\mathbf{H}_{k_i} \\ &\mathbf{G}_{i+1} = (\alpha \mathbf{I}_{\mathrm{N_R}} + \mathbf{H}_{\bar{k}_i}^H\mathbf{H}_{\bar{k}_i})^{-1}\mathbf{H}_{\bar{k}_i}^H \\ &k_{i+1} = \arg\min_{j\notin\{k_1\cdots k_i\}} \left\|\left(\mathbf{G}_{i+1}\right)_j\right\|^2 \\ &i \leftarrow i+1 \end{aligned} \tag{2.27}$$

where $\mathbf{G}_i$ is the MMSE estimate at the ith iteration stage, $Q(\cdot)$ denotes the quantization (slicing) operation depending upon the modulation constellation and $\mathbf{H}_{k_i}^{-}$ is a matrix obtained by zeroing columns $k_1,\ldots, k_j$ of $\mathbf{H}$.

2.4.4 Maximum Likelihood Receiver

Maximum likelihood receiver is the optimum MIMO receiver. It obtains the maximum likelihood estimate of the signal by finding the Euclidean distance between the received signal vector and the product of the all possible transmitted signal vectors with **H**, selecting the one with the minimum distance. If M denotes the set of signal constellation symbol points, Maximum likelihood estimate of **x** is obtained as

$$\hat{\mathbf{x}}_{\mathrm{ML}} = \arg\min_{\mathbf{x}\in \mathrm{M}^{\mathrm{N_T}}} \left\|\mathbf{y} - \mathbf{H}\mathbf{x}\right\|^2 \tag{2.28}$$

From eq. (2.28), it is clear that the complexity of the ML receiver increases exponentially with increase in the signal constellation or number of transmit antennas. For this reason, the ML receiver is rarely used with higher order modulation techniques or large number of antennas.

2.5 Results and Discussion

2.5.1 Simulation Details

The performance of the all receivers discussed above was studied. The details of simulation are given next. A total number of 100,000 random binary bits are generated and transmitted after Binary Phase Shift Keying (BPSK) modulation. No channel coding is used unless otherwise stated. The simulations are performed for two different antenna configurations, i.e. 2x2 and 4x4. It is assumed that channel state information at the receiver is perfectly known. The simulation is performed for Rayleigh and Rician fading channels which are described in sections 2.2.1 and 2.2.2 respectively. The Rayleigh fading channel characterizes the fading channel which has rich scattering and is considered as a Zero Mean Circularly Symmetric Gaussian (ZMCSG) random variable with CN (0, 1) and no LOS path unlike Rician fading which includes a dominant LOS component along with the scattering component. The Rician fading is described as the sum of the specular LOS component and a ZMCSG random variable with (0, 1).

2.5.2 Performance Comparison

The comparison of BER for different receivers for 2×2 antennas in uncorrelated Rayleigh fading channel is shown in Fig. 2.6. The ZF receiver has the worst performance whereas the ML receiver has the best performance. Similar results are observed for a 4×4 system in Fig. 2.7.

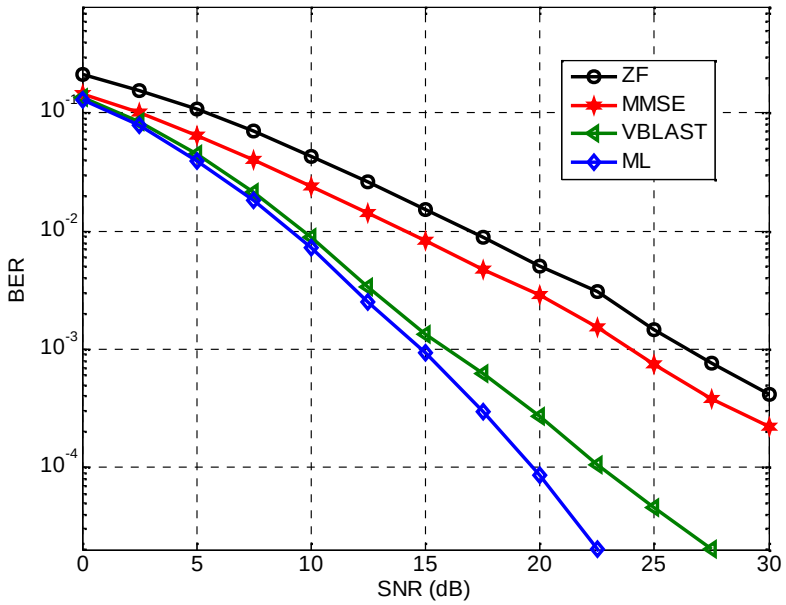

Figure 2.6: BER vs. SNR for N_T=N_R=2 system for a flat uncorrelated Rayleigh fading channel

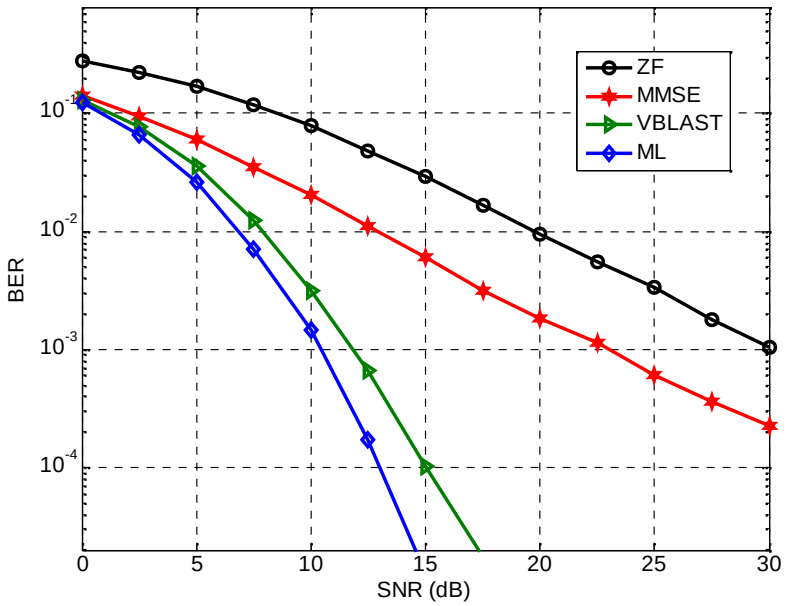

Figure 2.7: BER vs. SNR for N_T=N_R=4 system in flat uncorrelated Rayleigh fading channel

Table 2.1: Comparison of SNR of MIMO receivers for $N_T=N_R=2$ and $N_T=N_R=4$ to achieve a BER $=10^{-2}$ in uncorrelated Rayleigh fading channel

No. of Antennas	SNR required (in dB) for BER of 10^{-2}			
	ZF	MMSE	VBLAST	ML
2×2	16.99	14.09	9.64	9.12
4×4	19.8	12.91	7.88	6.82

Table 2.1 shows the comparison of SNR required by the receivers to achieve a BER of 10^{-2}. It is seen that ZF and MMSE receivers require higher SNR as compared to VBLAST and ML to achieve the same BER. Out of the four receivers, ML requires the least SNR.

In line with the previous results, Fig. 2.8 and 2.9 show the BER comparison of the different receivers in uncorrelated Rician fading channel with a K-factor of 10 for 2×2 and 4×4 antennas respectively. It is observed that the performance of all the receivers deteriorates due to the presence of a dominant LOS path and loss of scattering in the fading channel.

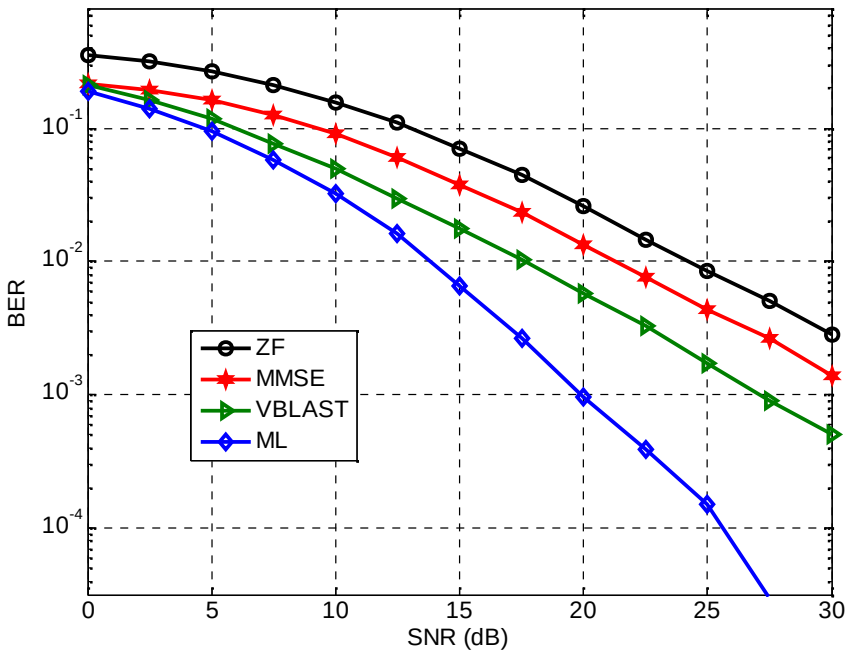

Figure 2.8: BER vs. SNR for $N_T=N_R=2$ system in flat uncorrelated Rician fading channel with *K*-factor=10

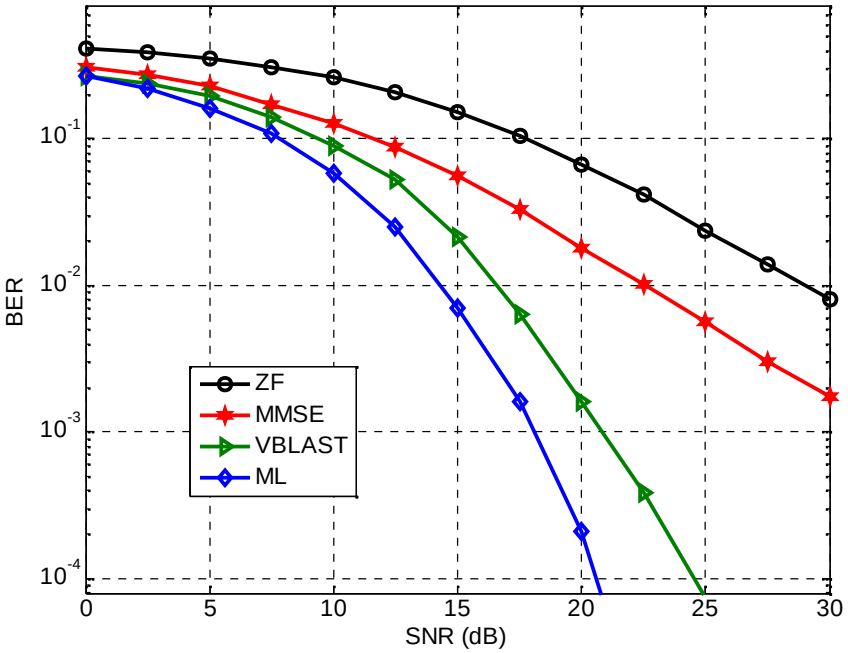

Figure 2.9: BER vs. SNR for N_T=N_R=4 system in flat uncorrelated Rician fading channel with *K*-factor=10

Table 2.2: Comparison of SNR of MIMO receivers for N_T=N_R=2 and N_T=N_R=4 to achieve a BER $=10^{-2}$ in uncorrelated Rician fading channel with *K*-factor=10

No. of Antennas	SNR required (in dB) for BER of 10^{-2}			
	ZF	MMSE	VBLAST	ML
2×2	24.21	21.3	17.64	13.82
4×4	29	22.57	16.57	14.28

From table 2.2, it is seen that in Rician fading with a K-factor=10dB, the performance of ML receiver deteriorates the least, whereas the performance of other three receiver degrades significantly.

Fig. 2.10 and 2.11 show the effect of increasing the K-factor (dB) of Rician fading on the BER of different receivers for a 2×2 system at a fixed SNR of 10dB and 30dB respectively. When the K-factor is 0, there is no dominant LOS path and the BER is less. With the increase in K-factor, the power of the dominant LOS path increases, the channel scattering decreases and thus the BER increases.

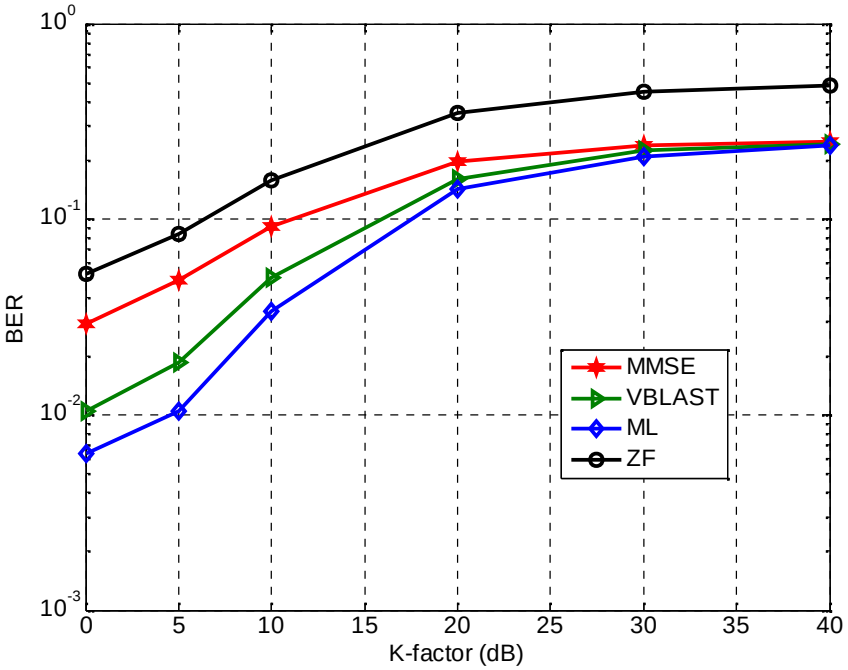

Figure 2.10: BER vs. Rician *K*-factor for N_T=N_R=2 at a fixed SNR of 10dB

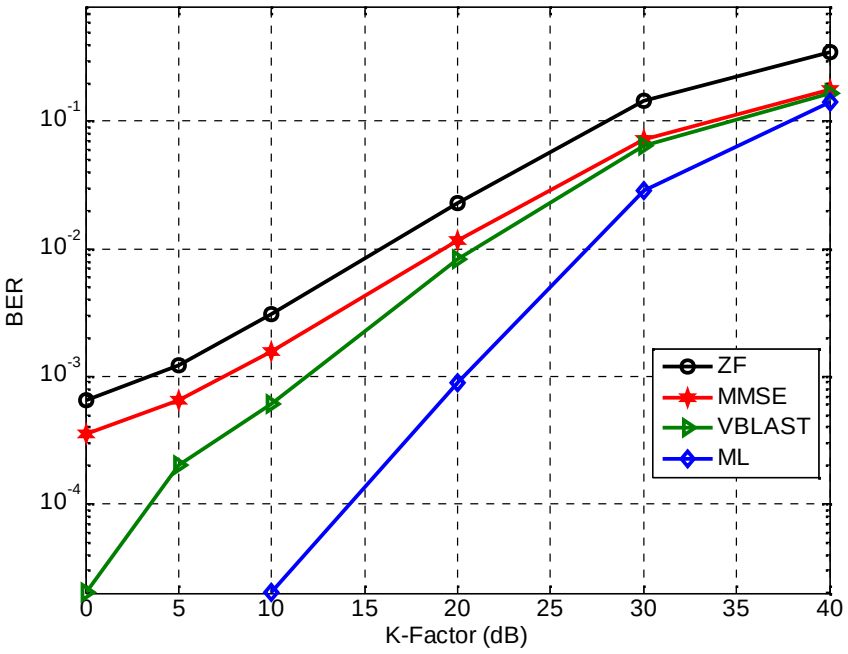

Figure 2.11: BER vs. Rician *K*-factor for N_T=N_R=2 at a fixed SNR of 30dB

Table 2.3: Comparison of BER of MIMO receivers at a fixed SNR and different values of K-factor in Rician fading channel for a 2x2 system

N_T=N_R=2	SNR=10dB				SNR=30dB			
K-factor	ZF	MMSE	VBLAST	ML	ZF	MMSE	VBLAST	ML
5	0.0843	0.0488	0.0183	0.0104	0.0012	0.00064	0.0002	-
10	0.1590	0.0913	0.0504	0.0337	0.0031	0.0015	0.0006	2×10^{-5}
20	0.3501	0.1970	0.1610	0.1432	0.0230	0.0116	0.0083	0.0008
30	0.4484	0.2400	0.2263	0.2099	0.1460	0.0726	0.0645	0.0288

The comparison of BER of MIMO receivers for different values of K-factor is shown in table 2.3. With an increase in the K-factor, the dominant LOS path becomes more powerful taking away the rich scattering advantage away from the fading channel. Due to this, the performance of all the receivers deteriorates with an increase in the K-factor. Fig. 2.12 and 2.13 show similar results for varying 'K' for a 4×4system. As observed in the previous results, the BER increases with increase in the K-factor of Rician fading.

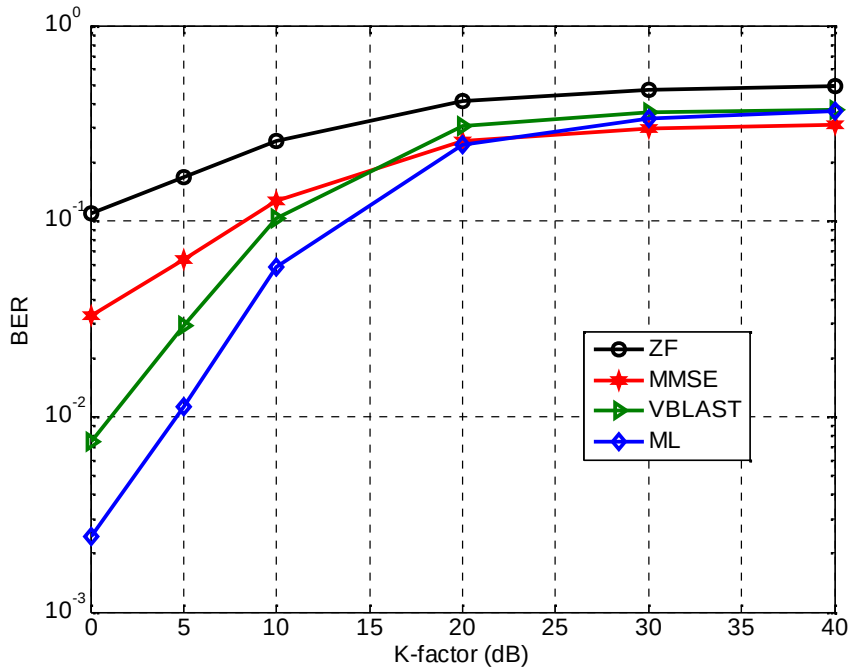

Figure 2.12: BER vs. Rician *K*-factor for N_T=N_R=4 at a fixed SNR of 10dB

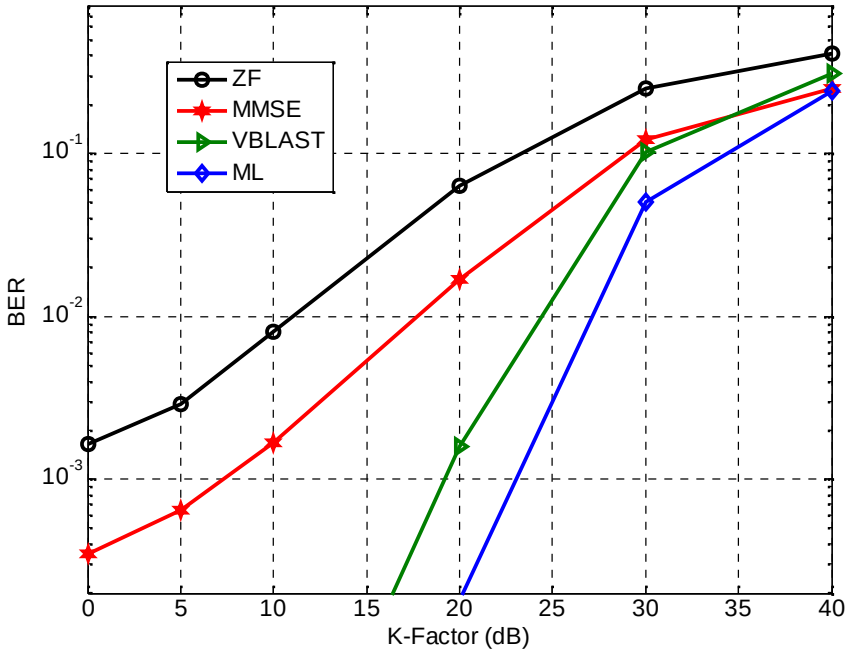

Figure 2.13: BER vs. Rician *K*-factor for N_T=N_R=4 at a fixed SNR of 30dB

Table 2.4: Comparison of BER of MIMO receivers at a fixed SNR and different values of K-factor in Rician fading channel for a 4x4 system

N_T=N_R=4	SNR=10dB				SNR=30dB			
K-factor	ZF	MMSE	VBLAST	ML	ZF	MMSE	VBLAST	ML
5	0.1678	0.0640	0.0290	0.0111	0.0028	0.0006	-	-
10	0.2583	0.1271	0.1036	0.0582	0.0080	0.0016	5×10^{-6}	-
20	0.4112	0.2550	0.3070	0.2448	0.0630	0.0167	0.0016	0.0002
30	0.4710	0.2988	0.3595	0.3346	0.2501	0.1218	0.1011	0.0506

From the previous results, it is clear that the dominant LOS path present in Rician fading hinders the communication and a higher BER is obtained as compared to NLOS channel. The dramatic success of MIMO systems is based on the fact that they exploit the additional space dimension along with time and frequency. However, the utilization of space dimension is based on the assumption that various channel are independent and uncorrelated. However, if the channels are correlated, they will fade identically and the advantage of space will be lost. In the following section, we observe the effects of spatial correlation on MIMO receivers. The single coefficient correlation model discussed in section 2.3 is used for simulating the correlated fading. The

results are presented in the form of BER vs. correlation coefficient and show the effect of spatial correlation from no correlation (r=0) case to fully correlated (r=1) case. For simplicity, it is assumed that the spatial correlation on both transmitter and receiver is equal; therefore, the correlation coefficient is denoted as $r_{TX}=r_{RX}=r$.

Fig. 2.14 and 2.15 show the BER vs. correlation coefficient for 2×2 system at a fixed SNR of 10 dB and 20 dB respectively. The minimum value of correlation coefficient is taken to be r=0 (no correlation) and maximum value is taken to r=1 (fully correlated). It is seen that when the channel is uncorrelated, the BER is lowest and with the increase in spatial correlation, the BER increases. Due to spatial correlation, the independence of the channels is lost and the space dimension cannot be exploited resulting in higher BER. Even the ML receiver, which is considered to be the optimum MIMO receiver (in terms of error rate performance), has a poor BER at high values of spatial correlation.

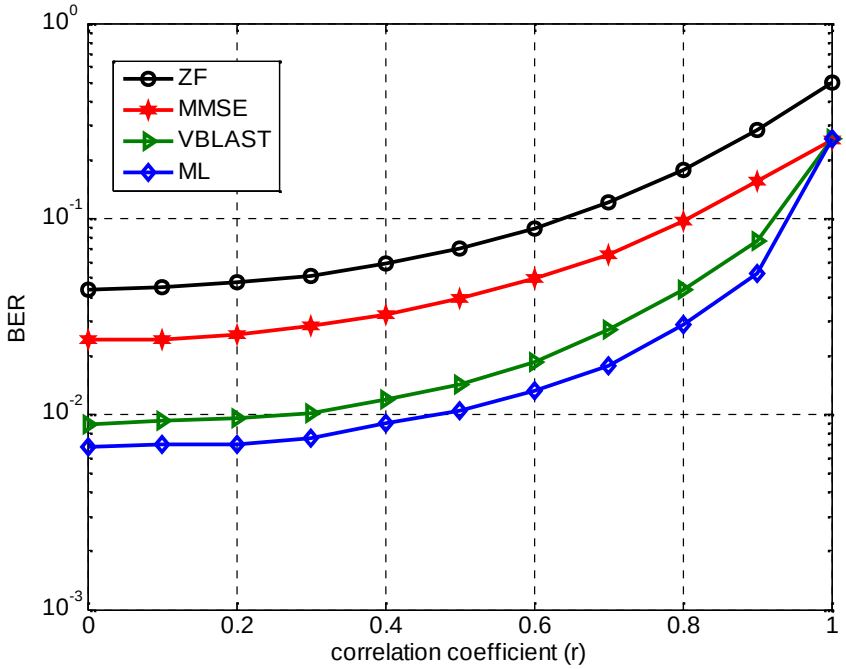

Figure 2.14: BER vs. correlation coefficient (r) for $N_T=N_R=2$ at a fixed SNR of 10 dB

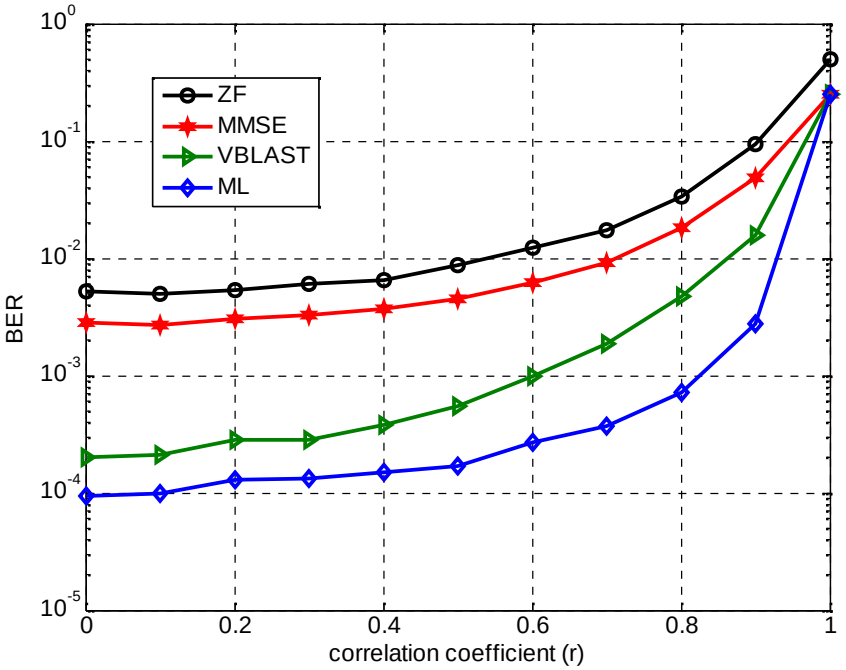

Figure 2.15: BER vs. correlation coefficient (r) for N_T=N_R=2 at a fixed SNR of 20 dB

Similar results are observed in Fig. 2.16 and 2.17 for a 4×4 system at fixed SNR of 10 dB and 20 dB respectively.

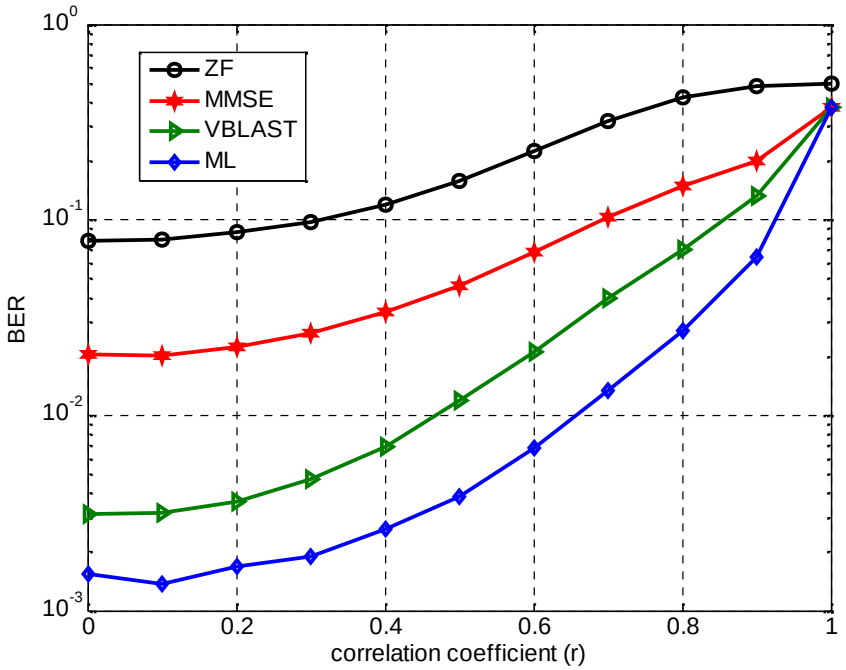

Figure 2.16: BER vs. correlation coefficient (r) for N_T=N_R=4 at a fixed SNR of 10 dB

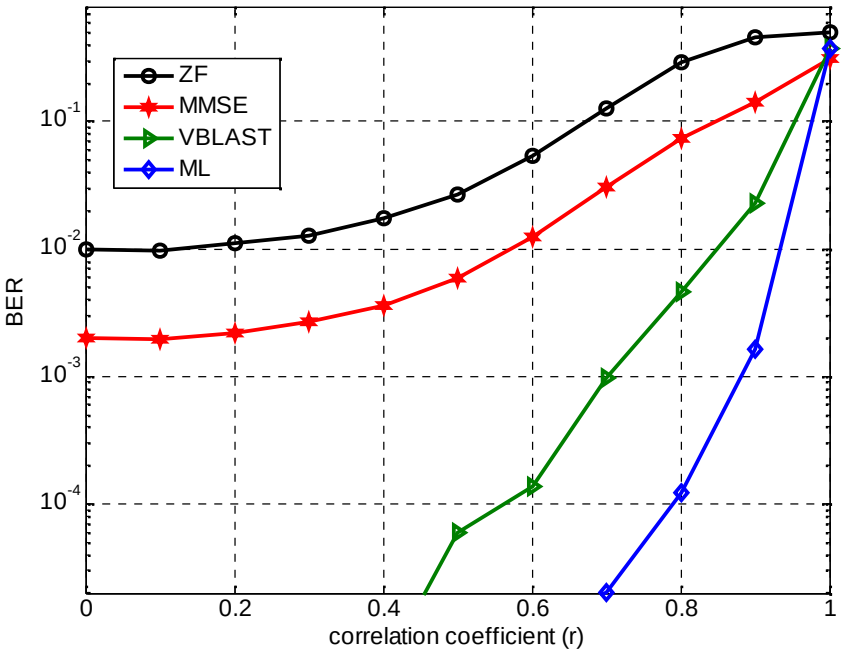

Figure 2.17: BER vs. correlation coefficient (r) for N_T=N_R=4 at a fixed SNR of 20 dB

It is seen from the results that increase in the spatial correlation can severely degrade the error performance of all the MIMO receivers. The error rate performance is acceptable up to r=0.5. At r>0.5, the error performance of all the receivers degrades very severely. Therefore, from the above results it can be concluded that for $r \leq 0.5$, the error performance of MIMO receivers is acceptable.

2.6 Complexity Analysis of MIMO Receivers

To compare the receivers completely, a comparison of the complexity of various receivers is also done [55]. The complexity is presented in terms of real additions and real multiplications. In this work, we assume equal number of transmit and receive antennas, therefore N_T=N_R=N. The complexity analysis has been divided into training phase and data phase.

Zero Forcing Receiver Complexity: For the ZF receiver, the training phase is given by (2.18) and its complexity is $4N^3 + N^2(8N-2) - 2N^2$ real additions and $12N^3$ real multiplications. The data phase of ZF receiver is given by (2.15) and its complexity is $2N^2 + 2N(N-1) + N\log_2(M)$ real additions and $4N^2$ real multiplications, where 'M' is the size of the modulation constellation.

MMSE Receiver Complexity: For the MMSE receiver, the training phase is given by (2.22) and the complexity of its training phase is $4N^3 + N^2(8N-2) - 2N^2$ real additions and $12N^3$ real multiplications. The data phase of MMSE receiver is given by (2.23) and its complexity is $2N^2 + 2N(N-1) + N\log_2(M)$ real additions and $4N^2$ real multiplications.

VBLAST Receiver Complexity: For VLAST, the complexity of training phase is $N(3N^2 + 4N^2(1+2N) + 3N(1+3N) + N - 1)/3$ real additions and $N^2(N+1)^2 + 8N^2(N+1)(2N+1)/6$ real multiplications and complexity of the data phase is $2N(4N-1) + N\log_2(M)$ real additions and $8N^2$ real multiplications.

ML Receiver Complexity: For ML receiver, if the maximum amount of memory is available, the complexity of the training phase is $2M^2N\frac{M^N-1}{M-1} + 2MN^2$ real additions and $4MN^2$ real multiplications and the complexity of data phase is $4N(I-1)$ real additions and $2NI$ real multiplications.

2.6.1 Simulation Details

To plot the complexity as one rather than separately in terms of additions and multiplications, the complexity is terms of equivalent additions. It is assumed that the algorithms are implemented by 8-bit operations; therefore, the complexity of an 8-bit multiplication is equal to 10 times the complexity of an 8-bit addition. All the results are presented in terms of equivalent additions for comparing the complexity of different receivers. The symbol time of the MIMO vector is assumed to be 10μs. The number of transmit and receive antennas is considered to be equal, therefore, N_T=N_R=N. The complexity is calculated for BPSK (M=2) modulation technique. The results are presented in the form of complexity (equivalent ADDs) vs. N.

2.6.2 Performance Comparison

The comparison of complexity of different receivers (in equivalent ADDs) vs. number of transmit/receive antennas (N) for BPSK modulation scheme is shown in Fig. 2.18. The complexity of ML receiver is the highest whereas the complexity of ZF and MMSE receivers is the lowest. Although, the MMSE receiver is better than the ZF receiver in terms of error rate performance, its complexity is equal to the ZF receiver.

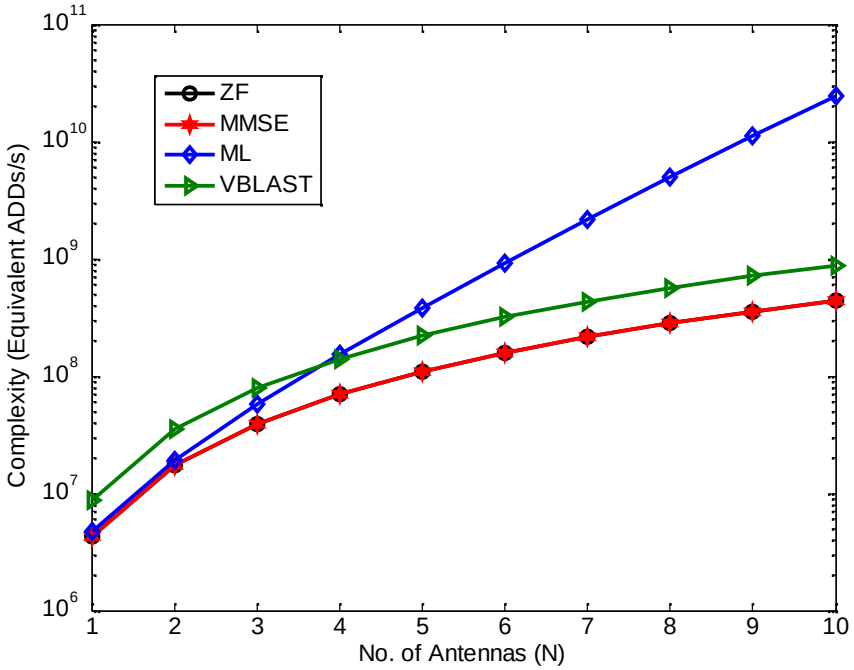

Figure 2.18: Complexity comparison of various MIMO receivers for BPSK modulation

Table 2.5: Comparison of Complexity (Eq. ADDs/s) for various MIMO receivers

$N_T=N_R=N$	ZF	MMSE	VBLAST	ML
2	1.74×10^7	1.74×10^7	3.5×10^7	1.91×10^7
4	7.001×10^7	7.001×10^7	1.404×10^8	1.535×10^8
8	2.809×10^8	2.809×10^8	5.626×10^8	4.915×10^9

From the above results, it can be seen that the ZF and MMSE receiver have the same complexity. The complexity of VBLAST is twice the complexity of ZF and MMSE receivers whereas the ML receiver has the highest complexity especially for antenna configurations greater than N=2.

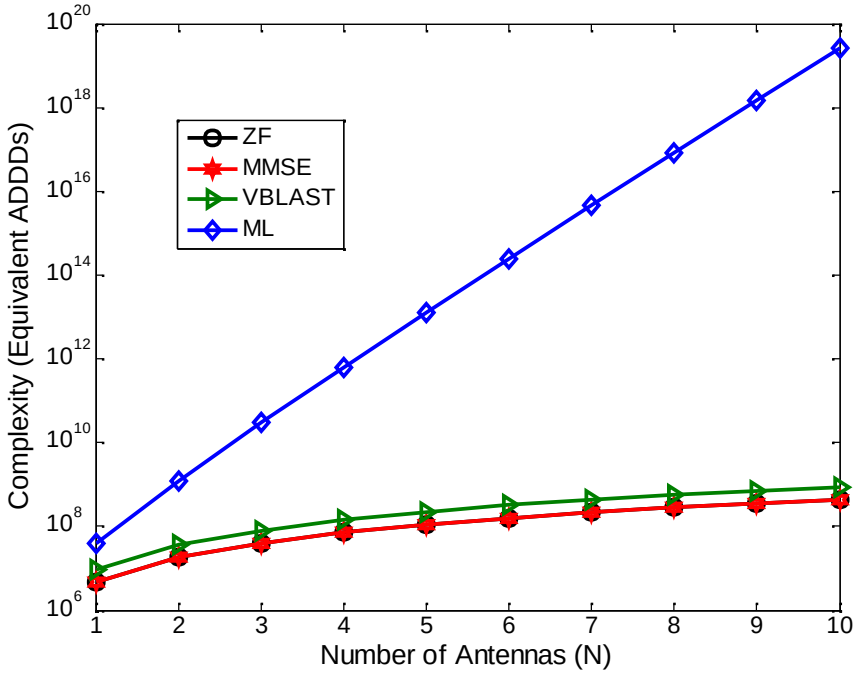

Figure 2.19: Complexity comparison of different receivers for 16-PSK modulation

Fig. 2.19 shows the complexity of various MIMO receivers with 16-PSK modulation. The complexity of the ML receiver is very high for 16-PSK due to the nature of its exhaustive search algorithm whereas the complexity of ZF, MMSE and VBLAST receivers is comparable to their complexity for BPSK.

2.7 Conclusions

In this chapter, the performance comparison of various MIMO receivers is done. The two criteria used for comparison are error performance and complexity. In terms of error performance, the two non linear receivers (VBLAST and ML) outperform the linear receivers (ZF and MMSE). ML receiver has the best error rate performance amongst all the receivers due to its exhaustive search algorithm. However, in terms of complexity, the ML receiver has the highest capacity which increases exponentially with increase in number of transmit antennas and modulation constellation. The complexity ZF and MMSE receiver is the same although MMSE receiver has a better error rate performance. The complexity of VBLAST is twice the complexity of ZF/MMSE receivers. Based on the BER and complexity tradeoff, as well as the simplicity of implementation of linear processing methods, we select the MMSE receiver.

Chapter 3
Improved Reception Scheme for Multi Antenna Systems

3.1 Introduction

In chapter 2, a comprehensive study of the MIMO receivers was done and it was concluded that MMSE receiver was preferable due to its linear nature and good error rate performance. With the increasing importance and application of MIMO systems in wireless communications and ever increasing demand for data rates, a receiver which gives lower BER performance as compared to the conventional MMSE receiver at a reasonably low computational complexity is desirable. In this section, we propose an improved MMSE receiver which gives a lower BER than the existing MMSE receiver. The improved receiver is based on Fractional Fourier Transform (FRFT) and filtering of the signal in fractional Fourier domain rather than time or frequency domain. Since, MMSE detection is based on Wiener filtering, a review of the Wiener filtering process has been given which serves as the background material for subsequent sections. We start by presenting the system model.

3.2 System Model

The transmitted signal which contains the desired information is denoted by **x**. It passes through the fading channel which is denoted by **H** and the additive noise is denoted by **n**. The received signal which is corrupted by fading and noise is given by **y**. Block diagram of the system model is shown in Fig. 3.1.

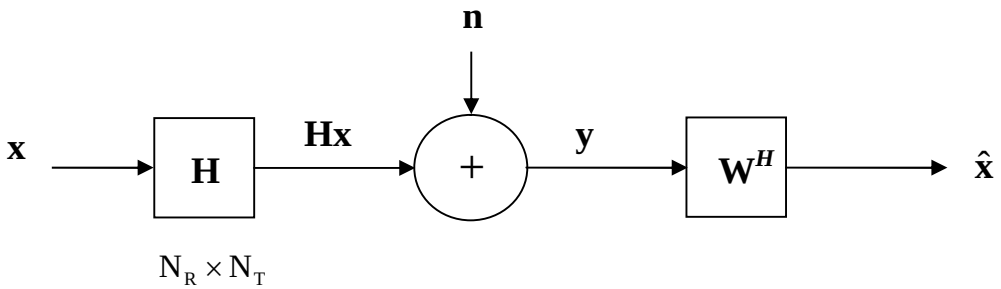

Figure 3.1: System Model

$$\mathbf{y} = \mathbf{H}\mathbf{x} + \mathbf{n} \tag{3.1}$$

where **x** is the transmitted data given by

$$\mathbf{x} = [x_1, x_2, x_3 \ldots, x_{\mathrm{N_T}}]^T. \tag{3.2}$$

H is a $\mathrm{N_R} \times \mathrm{N_T}$ random matrix that characterizes the degradation process and **y** is the received data given by

$$\mathbf{y} = [y_1, y_2, y_3 \ldots, y_{\mathrm{N_R}}]^T \tag{3.3}$$

and **n** is the additive noise with zero mean and unit variance, i.e. CN **(0, 1)**. It is assumed that the auto-correlation function of transmitted data and noise is known.

3.2.1 Wiener Filtering

Using linear processing, the estimate of the transmitted signal $\hat{\mathbf{x}}$ at the receiver can be found by multiplying it with the weight matrix **W**

$$\hat{\mathbf{x}} = \mathbf{W}^H \mathbf{y}, \tag{3.4}$$

where **W** is the $\mathrm{N_R} \times \mathrm{N_T}$ weight matrix given as

$$\mathbf{W} = \begin{bmatrix} w_{11} & w_{12} & w_{13} & \cdots & w_{1\mathrm{N_T}} \\ w_{21} & w_{22} & w_{23} & \cdots & w_{2\mathrm{N_T}} \\ w_{31} & w_{32} & w_{33} & \cdots & w_{3\mathrm{N_T}} \\ \vdots & \vdots & \vdots & \ddots & \vdots \\ w_{\mathrm{N_R}1} & w_{\mathrm{N_R}2} & w_{\mathrm{N_R}3} & \cdots & w_{\mathrm{N_R N_T}} \end{bmatrix} \tag{3.5}$$

The error vector '**e**' between the desired and the estimated signal is given by

$$\mathbf{e} = \mathbf{x} - \hat{\mathbf{x}}. \tag{3.6}$$

The MSE covariance matrix **E** is given by

$$\mathbf{E} = E\left\|\mathbf{e}\right\|^2 = E\left\|\mathbf{e}^H\mathbf{e}\right\| = E\left\|\mathbf{x} - \hat{\mathbf{x}}\right\|^2, \tag{3.7}$$

where **E** is the error covariance matrix, now inserting the value of $\hat{\mathbf{x}}$ from eq. (3.4), we get

$$\mathbf{E} = E\left\|\mathbf{x} - \mathbf{W}^H\mathbf{y}\right\|^2 \tag{3.8}$$

$$= \mathbf{R}_{xx} - \mathbf{W}^H\mathbf{R}_{yx} - \mathbf{W}\mathbf{R}_{yx}^H + \mathbf{W}^H\mathbf{R}_{yy}\mathbf{W}, \tag{3.9}$$

where, $\mathbf{R}_{xx}$ is the auto correlation matrix of the transmitted signal, $\mathbf{R}_{yy}$ is the auto correlation matrix of the received signal and $\mathbf{R}_{yx}$ is the cross correlation matrix of the desired signal and the received signal.

From (3.8), the gradient of the mean square error function with respect to the filter coefficient matrix is given by

$$\frac{\partial}{\partial \mathbf{W}} E\left[\mathbf{e}^2\right] = -2\mathbf{R}_{yx} + 2\mathbf{W}\mathbf{R}_{yy}. \tag{3.10}$$

To obtain the minimum mean square error, the left hand side (L.H.S) of (3.10) is set to zero:

$$-2\mathbf{R}_{yx} + 2\mathbf{W}\mathbf{R}_{yy} = 0 \tag{3.11}$$

Therefore, from (3.11) the optimal weight matrix can be given as

$$\mathbf{W} = \mathbf{R}_{yy}^{-1}\mathbf{R}_{yx} \tag{3.12}$$

$$\mathbf{R}_{yy} = E[\mathbf{y}\mathbf{y}^H] = \mathbf{H}\mathbf{R}_{xx}\mathbf{H}^H + \mathbf{R}_{nn} \tag{3.13}$$

$$\mathbf{R}_{yx} = E[\mathbf{y}\mathbf{x}^H] = \mathbf{R}_{xx}\mathbf{H}^H \tag{3.14}$$

The autocorrelation of the transmitted signal R_{xx} is given by

$$\mathrm{R}_{xx} = E[\mathbf{x}\mathbf{x}^*] \tag{3.15}$$

and the autocorrelation of noise R_{nn} is given by

$$\mathrm{R}_{nn} = E[\mathbf{n}\mathbf{n}^*] \tag{3.16}$$

The SINR and MSE are related to each other by [61-62]

$$\mathrm{SINR} = \frac{1}{\mathrm{MSE}} - 1 \tag{3.17}$$

From the above equation, it is clear that by reducing MSE, the value of SINR increases. Once the MSE is obtained, the SINR can be easily calculated using the above equation. Assuming that

interference-plus-noise component is Gaussian distributed, the symbol error probability (P_e) can be analytically expressed as a function of SINR as

$$P_e = \alpha \mathbf{Q}\left(\sqrt{\beta(\text{SINR})}\right), \tag{3.18}$$

where $\alpha \geq 1$ and $\beta \leq 1$ are real valued parameters that depend on the modulation scheme. In this work, BPSK is selected to be the digital modulation scheme for which $\alpha = \beta = 1$. $Q(\cdot)$ is the one dimensional Q-function defined by

$$\mathbf{Q}(x) = \frac{1}{2\pi}\int_{x}^{\infty} \mathrm{e}^{-\frac{\lambda^2}{2}}\,\mathrm{d}\lambda\ . \tag{3.19}$$

Since, the conventional Q-function has upper limit up to infinity, it makes it computationally difficult to evaluate. To approximate the Symbol Error Probability (SEP), a simple but accurate approximation of the one dimensional Q-function as derived in [63] is used.

$$\mathbf{Q}(x) \cong 0.49 e^{-\frac{8x}{13}} e^{-\frac{x^2}{2}}. \tag{3.20}$$

To verify the tightness of the approximation, a comparison of both the Q-function and its approximation is shown in Fig. 3.2. Using (3.18) and (3.20), P_e is given by

$$\mathrm{P}_e \cong 0.49\alpha e^{-\frac{8(\sqrt{\beta(\text{SINR})})}{13}} e^{-\frac{\beta(\text{SINR})}{2}}. \tag{3.21}$$

The BER can be obtained from SEP by

$$BER = \frac{P_e}{k}, \tag{3.22}$$

where $k=\log_2 M$. M is the constellation size of the modulation scheme.

The BER is bounded by $0 \leq \text{BER} \leq 0.5$, the lower bound cannot be achieved until the channel is noiseless and the upper bound can easily be achieved by choosing a random bit as the estimated bit which means no effective communication. The comparison of approximation of one dimensional Q-function given in (3.20) and Chernoff upper bound is shown in Fig 3.3. From (3.17) to (3.22) it is clear that BER, MSE and SINR are all inter related. Writing the expression for SEP, in terms of MSE, we get:

$$P_e = \alpha \mathbf{Q}\left(\sqrt{\beta\left(\frac{1}{\text{MSE}} - 1\right)}\right) \text{ or } P_e = \alpha \mathbf{Q}\left(\sqrt{\beta\left(\text{MSE}^{-1} - 1\right)}\right). \tag{3.23}$$

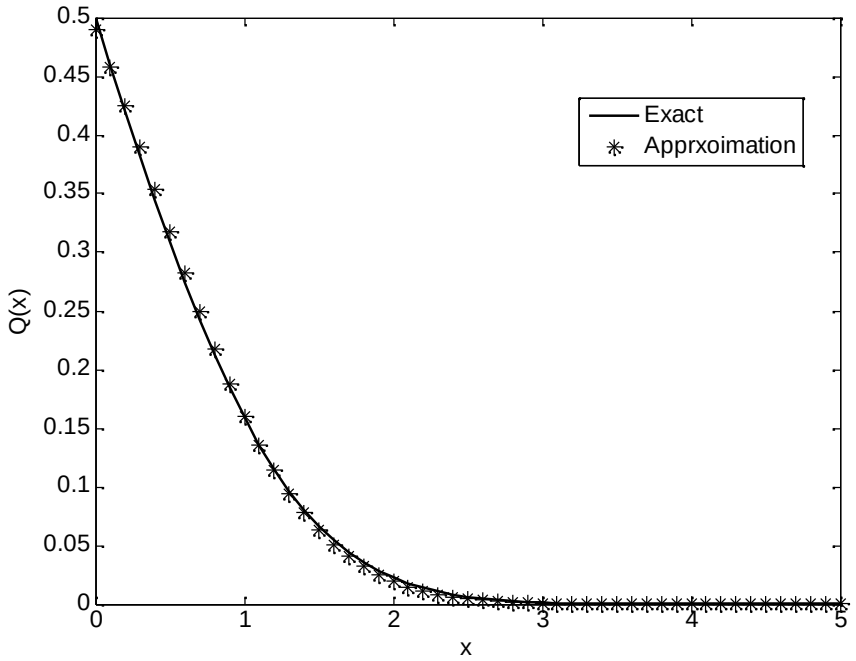

Figure 3.2: Comparison of Exact value of Q(x) versus approximate value

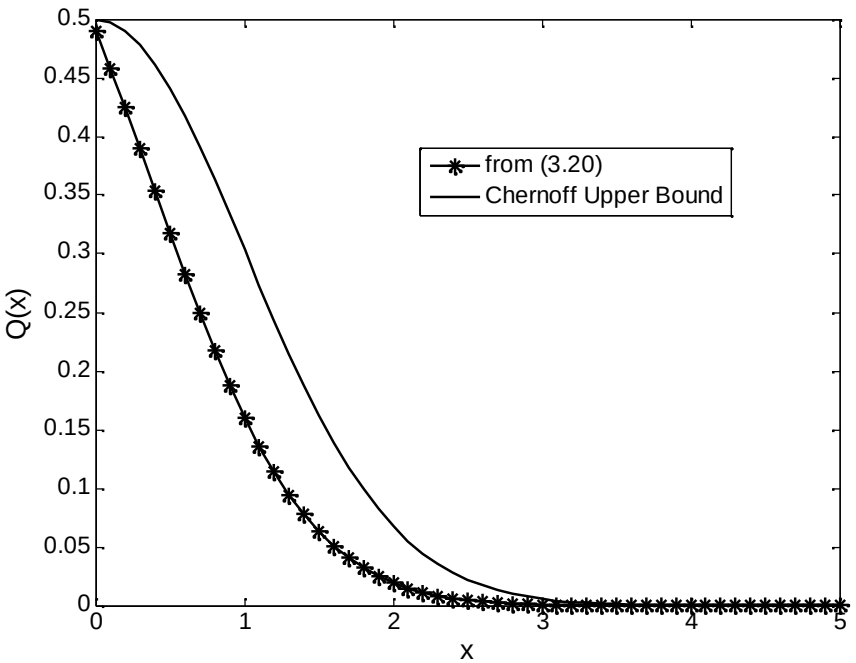

Figure 3.3: Comparison of the Q function approximation in (3.20) with Chernoff bound

Again, using the approximation for the Q-function described above, we get:

$$P_e \cong 0.49\alpha e^{-\frac{8(\sqrt{\beta(MSE^{-1}-1)})}{13}} e^{-\frac{\beta(MSE^{-1}-1)}{2}}. \quad (3.24)$$

By calculating the MSE of the system and putting its value in (3.24), BER can be calculated. To demonstrate the relation between P_e, SINR and MSE, P_e vs. MSE, P_e vs. SINR and MSE vs. SINR are plotted in Fig. 3.4-3.6. From Fig 3.4, it can be seen that BER decreases with a decrease in MSE. The MSE is taken to be from 0.1 to 0.01 in decreasing order. The x-axis (MSE) is linear while the y-axis (BER) is logarithmic. From the graph, it is observed that reducing the MSE is tantamount to reducing the BER of the system. In Fig. 3.5, BER vs. SINR is plotted for increasing values of SINR from 0 to 30 dB. As expected, BER decreases with increase in the SINR.

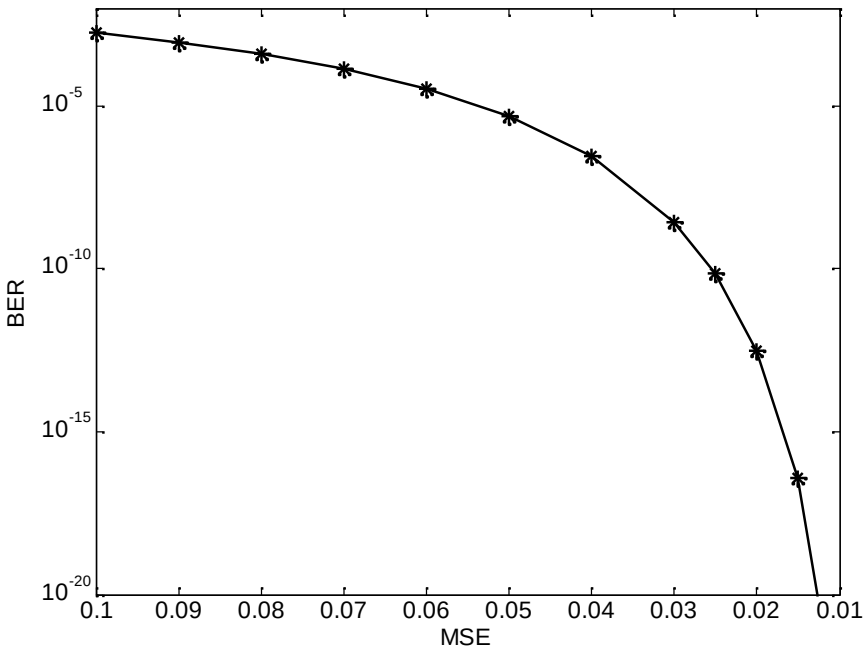

Figure 3.4: Analytical BER vs. MSE plotted using (3.24)

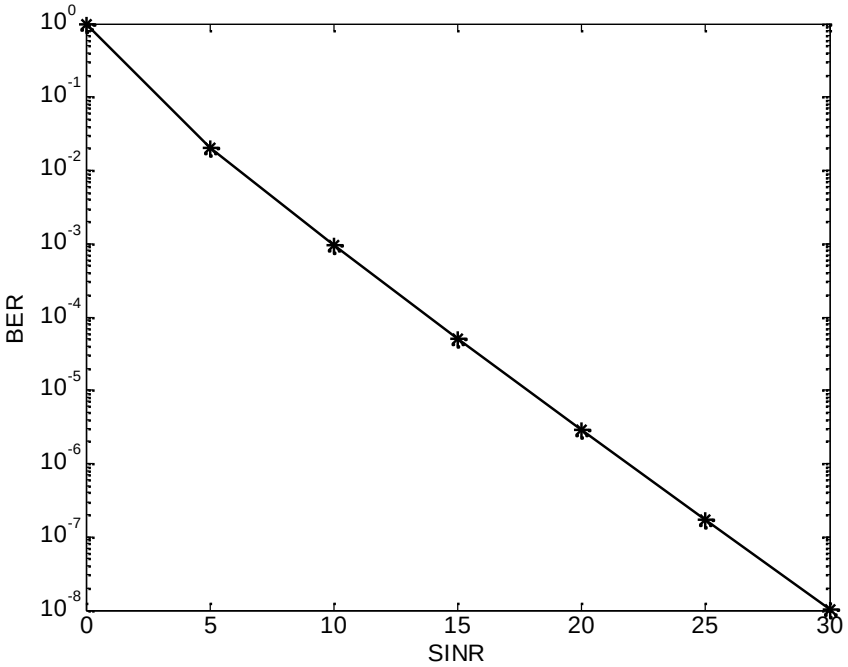

Figure 3.5: Analytical BER vs. SINR plotted using (3.21)

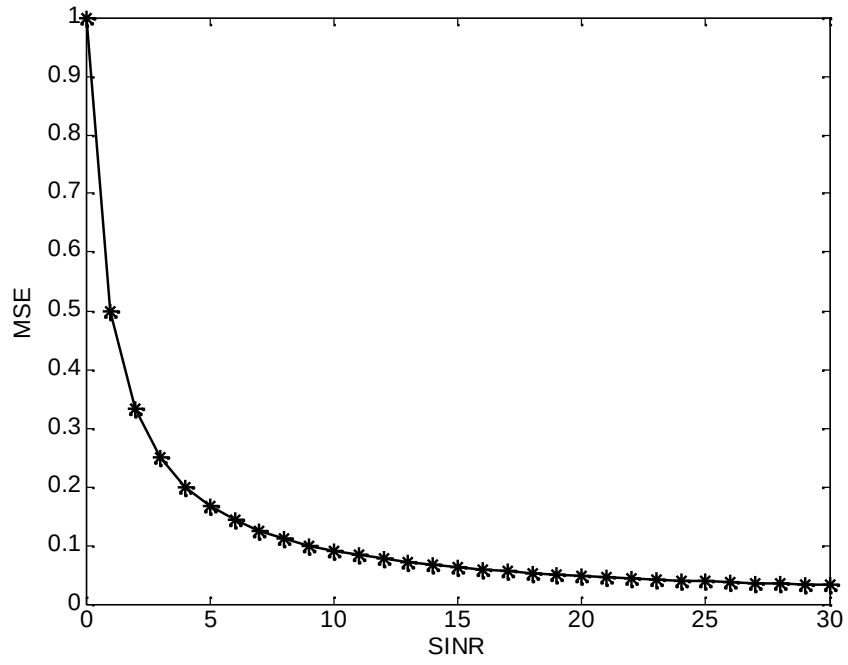

Figure 3.6: MSE vs. SINR plotted using (3.17)

It is clear from the above results that as MSE decreases, P_e decreases and the SINR increases. Therefore, now it can be safely said that any technique which decreases the MSE beyond the MSE of the conventional MMSE receiver will further decrease the BER of the system owing to lesser number of errors at the same SINR.

A novel method of reducing the MSE of a conventional Wiener filter was proposed in [20-21]. In this work, the authors proposed and proved that filtering of the signal in optimum fractional Fourier domain reduces the MSE and BER as compared to the conventional time domain MMSE receiver. The fractional Fourier transform is a method of transforming a time domain signal into fractional Fourier domains [64]. Conventional Fourier transform converts a signal directly to the frequency domain. FRFT enables the transformation of a signal to domains which lie between the time and frequency domains, i.e. fractional Fourier domains. The fractional domains are characterized by a parameter 'a' or the angle of rotation 'α' as shown in Fig. 3.7.

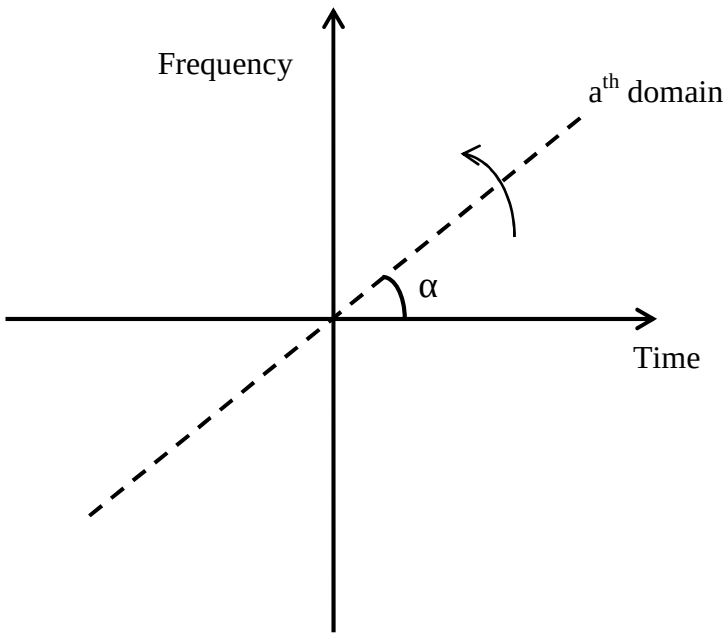

Figure 3.7: A graphical representation of a^{th} fractional Fourier domain

The angle of rotation 'α' and 'a' are related to each other by:

$$\alpha = \frac{a\pi}{2} \tag{3.25}$$

Throughout the thesis, we refer to the fractional domain in terms of 'a'. The domain 'a'=0 corresponds to time domain and 'a'=1 corresponds to frequency domain. The following section gives a brief explanation of the fractional Fourier transform operator and the filtering process.

3.3 Fractional Fourier Transform

Since, the scope of this dissertation is limited to discrete signals, only discrete fractional Fourier transform operator is discussed. Fourier analysis is one of the most frequently used tools in signal processing and many other scientific fields. A while back, a generalization of the Fourier Transform (FT) called fractional Fourier transform was proposed in mathematics literature. Since, it is a generalization of the FT, the FRFT has something to offer in every area in which FT and related concepts are used [65-68]. The FRFT also leads to generalization of notion of time (or space) and frequency domains which are central concepts in the signal processing field. In all the time-frequency representations, a plane with two orthogonal axes corresponding to time and frequency is used. If a signal x(t) is represented along the time axis and its ordinary Fourier transform X(f) is represented along the frequency axis, then the Fourier transform operator (denoted by 'F') can be visualized as a change in the representation of the signal corresponding to a counter clockwise rotation of the signal by an angle $\pi/2$. This is consistent with some of the observed properties of the Fourier transform. For example, two successive rotations of the signal through $\pi/2$ will result in an inversion of the time axis. Moreover, four successive rotations will leave the signal unaltered.

Just like discrete FT can be obtained from continuous FT, the discrete FRFT can also be obtained from continuous FRFT [69-71]. Therefore, we begin the discussion with a brief explanation of continuous FRFT extending it to discrete FRFT later.

3.3.1 Continuous and Discrete Fractional Fourier Transform

The continuous FRFT for a-th order can be defined by using a transformation kernel K_a by

$$\left\{F^a f\right\}(t_a) = \int_{-\infty}^{\infty} K_a(t_a, t) f(t) dt \tag{3.26}$$

$$K_a(t_a, t) = K_\alpha \exp\left(j\pi(t_a^2 \cot\alpha - 2t_a t \csc\alpha + t^2 \cot\alpha)\right), \tag{3.27}$$

where K_α is the transformation kernel given by:

$$K_\alpha = \frac{\exp\left[-j\left(\pi \operatorname{sgn}(\phi)/4 - \phi/2\right)\right]}{\left|\sin(\phi)\right|^{0.5}} \tag{3.28}$$

The spectral expansion of the transformation kernel is given by [73]

$$K_a(t_a, t) = \sum_{k=0}^{\infty} \psi_k(t_a) \exp\left(-j\frac{\pi}{2}ka\right) \psi_k(t) \tag{3.29}$$

where $\psi_k(t)$ represents kth Hermite-Gaussian function and t_a denotes the variable in ath fractional Fourier domain (FFD). In (3.29), $\exp\left(-j\frac{\pi}{2}ka\right)$ denotes the eigenvalues of the FRFT which are defined as eigenvalues of FT $\left(\exp\left(-j\frac{\pi}{2}k\right)\right)$ raised to the power a.

The kth order Hermite-Gaussian function is defined as:

$$\psi_k = \frac{2^{1/4}}{\sqrt{2^k k!}} H_k(\sqrt{2\pi}t) \exp(-\pi t^2), \tag{3.30}$$

where H_k is the kth Hermite polynomial having k real zeros. The differential equation of Hermite Gaussians is defined as:

$$\frac{d^2 f(t)}{dt^2} - 4\pi^2 t^2 f(t) = \lambda f(t) \tag{3.31}$$

The LHS can be expressed in abstract operator notation as:

$$\left(D^2 + FD^2F^{-1}\right) f(t) = \lambda f(t) \tag{3.32}$$

where D is the differentiation operation and F denotes the ordinary FT.

$$\left(D^2 + FD^2F^{-1}\right) = S \tag{3.33}$$

$$Sf(t) = \lambda f(t)$$

If it can be proved that if S commutes with F, then there exists an eigenvector set which is common to both S and F. The same concept can be extended to obtain the discrete FRFT. So, to find the Discrete Fractional Fourier Transform (DFRFT), we use the Eigen decomposition of the transform matrix of the discrete Fourier transform. The N-point Discrete Fourier Transform (DFT) and its inverse are defined as:

$$X(k) = \frac{1}{\sqrt{N}} \sum_{n=0}^{N-1} x(n) e^{-j2\pi \frac{nk}{N}}, \quad k = 0,1,\ldots,N-1, \tag{3.34}$$

$$x(n) = \frac{1}{\sqrt{N}} \sum_{k=0}^{N-1} X(k) e^{j2\pi \frac{nk}{N}}, \quad n = 0,1,\ldots,N-1, \tag{3.35}$$

where $\frac{1}{\sqrt{N}}$ is a normalization factor for making both the DFT and Inverse Discrete Fourier Transform (IDFT) unitary. The discrete Fourier transform can be written in matrix form as:

$$\mathbf{F}_N = \frac{1}{\sqrt{N}} \begin{bmatrix} 1 & 1 & 1 & \cdots & \cdots & 1 \\ 1 & e^{-j\frac{2\pi}{N}1} & e^{-j\frac{2\pi}{N}2} & \cdots & \cdots & e^{-j\frac{2\pi}{N}(N-1)} \\ 1 & e^{-j\frac{2\pi}{N}2} & e^{-j\frac{2\pi}{N}4} & \cdots & \cdots & e^{-j\frac{2\pi}{N}2(N-1)} \\ \vdots & \vdots & \vdots & \ddots & \cdots & \vdots \\ \vdots & \vdots & \vdots & \cdots & \ddots & \vdots \\ 1 & e^{-j\frac{2\pi}{N}(N-1)} & e^{-j\frac{2\pi}{N}(N-1)2} & \cdots & \cdots & e^{-j\frac{2\pi}{N}(N-1)(N-1)} \end{bmatrix} \tag{3.36}$$

It can be seen from (3.36) that $\mathbf{F}_N$ is a symmetric matrix and from matrix theory, it is known that a symmetric matrix is orthogonally diagonalizable. If $\mathbf{F}_N$ is diagonalizable then it can be decomposed as:

$$\mathbf{F}_N = \mathbf{U}\mathbf{R}\mathbf{U}^T, \tag{3.37}$$

where $\mathbf{R}$ is the diagonal matrix consists of eigenvalues of $\mathbf{F}_N$ and $\mathbf{U}$ is the orthogonal matrix. The ordinary DFT has only four distinct eigenvalues given by [71]:

$$\lambda_k = \exp(-j\pi k/2) \in \{1, -1, j, -j\} \tag{3.38}$$

The N-point Discrete Fourier Transform can be written as:

$$\mathbf{X}_\mathbf{F} = \mathbf{F}_N \mathbf{x} \tag{3.39}$$

Since the α^{th} order FRFT shares the same eigenvector set as FT except that the eigenvalues are α^{th} power the eigenvalues of conventional FT, FRFT can be thought of as FT to the power α and is defined as [69]:

$$\mathbf{F}_N^{\alpha} = \mathbf{U}\mathbf{R}^{\alpha}\mathbf{U}^T \tag{3.40}$$

U is again a Hermite-Gaussian function and analogous to the continuous case, it can be defined as the solution of a difference equation as:

$$\tilde{D}^2 f(t) = \frac{f(t+h) - 2f(t) + f(t-h)}{h^2} \tag{3.41}$$

where $\tilde{D}^2$ is the second difference operator which serves an approximation to d^2/dt^2.

$$\tilde{D}^2 = \frac{e^{hD} - 2 + e^{-hD}}{h^2} \tag{3.42}$$

Using (3.33) to calculate $\tilde{S}$, using finite difference analog of FD^2F^{-1} we first calculate $F\tilde{D}^2F^{-1}$ as:

$$F\tilde{D}^2F^{-1} = F\left[\frac{e^{hD} - 2 + e^{-hD}}{h^2}\right]F^{-1} \tag{3.43}$$

Now, we replace D^2 in (3.33) by $\tilde{D}^2$ to obtain an approximation of S denoted by $\tilde{S}$ by:

$$\tilde{S} = D^2 - 4\pi t^2 + \frac{h^2}{12}(D^4 + 16\pi^4 t^4) + O(h^4) \tag{3.44}$$

Writing the analogous difference equation explicitly, we obtain:

$$\tilde{S}f(t) = \lambda f(t), \tag{3.45}$$

$$f(t+h) - 2f(t) + f(t-h) + 2(\cos(2\pi ht) - 1)f(t) = h^2\lambda f(t). \tag{3.46}$$

The difference equation can also be written in matrix form:

$$\mathbf{Sf} = \boldsymbol{\lambda}\mathbf{f}. \tag{3.47}$$

When $h = 1/\sqrt{N}$, the difference equation has periodic coefficients. Therefore, the solution of difference equation is also periodic and can be written as the eigenvectors of the following matrix **S**:

$$\mathbf{S}=\begin{bmatrix} 2 & 1 & 0 & \cdots & 0 & 1 \\ 1 & 2\cos\left(\frac{2\pi}{N}\right) & 1 & \cdots & 0 & 0 \\ 0 & 1 & 2\cos\left(\frac{2\pi}{N}2\right) & \cdots & 0 & 0 \\ \vdots & \vdots & \vdots & \ddots & \vdots & \vdots \\ 0 & 0 & 0 & \cdots & 2\cos\left[\frac{2\pi}{N}(N-2)\right] & 1 \\ 1 & 0 & 0 & \cdots & 1 & 2\cos\left[\frac{2\pi}{N}(N-1)\right] \end{bmatrix}. \quad (3.48)$$

If we let $\omega = 2\pi/N$, we get:

$$\mathbf{S}=\begin{bmatrix} 2 & 1 & 0 & \cdots & 0 & 1 \\ 1 & 2\cos\omega & 1 & \cdots & 0 & 0 \\ 0 & 1 & 2\cos(2\omega) & \cdots & 0 & 0 \\ \vdots & \vdots & \vdots & \ddots & \vdots & \vdots \\ 0 & 0 & 0 & \cdots & 2\cos[(N-2)\omega] & 1 \\ 1 & 0 & 0 & \cdots & 1 & 2\cos[(N-1)\omega] \end{bmatrix}. \quad (3.49)$$

Just as in continuous FRFT, it can be shown that the matrix S commutes with DFT matrix F, i.e. $\mathbf{FS}=\mathbf{SF}$, therefore, there exists a common eigenvector between S and F. As, $\mathbf{S}$ is a real and symmetric matrix, its eigenvectors will be real and orthogonal and the eigenvalues of $\mathbf{F}$ are $\{+1,-1,+j,-j\}$, therefore, eq. (3.40) can be written as:

$$\mathbf{F}_N^{\alpha}=\begin{bmatrix}\mathbf{U}_1 & \mathbf{U}_2 & \mathbf{U}_3 & \mathbf{U}_4\end{bmatrix}\begin{bmatrix} (\mathbf{I}_1)^{\alpha} & 0 & 0 & 0 \\ 0 & (-\mathbf{I}_2)^{\alpha} & 0 & 0 \\ 0 & 0 & (-j\mathbf{I}_3)^{\alpha} & 0 \\ 0 & 0 & 0 & (j\mathbf{I}_4)^{\alpha} \end{bmatrix}\begin{bmatrix}\mathbf{U}_1^{T} \\ \mathbf{U}_2^{T} \\ \mathbf{U}_3^{T} \\ \mathbf{U}_4^{T}\end{bmatrix}, \quad (3.50)$$

where α is the order of discrete Fractional Fourier Transform and U_i are given by

1. $\mathbf{U}_1$ is constructed by the eigenvectors $\mathbf{v}$ of matrix $\mathbf{S}$ which satisfy $\mathbf{Fv} = \mathbf{v}$
2. $\mathbf{U}_2$ is constructed by the eigenvectors $\mathbf{v}$ of matrix $\mathbf{S}$ which satisfy $\mathbf{Fv} = -\mathbf{v}$
3. $\mathbf{U}_3$ is constructed by the eigenvectors $\mathbf{v}$ of matrix $\mathbf{S}$ which satisfy $\mathbf{Fv} = -j\mathbf{v}$
4. $\mathbf{U}_4$ is constructed by the eigenvectors $\mathbf{v}$ of matrix $\mathbf{S}$ which satisfy $\mathbf{Fv} = j\mathbf{v}$

Finally, the $\mathbf{F}_N^{\alpha}$ matrix is obtained which is the DFRFT matrix. The rest of the process for transforming the signal to the fractional domain is similar to the ordinary DFT process. Since DFRFT is a generalization of DFT, it can be used in all applications where DFT is used.

3.3.2 Filtering in Fractional Fourier Domains

In the previous section, Wiener filtering process in time domain was discussed and it was suggested that the performance of Wiener filtering can be improved if this filtering can be improved by filtering in fractional Fourier domain. In the following section, we discuss the fractional Wiener filtering and the reason why lower MSE can be obtained by filtering in the fractional domains. The weight vector given by eq. (3.12) is calculated in the ath domain by:

$$\mathbf{W}_a = \boldsymbol{R}_{\mathrm{y_a y_a}}^{-1} \boldsymbol{R}_{\mathrm{y_a x_a}}, \tag{3.51}$$

where $\boldsymbol{R}_{\mathrm{y_a y_a}}$ is the autocorrelation in the ath domain and $\mathbf{R}_{\mathrm{y_a x_a}}$ is the cross correlation in the ath domain.

$$\boldsymbol{R}_{\mathrm{y}_a\mathrm{x}_a} = F^a(\mathbf{R}_{\mathrm{xx}}\mathbf{H}^H)F^{-a} = \mathbf{R}_{\mathrm{x_a x_a}}\mathbf{H}_a^H \tag{3.52}$$

$$\boldsymbol{R}_{\mathrm{y}_a\mathrm{y}_a} = F^a\left(\mathbf{H}\mathbf{R}_{\mathrm{xx}}\mathbf{H}^H + \mathbf{R}_{\mathrm{nn}}\right)F^{-a} = \mathbf{H}_a\mathbf{R}_{\mathrm{x_a x_a}}\mathbf{H}_a^H + \mathbf{R}_{\mathrm{n_a n_a}} \tag{3.53}$$

where F^a and F^{-a} are used to describe the ath order fractional Fourier transform and ath order Inverse Fractional Fourier Transform (IFRFT) respectively. The estimated signal is obtained from the received signal **y** and weight matrix $\mathbf{W}_a$ by:

$$\hat{\mathbf{x}} = F^{-a}\mathbf{W}_a^H F^a \mathbf{y} \tag{3.54}$$

The MSE according to the weight vector in the a^{th} domain is given by:

$$\mathrm{MSE}(\mathbf{W}_a) = E\left\{\left\|\mathbf{x} - F^{-a}\mathbf{W}_a^H F^a \mathbf{y}\right\|^2\right\} \tag{3.55}$$

In general, the optimum domain cannot be found analytically. Therefore, to find the optimum domain, the MSE is calculated for discrete values of 'a' between (-1, 1) for a given step size. The domain in which the MSE is lowest is considered to be the optimum domain. If a more accurate fractional domain is required, then we can simply increase the step size to 0.01. However, this method of increasing the accuracy increases the computational complexity immensely. An alternate method of improving the accuracy is to find the optimum domain with a step size of 0.1 first and then run the experiment again around the optimum domain with a smaller step size. By using this method, the accuracy can be improved with a little increase in computational complexity. However, till date no method has been discovered to find the optimum domain analytically.

To understand why the fractional domain filtering results in lower MSE, let us consider a simple example. In this example, the Wigner distribution of the desired signal and the distortion is taken and plotted on the same graph as shown in Fig. 3.8-3.10. Fig. 3.8 shows the time domain ('a'=0) filtering process where the filtering is done along the xx' line. It is clear that after filtering, some distortion (the one to the left of the xx' line) still overlaps with the desired signal thereby resulting in high MSE. Similarly, the case for frequency domain ('a'=1) filtering is shown in Fig. 3.9 where the filtering is done along yy' line. In this case also the distortion is not completely filtered and some of it overlaps with the signal. In the case of optimum domain filtering as shown in Fig. 3.10, an attempt is made to find the domain in which there is minimum distortion. When the filtering is done along the zz' line, the distortion is completely separated from the signal, therefore, the errors in this domain will be the minimum. This domain is known as the optimum domain ('a'=a_{opt}) and the process is called optimum fractional domain filtering.

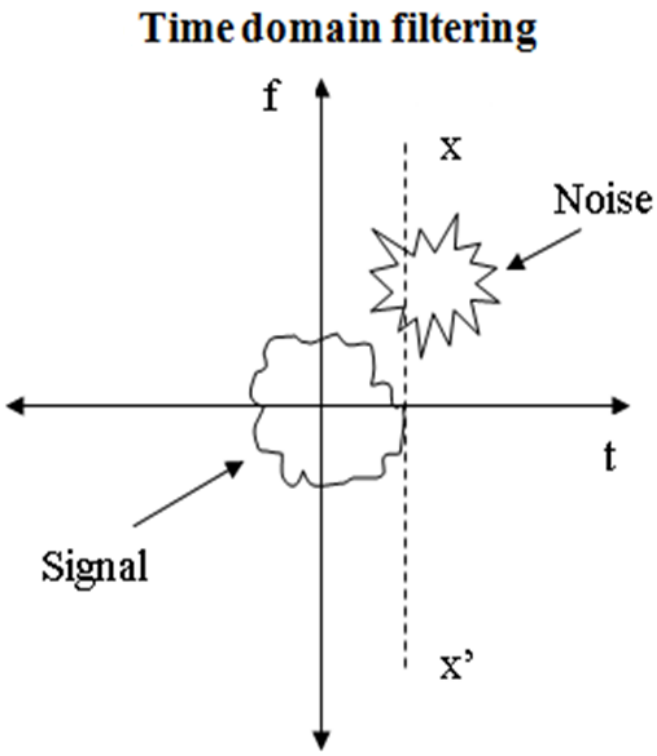

Figure 3.8: Filtering of signal in the time domain

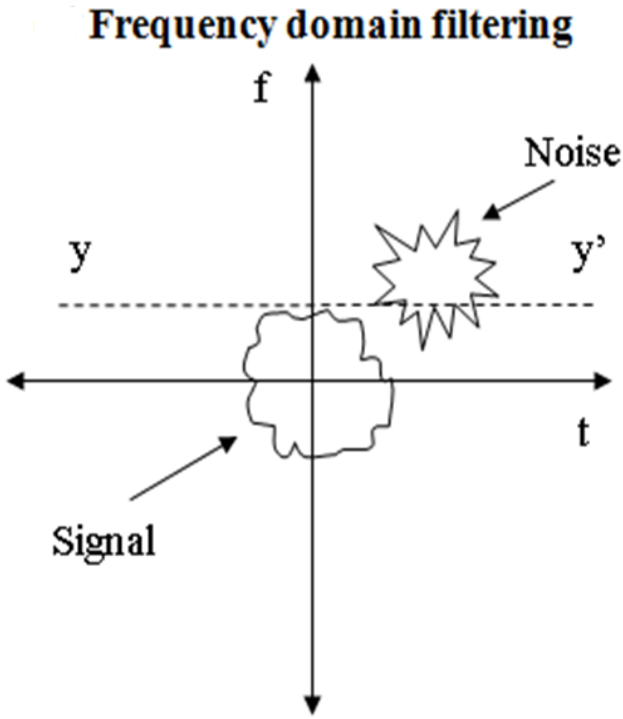

Figure 3.9: Filtering of signal in the frequency domain

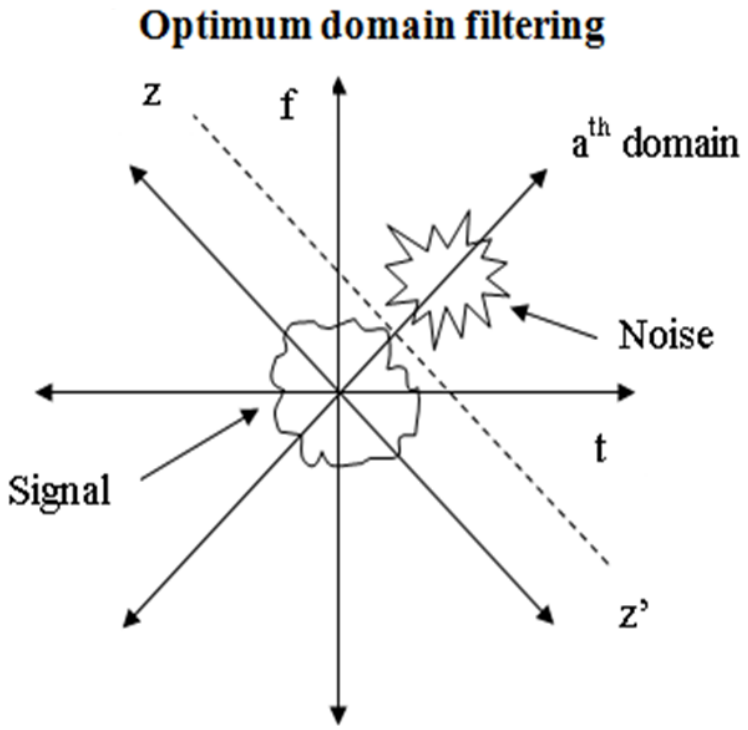

Figure 3.10: Filtering of signal in the optimum domain

3.4 Optimum Linear Receiver for Multiple Antenna Systems

Let us first consider the case when there is one transmit antenna (N_T=1) and multiple receive antennas (N_R=2, 4, 8). As discussed earlier in chapter 2, receive diversity is achieved when there is a single antenna at the transmitter and multiple antennas at the receiver and the fading channel is uncorrelated. This helps in improving the link reliability because the probability that all the channels will be in a deep fade at the same time is small. At the receiver, replicas of the transmitted signal with different distortions are obtained and processed to get the desired information. This process is known as diversity combining. To obtain the best results, different diversity techniques to process the distorted replicas of the transmitted signal have been proposed along the years. All the diversity techniques have been discussed previously in chapter 1. In this work, we consider the reception scheme based on Wiener filtering which when used with receive diversity acts as an optimum combiner [18]. Optimum combining uses the MSE criteria for the calculation of weights of the respective received signals on different branches to maximize the SINR. Shah et al. showed that in an interference dominated environment, this technique performs better than MRC and is very effective even when the number of interferers

exceeds the number of receive antennas [75]. Below we present the system model and the fractional optimum combining technique.

$$\mathbf{y} = \mathbf{hx} + \mathbf{n} \tag{3.56}$$

where **y** is the received signal, **h** is the fading channel whose envelope is characterized by Rayleigh distribution.

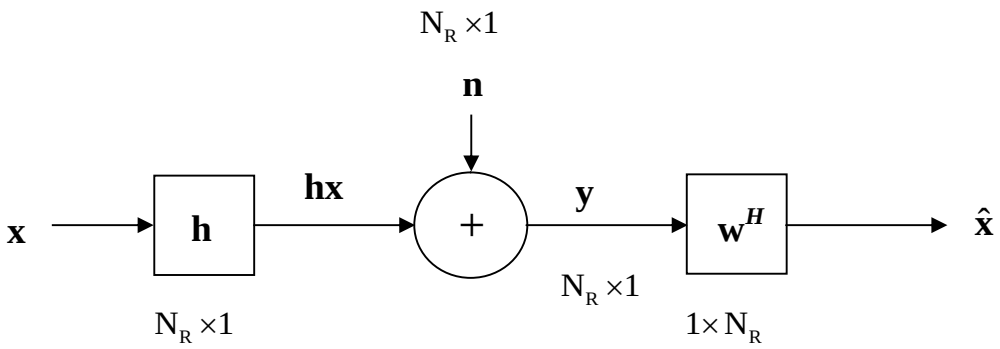

Figure 3.11: System model for optimum combining technique

Let us recall the definition of the optimal weight matrix **W** from eq. (3.5):

$$\mathbf{W} = \begin{bmatrix} w_{11} & w_{12} & w_{13} & \cdots & w_{1N_T} \\ w_{21} & w_{22} & w_{23} & \cdots & w_{2N_T} \\ w_{31} & w_{32} & w_{33} & \cdots & w_{3N_T} \\ \vdots & \vdots & \vdots & \ddots & \vdots \\ w_{N_R 1} & w_{N_R 2} & w_{N_R 3} & \cdots & w_{N_R N_T} \end{bmatrix}$$

Now, the number of transmit antennas in this case is one. Therefore, the optimal weight matrix reduces to a vector given by:

$$\mathbf{w} = \begin{bmatrix} w_{11} \\ w_{12} \\ w_{13} \\ \vdots \\ w_{N_R 1} \end{bmatrix} \tag{3.57}$$

To find the optimal weight vector in the optimum fractional domain, we use the autocorrelation and cross-correlation functions given above:

$$\boldsymbol{r}_{y_a x_a} = F^a(\mathbf{R}_{xx}\mathbf{H}^H)F^{-a} = \mathbf{R}_{x_a x_a}\mathbf{H}_a^H \tag{3.58}$$

$$\boldsymbol{R}_{y_a y_a} = F^a\left(\mathbf{H}\mathbf{R}_{xx}\mathbf{H}^H + \mathbf{R}_{nn}\right)F^{-a} = \mathbf{H}_a\mathbf{R}_{x_a x_a}\mathbf{H}_a^H + \mathbf{R}_{n_a n_a} \tag{3.59}$$

$$\hat{\boldsymbol{x}} = \boldsymbol{F}^{-a}\left\{\boldsymbol{w}^H\left(\boldsymbol{F}^a\{\boldsymbol{y}\}\right)\right\} \tag{3.60}$$

Above equations describe the complete combining process at the receiver. First, the received signal is transformed to the ath domain, then the weights are calculated in that domain and finally the estimated signal is transformed back to time domain. The minimum mean squared error is obtained in the optimum domain and is given by:

$$\text{MMSE}(\boldsymbol{w}_{opt}) = E\left\{\left\|\boldsymbol{x} - \boldsymbol{F}^{-aopt}\boldsymbol{w}^H\boldsymbol{F}^{aopt}\boldsymbol{y}\right\|^2\right\} \tag{3.61}$$

3.4.1 Simulation Details

In this section, the performance of optimum combining diversity technique for N_R=2, N_R=4 and N_R=8 in time and frequency domains has been compared with the proposed fractional domain optimum combining technique. The fading is taken to be Rayleigh distributed and it is assumed that the fading is uncorrelated and comprises of independent and identically distributed Gaussian random variables with CN **(0, 1)**. The modulation is assumed to be Quadrature Phase Shift Keying (QPSK). The transmission is done in the form of blocks of bits and the block length is taken to be 100. The value of the fractional domain parameter 'a' is varied from -1 to +1 with a step size of 0.1. For each value of 'a', total number of 10000 independent realizations of faded signal plus noise are considered. The value of 'a' which gives the minimum mean squared error is considered to be the optimum domain (*aopt*) for signal processing.

3.4.2 Results and Discussion

In the previous section, we discussed a method for the fractional implementation of the optimum combining diversity technique using the fractional Fourier transform. It was stated that this technique performs better than the conve

In this section, the results are presented in the terms of BER vs. SNR, MSE vs. SNR and block error rate (BLER) vs. SNR. Fig. 3.12 shows the MSE vs. SNR performance of time domain (red line), frequency domain (dotted green line) and proposed combiner (dashed blue line) for 2 receive antennas. It can be seen that the proposed combiner gives lowest MSE at all SNRs as compared to its time domain and frequency domain counterparts. Fig. 3.13 and 3.14 show similar results for 4 and 8 receive antennas. Again the proposed combiner outperforms the two existing combiners in terms of MSE.

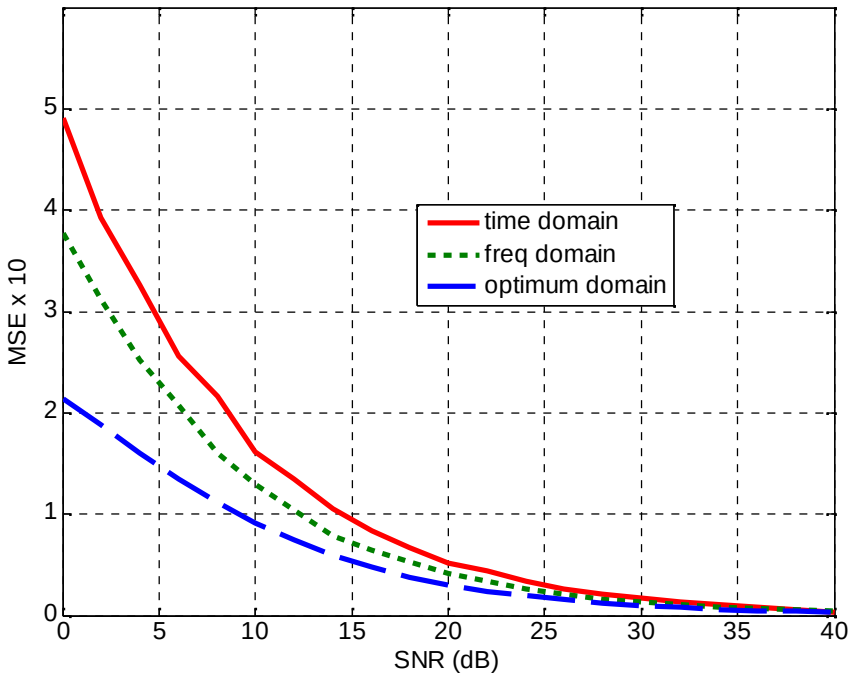

Figure 3.12: MSE vs. SNR comparison of different combiners in Rayleigh fading for N_R=2

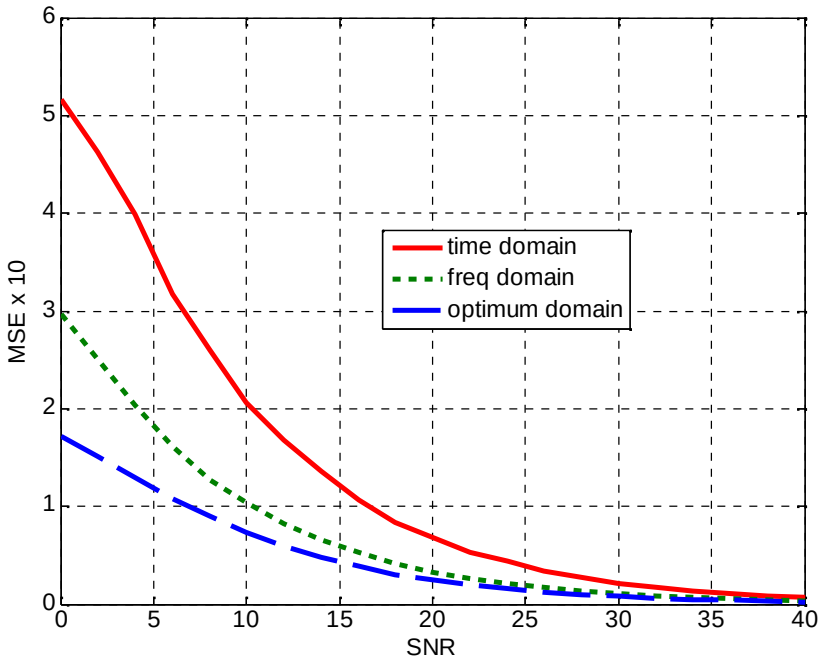

Figure 3.13: MSE vs. SNR comparison of different combiners in Rayleigh fading for N_R=4

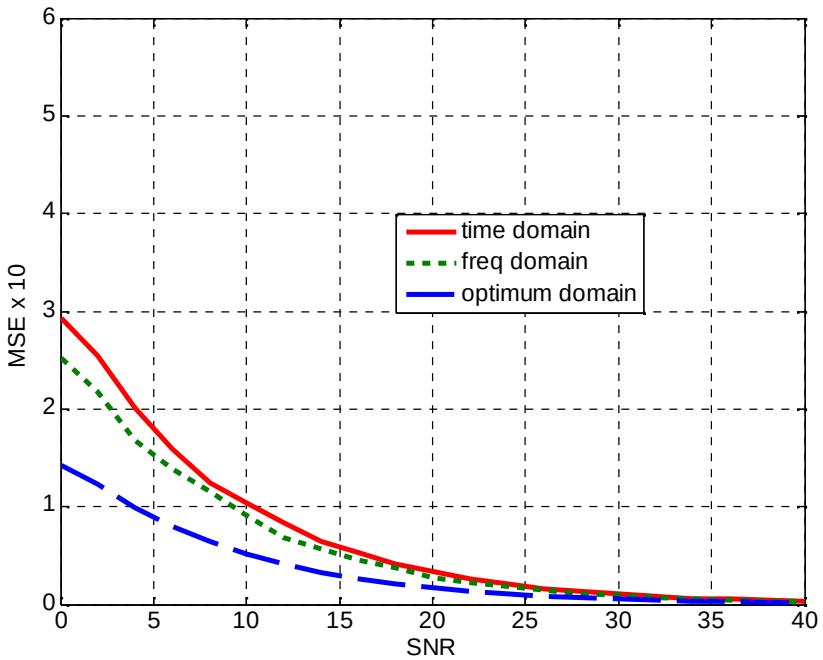

Figure 3.14: MSE vs. SNR comparison of different combiners in Rayleigh fading for N_R=8

Fig. 3.15 shows the BER vs. SNR performance of the three combiners for 2 receive antennas. It can be clearly seen that there is a significant improvement in performance of proposed combiner in optimum domain at all SNRs. For a BER of 10^{-2} the proposed combiner gives an improvement of 7.2 dB and 2.4 dB over time and frequency domain combiners respectively. Fig. 3.16 and 3.17 show the performance of proposed combiner with 4 and 8 receive antennas respectively. Table 1 summarizes the SNR improvement in performance of that the proposed combiner for all the three cases of 2, 4 and 8 antennas at a BER of 10^{-2}.

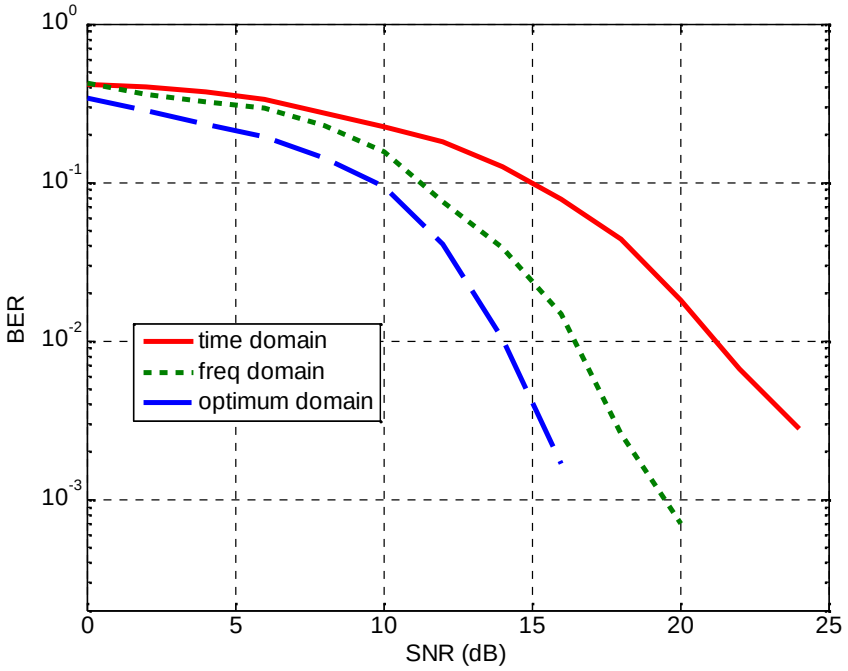

Figure 3.15: BER vs. SNR comparison of different combiners in Rayleigh fading for N_R=2

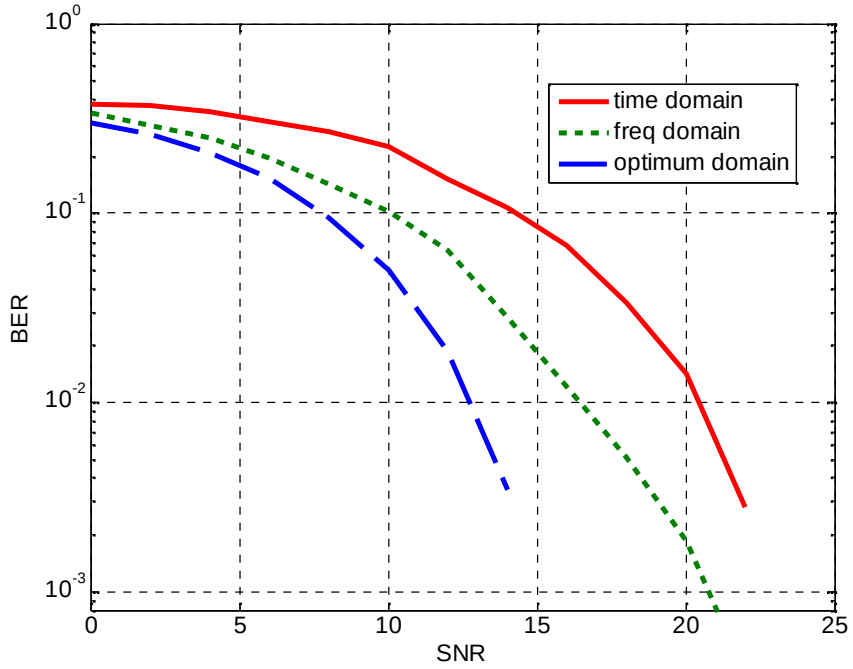

Figure 3.16: BER vs. SNR comparison of different combiners in Rayleigh fading for N_R=4

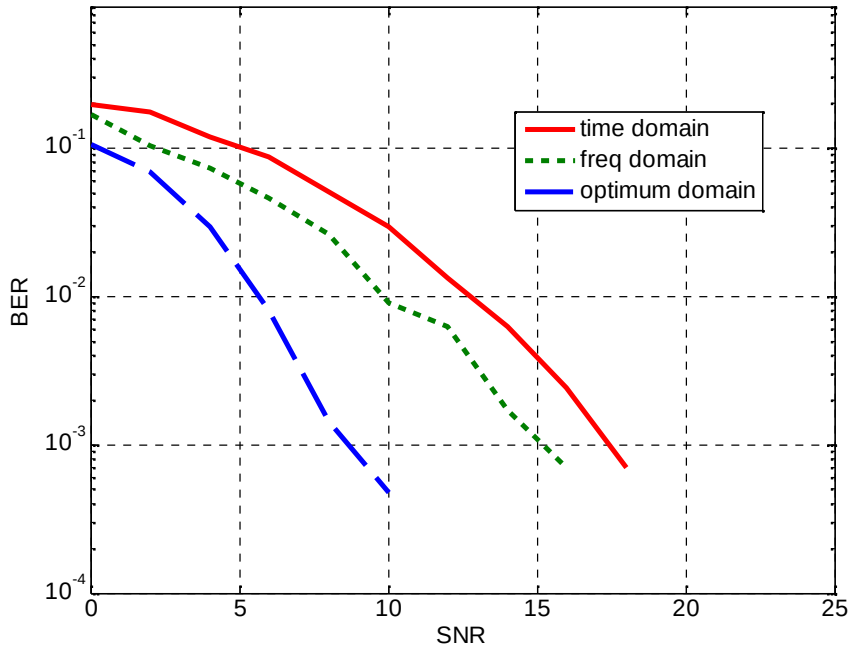

Figure 3.17: BER vs. SNR comparison of different combiners in Rayleigh fading for N_R=8

Table 3.1: SNR improvement of fractional optimum combiner over the time and freq. domain combiners for a BER of 10^{-2}

N_T, N_R	At a BER of 10^{-2}, SNR improvement of optimum domain combiner over	
	time domain combiner	freq. domain combiner
1,2	7.2 dB	2.4 dB
1,4	7.5 dB	3.4 dB
1,8	7.3 dB	4.3 dB

Table 3.1 shows the SNR improvement of the proposed receiver over the time and freq domain receivers for a fixed BER of 10^{-2} and N_R=2, 4 and 8. For 2 receive antennas, the proposed receiver requires 7.2 dB less SNR than the time domain receiver and 2.4 dB less SNR than the frequency domain receiver to achieve BER of 10^{-2}. Similar results are observed for N_R=4 and 8. It is also clear that as the number of receiver antennas increases, the BER of all the three receivers decreases due to increase in receive diversity.

The following Fig. 3.18, 3.19 and 3.20 show the BER vs. normalized MSE performance of the time domain, frequency domain and proposed combiner for 2, 4 and 8 receive antennas respectively. The MSE has to be normalized so that the values of all the three receivers are comparable. For any given value of normalized MSE, the proposed combiner gives the lowest BER which means that the performance optimum combiner is better even when the normalized MSE value is same for all the three combiners. Also, it can be seen that with the increase in the number of receive antennas, the BER at a fixed value of normalized MSE decreases due to increase in the receive diversity.

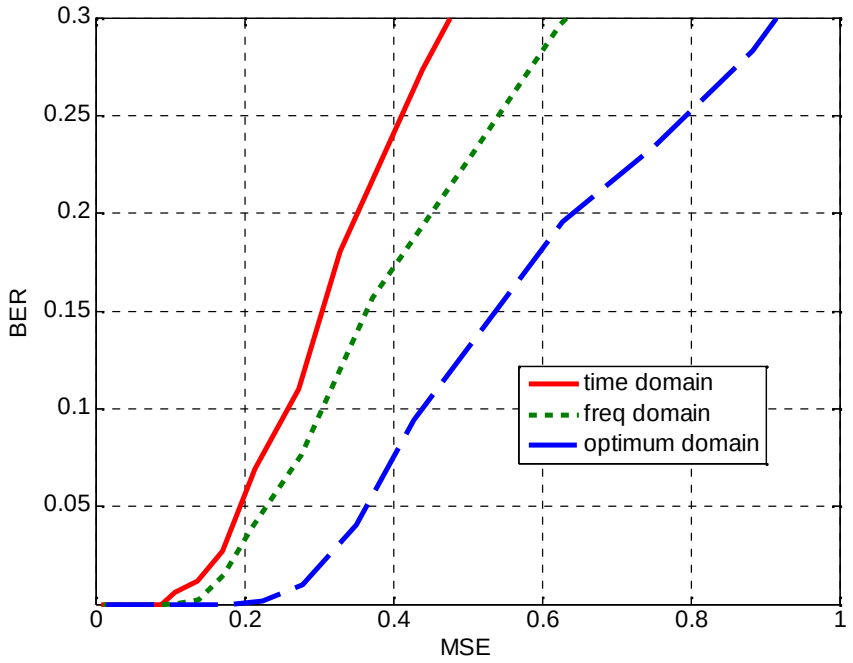

Figure 3.18: BER vs. normalized MSE for different combiners in Rayleigh fading for N_R=2

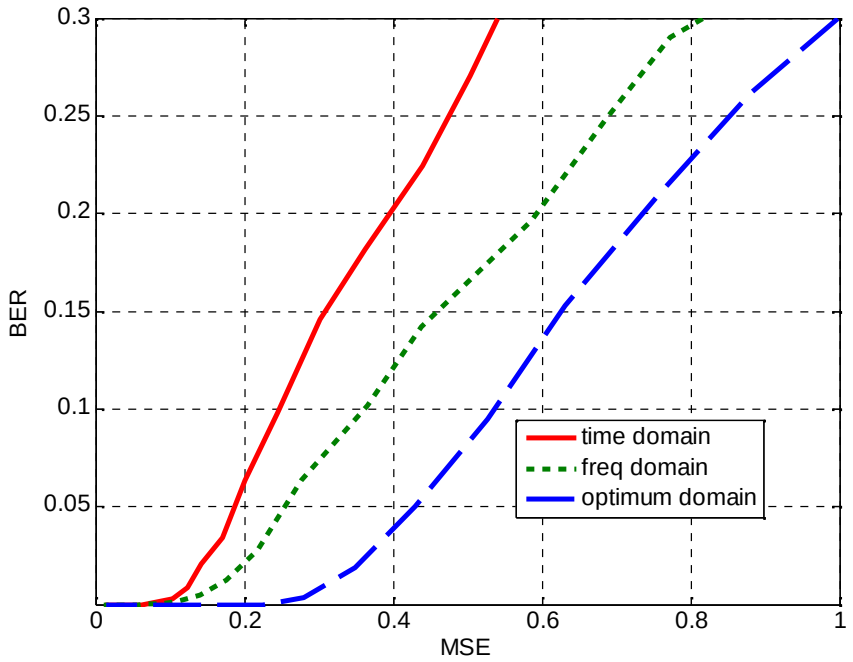

Figure 3.19: BER vs. normalized MSE for different combiners in Rayleigh fading for N_R=4

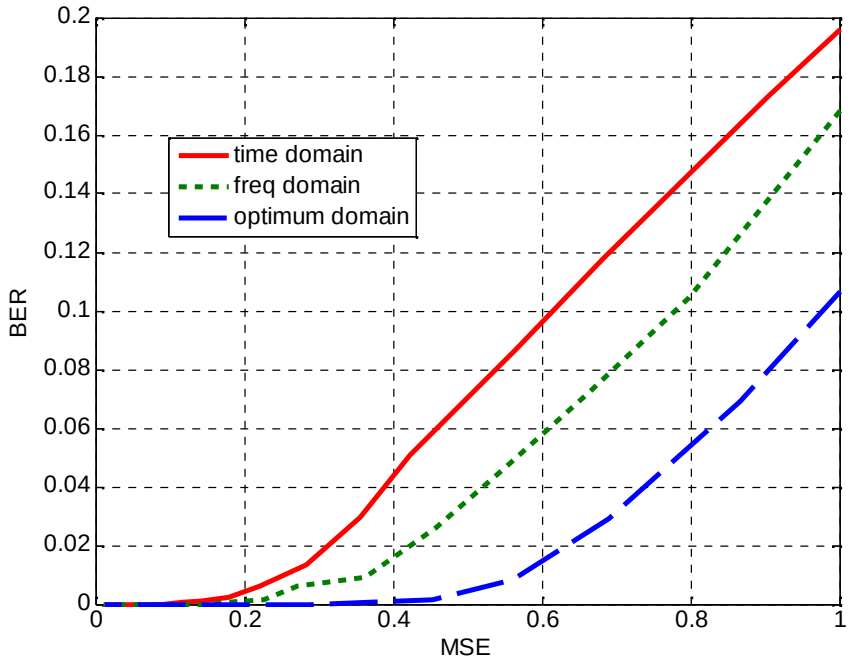

Figure 3.20: BER vs. normalized MSE for different combiners in Rayleigh fading for N_R=8

Table 3.2 shows the performance comparison of BER of the three receivers for a fixed normalized MSE of 0.5 for 2, 4 and 8 receive antennas. It can be seen that for the same MSE, the proposed receive has the lowest BER whereas the time domain receiver has the highest BER.

Table 3.2: BER performance for a normalized MSE of 0.5

N_T, N_R	Time domain	Freq domain	Optimum domain
1,2	0.3324	0.231	0.137
1,4	0.269	0.161	0.078
1,8	0.07	0.036	0.004

3.5 Optimum Linear Receiver for MIMO Systems in Correlated Channels

In line with the previous section, we now consider multiple antennas at both transmitter and receiver, i.e. the performance of fractional MMSE receiver in MIMO systems. When there is a single antenna at the transmitter and multiple antennas at the receiver, the weight matrix reduces to a vector, however, with multiple antennas on both ends; the weight matrix is given by (3.51) and the weights are calculated by using the following equation:

$$\mathbf{W}_a = \mathbf{R}_{\mathrm{y_a y_a}}^{-1} \mathbf{R}_{\mathrm{y_a x_a}},$$

$$\boldsymbol{R}_{\mathrm{y}_a \mathrm{x}_a} = F^a(\mathbf{R}_{\mathrm{xx}}\mathbf{H}^H)F^{-a} = \mathbf{R}_{\mathrm{x_a x_a}}\mathbf{H}_a^H$$

$$\boldsymbol{R}_{\mathrm{y}_a \mathrm{y}_a} = F^a\left(\mathbf{H}\mathbf{R}_{\mathrm{xx}}\mathbf{H}^H + \mathbf{R}_{\mathrm{nn}}\right)F^{-a} = \mathbf{H}_a\mathbf{R}_{\mathrm{x_a x_a}}\mathbf{H}_a^H + \mathbf{R}_{\mathrm{n_a n_a}}$$

After calculating the weight matrix in the ath domain, the estimated received signal is given by

$\hat{\mathbf{x}} = F^{-a}\mathbf{W}_a^H F^a \mathbf{y}$.

The MSE in the ath domain is calculated using (3.55) as

$$\mathrm{MSE}(\mathbf{W}_a) = E\left\{\left\|\mathbf{x} - F^{-a}\mathbf{W}_a^H F^a \mathbf{y}\right\|^2\right\}.$$

The MSE is calculated for closely spaced discrete values of 'a' $\in (-1, +1)$ with a step size of 0.1. The domain in which MSE is minimum is then selected as the optimum domain (a_{opt}). The MSE in the optimum domain is given as:

$$\mathrm{MMSE}(\mathbf{W}_{opt}) = E\left\{\left\|\mathbf{x} - F^{-a}\mathbf{W}_{opt}^H F^a \mathbf{y}\right\|^2\right\}$$

From the above equations, it is seen that the optimum domain receiver outperforms the time and frequency domain receivers in terms of MSE. It was discussed earlier that as MSE reduces, the BER reduces too; therefore, reducing the MSE is equivalent to reducing the BER. In the following sections, the performance assessment of the proposed receiver is done in correlated and uncorrelated wireless environment.

3.5.1 Simulation Details

Performance of the proposed fractional MMSE receiver is compared with time and frequency domain MMSE receivers for MIMO systems. A stream of 100,000 random bits (0, 1) is generated. After generation, the bit stream is modulated using BPSK modulation $(0 \to -1,\ 1 \to +1)$. Two fading channels are considered for simulations, i.e. Rayleigh and Rician fading (described previously in sections 2.2.1 and 2.2.2). The noise vector (**n)** is considered to have zero mean uncorrelated Gaussian distributed random variables with variance σ_n^2. Inadequate antenna spacing in wireless devices leads to spatial correlation. The process of generating spatially correlated fading channels was discussed in section 2.3. For the sake of simplicity the single coefficient correlation model assumes the transmit (r_{TX}) and receive correlation (r_{RX}) to be equal and represented by *r*. In this work we consider transmission through four levels of

correlation, i.e. no correlation $(r = 0)$, low correlation $(r = 0.2)$, medium correlation $(r = 0.5)$ and high correlation $(r = 0.8)$. In practical wireless systems, the inadequate antenna spacing constraint might be present only at one end (transmitter or receiver), therefore, the case of spatial correlation at only one end (transmitter/receiver) is also considered. No channel estimation is used and CSIR is assumed to be perfectly known. All simulations as well as analytical calculations have been performed using MATLAB.

3.5.2 Performance Comparison

In this section the error rate performance of the proposed receiver is compared with its time and frequency domain counterparts in uncorrelated and correlated fading environments. It is already known from the analysis in literature that spatial correlation degrades the BER of wireless systems significantly [76-79]. In the following section, the effect of spatial correlation on the BER of time, frequency and optimum domain MMSE receivers is considered.

Fig. 3.21 shows the comparison of simulated BER vs. SNR for the three receivers in uncorrelated frequency flat Rayleigh fading for N_T=N_R=2. The solid red line represents the time domain MMSE, the dotted green line represents the freq domain MMSE and the dashed blue line represents the fractional MMSE receiver. It can be seen that the proposed receiver (dashed blue line) has the lowest BER out of all the three receivers. Fig. 3.22-3.24 show similar results as Fig. 3.21 but with spatial correlation coefficient $r_{TX} = r_{RX} = r$ of 0.2, 0.5 and 0.8 respectively. As discussed earlier, spatial correlation deteriorates the performance of the system by reducing the advantage of independent propagation paths for signals between different sets of antennas, thereby reducing the capacity. It can be observed from Fig. (3.22-3.24) that with increase in spatial correlation, the BER of all the receivers reduces considerably but the proposed receiver outperforms the other two in all the three cases.

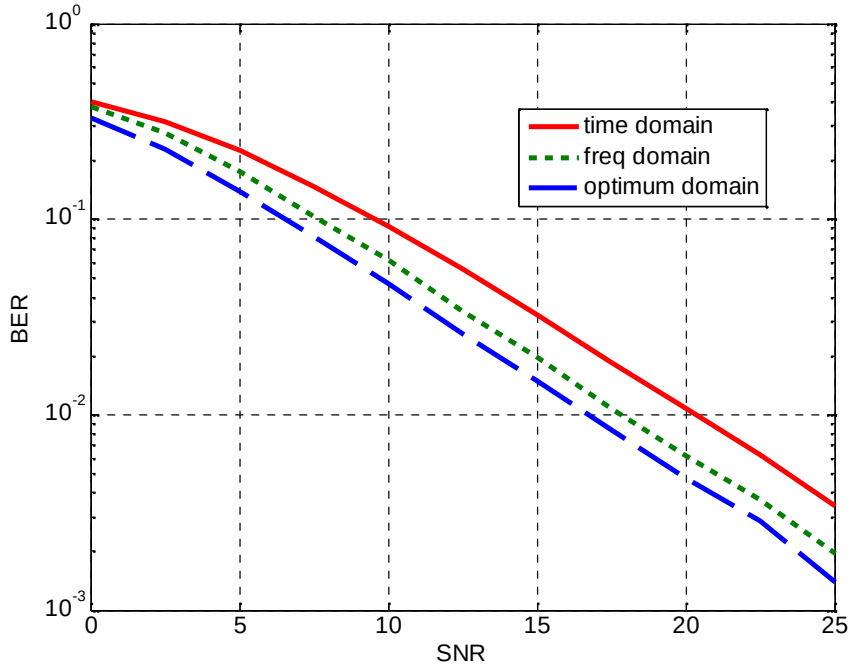

Figure 3.21: Comparison of BER of FRFT domain MMSE receiver with time and frequency domain MMSE receiver for N_T=N_R=2 in uncorrelated Rayleigh fading channel.

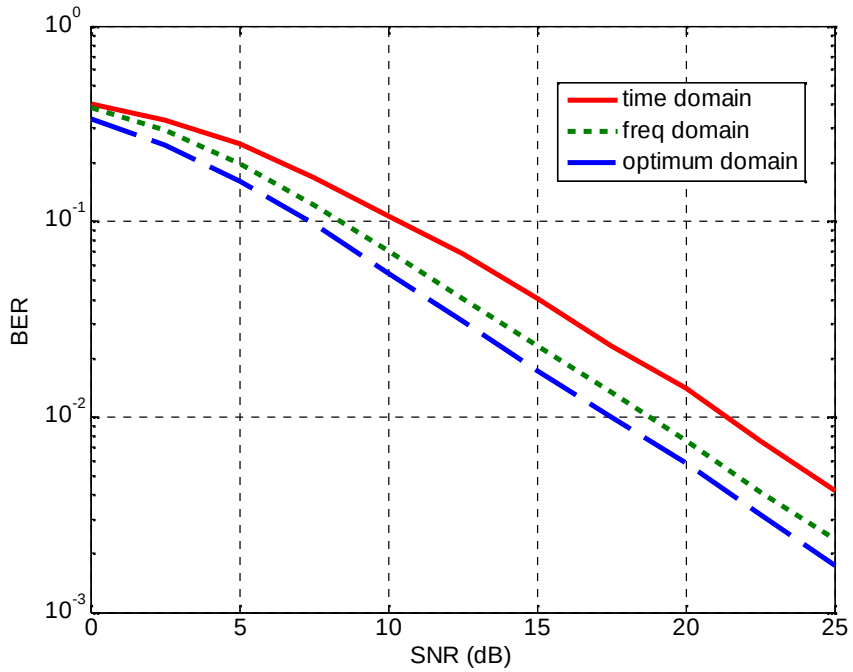

Figure 3.22: Comparison of BER of FRFT domain MMSE receiver with time and frequency domain MMSE receiver for N_T=N_R=2 in correlated Rayleigh fading channel with rtx=rrx=0.2

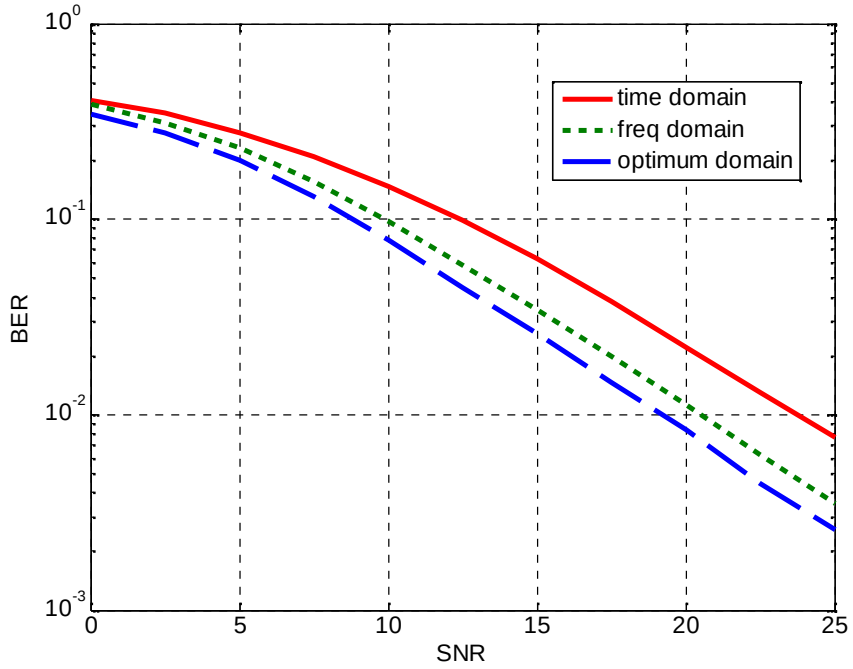

Figure 3.23: Comparison of BER of FRFT domain MMSE receiver with time and frequency domain MMSE receiver for $N_T=N_R=2$ in correlated Rayleigh fading channel with rtx=rrx=0.5

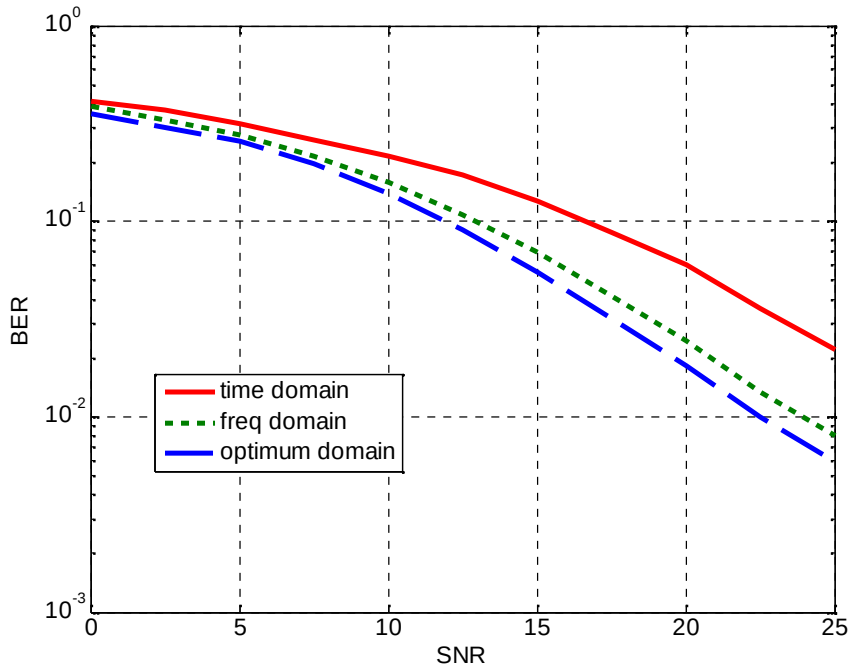

Figure 3.24: Comparison of BER of FRFT domain MMSE receiver with time and frequency domain MMSE receiver for $N_T=N_R=2$ in correlated Rayleigh fading channel with rtx=rrx=0.8

Table 3.3 summarizes the results shown in Fig. 3.21-24 giving the SNR required to achieve a fixed BER by all the three receivers for four different levels of spatial correlation. It is clear that the proposed receiver requires the least SNR to achieve a fixed BER. The table also shows the amount SNR improvement (in dB) of the proposed receiver over the other two receivers.

Table 3.3: SNR improvement of proposed MMSE receiver over the time and frequency domain MMSE receivers for a fixed BER and $N_T=N_R=2$

Spatial Correlation/BER	Time domain (dB)	Freq domain (dB)	Optimum domain (dB)	SNR Advantage over Time domain MMSE	SNR Advantage over Freq domain MMSE
$0/10^{-2}$	20.34	17.872	16.74	3.6 dB	1.132 dB
$0.2/10^{-2}$	21.35	18.78	17.48	3.87 dB	1.3 dB
$0.5/10^{-2}$	23.74	20.5	19.21	4.53 dB	1.29 dB
$0.8/10^{-1.5}$	23.14	18.8	17.53	5.61 dB	1.27 dB

In line with the previous simulation results, Fig. 3.25-3.28 show the results for a $N_T=N_R=4$ system. According to the theory, the capacity of MIMO systems increases linearly when there is no spatial correlation. Spatial correlation has the effect of limiting the capacity that can be achieved by MIMO systems due to nullifying the effect of rich scattering in the channel and cancelling out independent channels between different sets of antennas. Therefore, in the following results, the deterioration of BER of a 4×4 system with increase in spatial correlation is much more as compared to a 2×2 system.

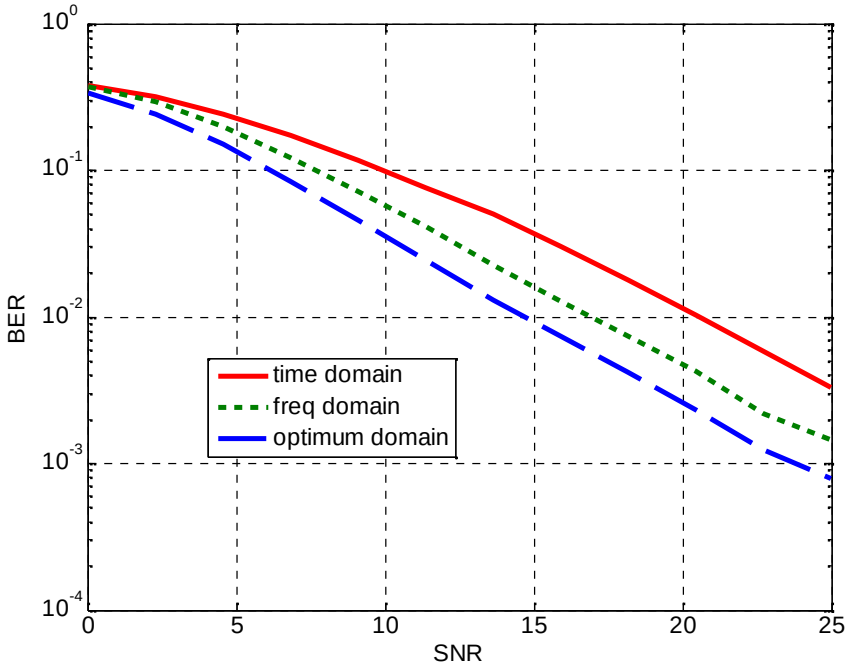

Figure 3.25: Comparison of BER of FRFT domain MMSE receiver with time and frequency domain MMSE receiver for $N_T=N_R=4$ in uncorrelated Rayleigh fading channel.

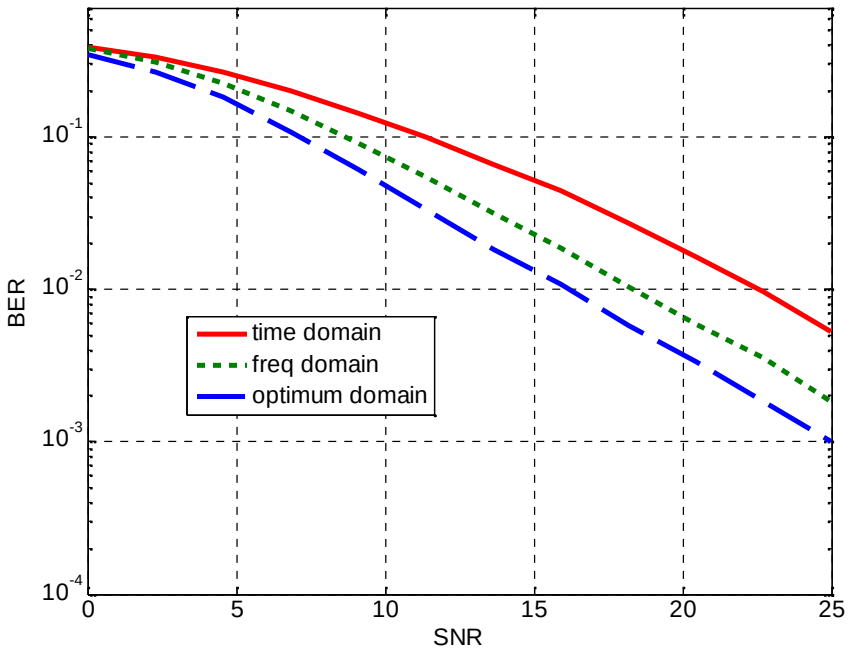

Figure 3.26: Comparison of BER of FRFT domain MMSE receiver with time and frequency domain MMSE receiver for $N_T=N_R=4$ in correlated Rayleigh fading channel with rtx=rrx=0.2

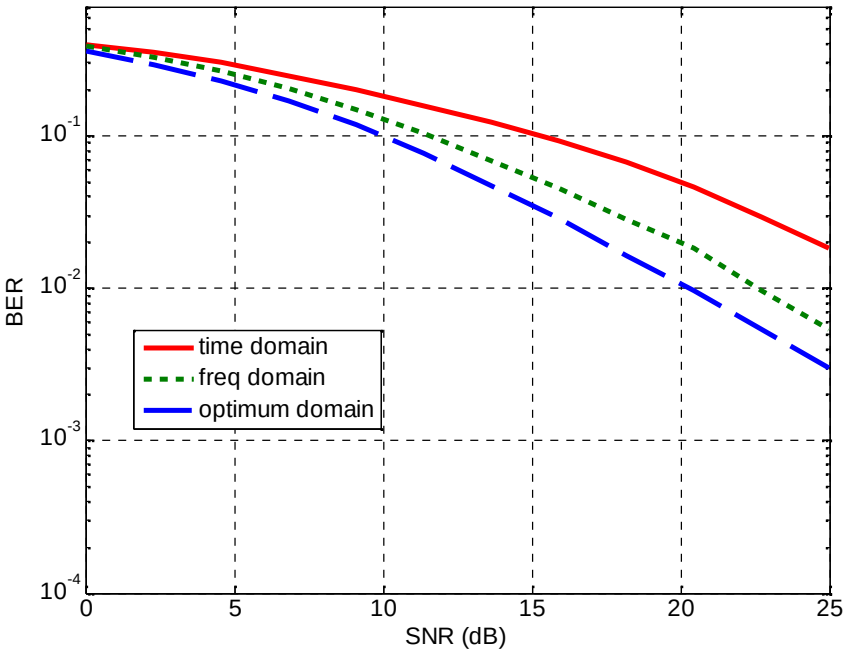

Figure 3.27: Comparison of BER of FRFT domain MMSE receiver with time and frequency domain MMSE receiver for $N_T=N_R=4$ in correlated Rayleigh fading channel with rtx=rrx=0.5

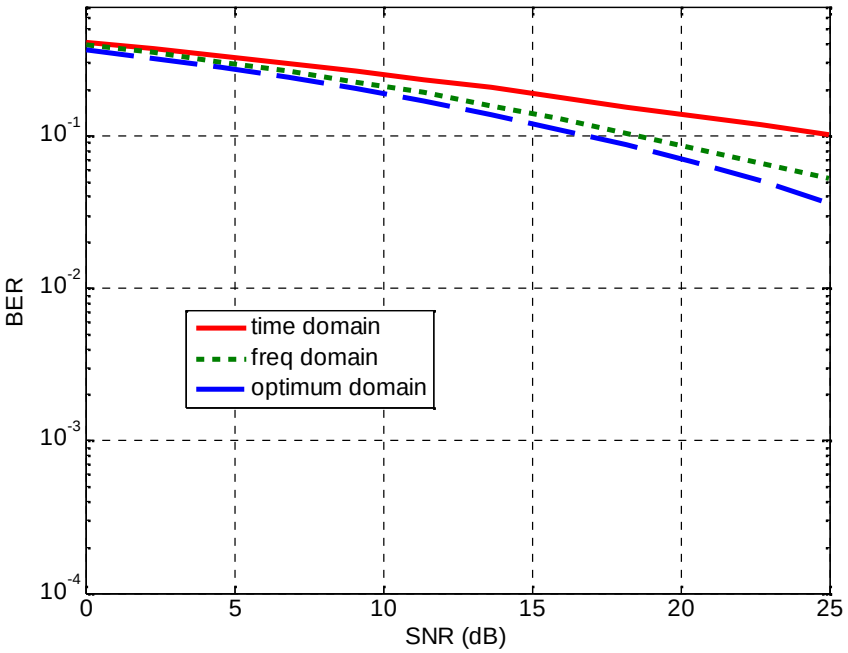

Figure 3.28: Comparison of BER of FRFT domain MMSE receiver with time and frequency domain MMSE receiver for $N_T=N_R=4$ in correlated Rayleigh fading channel with rtx=rrx=0.8

It is observed from the results that the BER deteriorates very severely with increase in spatial correlation for $N_T=N_R=4$ as compared with results for $N_T=N_R=2$. Table 3.4 summarizes the results shown in Fig. 3.25-3.28 presenting the SNR improvement (in dB) of the proposed receiver over the other two receivers at a fixed BER for four different levels of correlation.

Table 3.4: SNR improvement of proposed MMSE receiver over the time and frequency domain MMSE receivers for a fixed BER and $N_T=N_R=4$

Correlation Coefficient/BER	Time domain (dB)	Freq domain (dB)	Optimum domain (dB)	SNR Advantage over Time domain MMSE	SNR Advantage over Freq domain MMSE
$0/10^{-2}$	20.57	16.95	14.70	5.87 dB	2.25 dB
$0.2/10^{-2}$	22.53	18.36	16.18	6.35 dB	2.18 dB
$0.5/10^{-1.7}$	24.60	19.96	17.35	7.25 dB	2.61 dB
$0.8/10^{-1}$	25	18.55	16.79	8.21 dB	1.76 dB

The previous results show the effect of spatial correlation on the BER performance of the three receivers. To understand the effect of spatial correlation in greater detail, BER vs. correlation coefficient is presented for a $N_T=N_R=2$ for SNR=10 dB in Fig. 3.29 and SNR=20 dB in Fig. 3.30. The channel is considered to be correlated Rayleigh fading. It can be clearly seen from the results that the BER deteriorates with increase in the correlation coefficient (r). At high values of correlation coefficient, the BER of all the three receivers becomes almost equal. Similar results are observed in Fig. 3.31 and 3.32 for $N_T=N_R=4$.

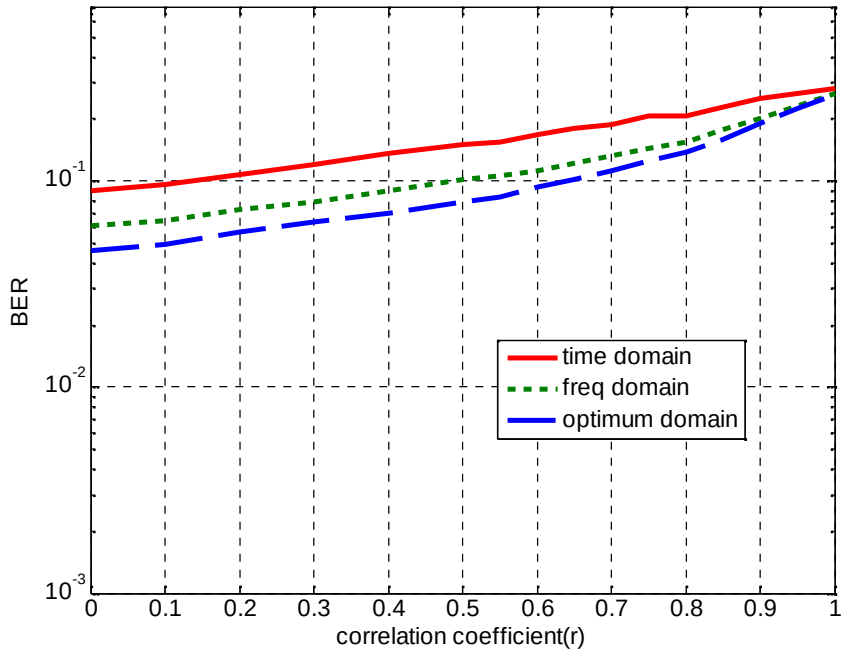

Figure 3.29: BER vs. correlation coefficient (r_{TX}=r_{RX}=r) for N_T=N_R=2 and a fixed SNR=10dB in flat Rayleigh fading channel

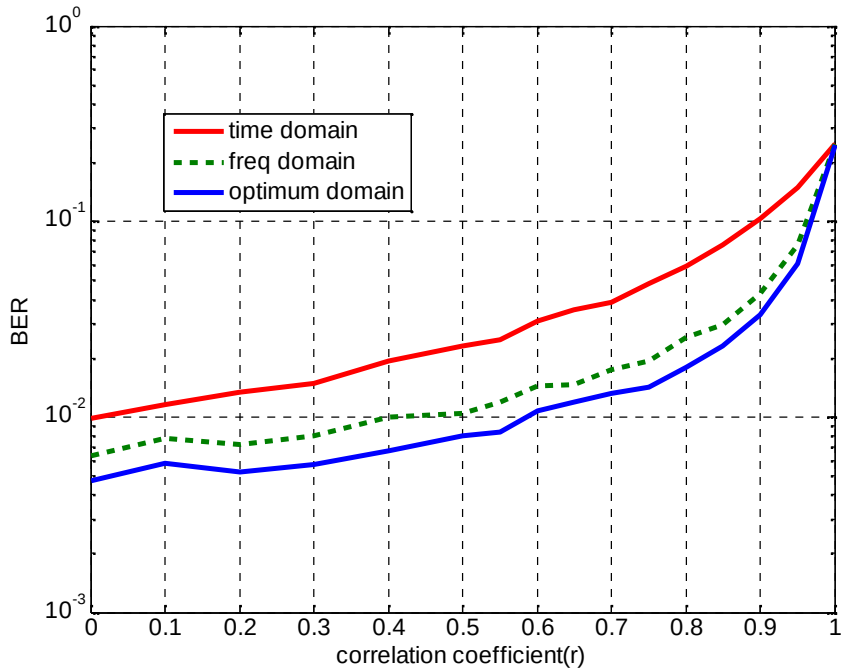

Figure 3.30: BER vs. correlation coefficient (r_{TX}=r_{RX}=r) for N_T=N_R=2 and a fixed SNR=20dB in flat Rayleigh fading channel

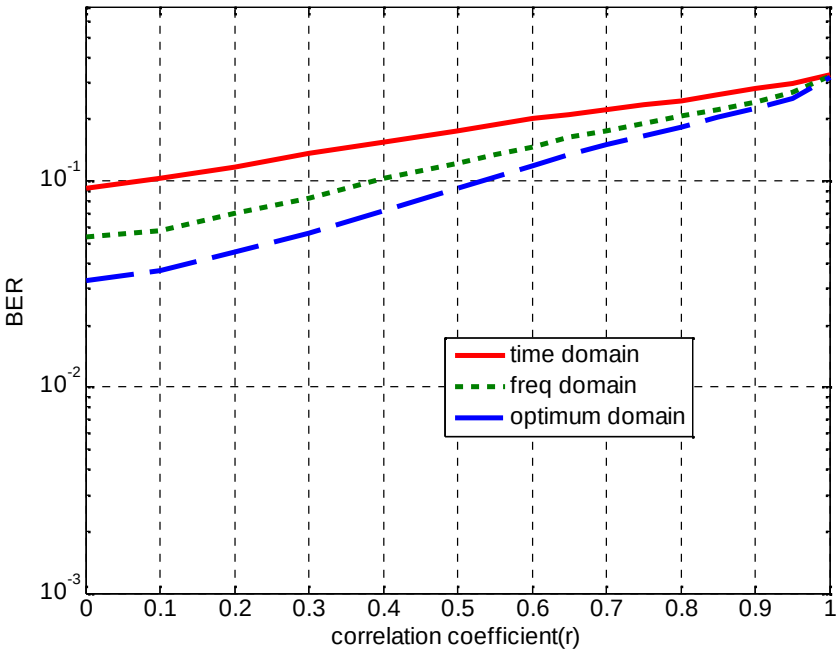

Figure 3.31: BER vs. correlation coefficient (r_{TX}=r_{RX}=r) for N_T=N_R=4 and a fixed SNR=10dB in flat Rayleigh fading channel

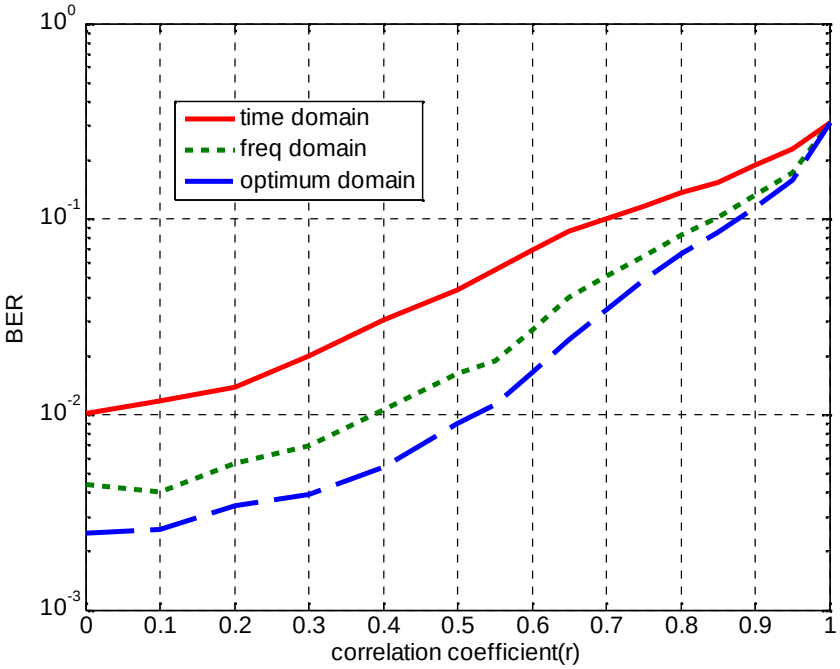

Figure 3.32: BER vs. correlation coefficient (r_{TX}=r_{RX}=r) for N_T=N_R=4 and a fixed SNR=20dB in flat Rayleigh fading channel

The results in Fig. 3.29-3.32 are summarized in table 3.5. As evident from previous results, the performance of all the three receivers deteriorates with increase in the correlation coefficient. It can be seen that the proposed receiver gives the lowest BER out of the three receivers. It can also be observed that at full correlation (r=1), all the receivers have the same BER. It is seen that for r=0.2 and 0.5, the optimum receiver outperforms the other two receivers whereas for r=0.8, all receivers have a similar error rate performance.

Table 3.5: Comparison of BER of proposed receiver with the time and frequency domain receivers for different correlation coefficients at a fixed SNR

	$N_T=N_R=2$			$N_T=N_R=4$		
Spatial Correlation / SNR	Time domain	Freq domain	Optimum domain	Time domain	Freq domain	Optimum domain
0.2 / 10 dB	0.1069	0.07252	0.05633	0.1174	0.07011	0.04511
0.5 / 10 dB	0.1503	0.1009	0.07952	0.1754	0.1219	0.09245
0.8 / 10 dB	0.2069	0.1553	0.1388	0.2451	0.2054	0.1829
0.2 / 20 dB	0.0133	0.0072	0.00519	0.0137	0.0055	0.0034
0.5 / 20 dB	0.02312	0.01043	0.0079	0.04364	0.01623	0.0089
0.8 / 20 dB	0.05883	0.02571	0.01805	0.137	0.08256	0.06686

In previous simulations, it was assumed that the correlation coefficient (r) was equal at both transmitter and receiver. However, in practical wireless systems, this might not be the case with either of the transmitter or receiver being large enough to have adequate spacing between the elements to avoid spatial correlation. In that case, we would encounter correlation at one end and uncorrelated system at the other. The effect spatial correlation on transmitter/receiver only on the BER of the system is plotted below in Fig. 3.33-3.40. It can be seen that the BER deteriorates with increase in transmit/receive correlation but the deterioration is less even at higher correlation values as compared to the previous case where spatial correlation was considered at both ends.

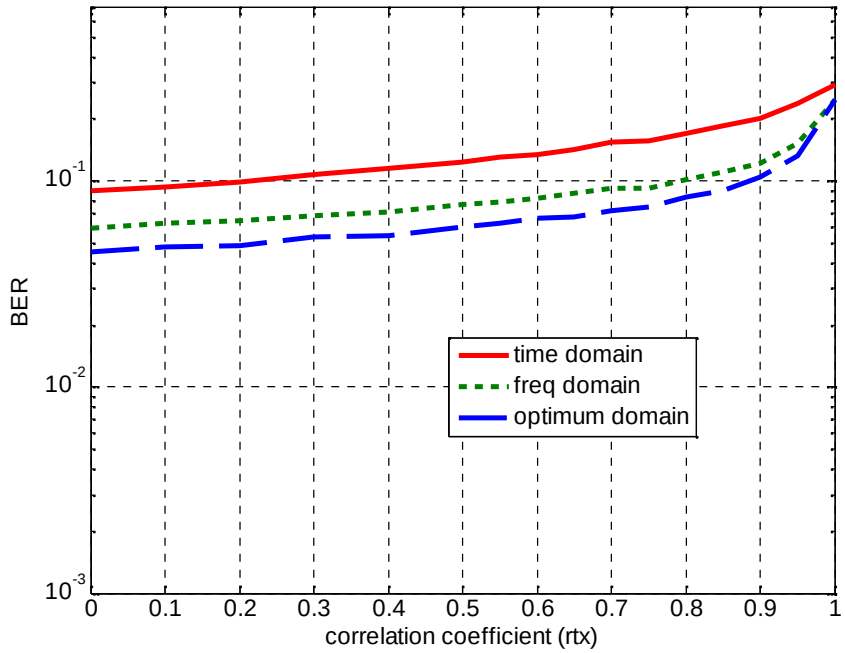

Figure 3.33: BER vs. transmit correlation (r_{TX}) for N_T=N_R=2 and a fixed SNR=10dB (r_{RX}=0) in flat Rayleigh fading channel

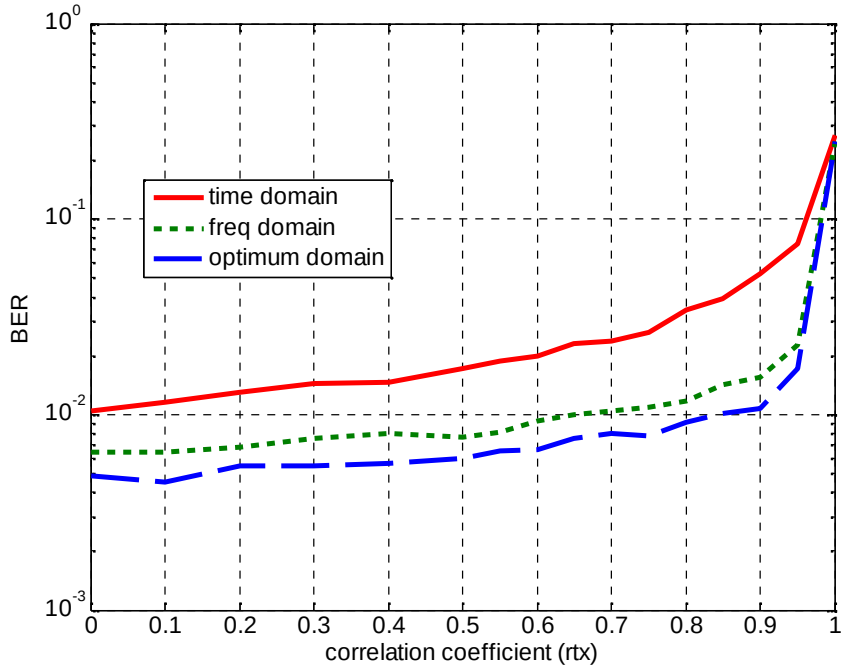

Figure 3.34: BER vs. transmit correlation (r_{TX}) for N_T=N_R=2 and a fixed SNR=20dB (r_{RX}=0) in flat Rayleigh fading channel

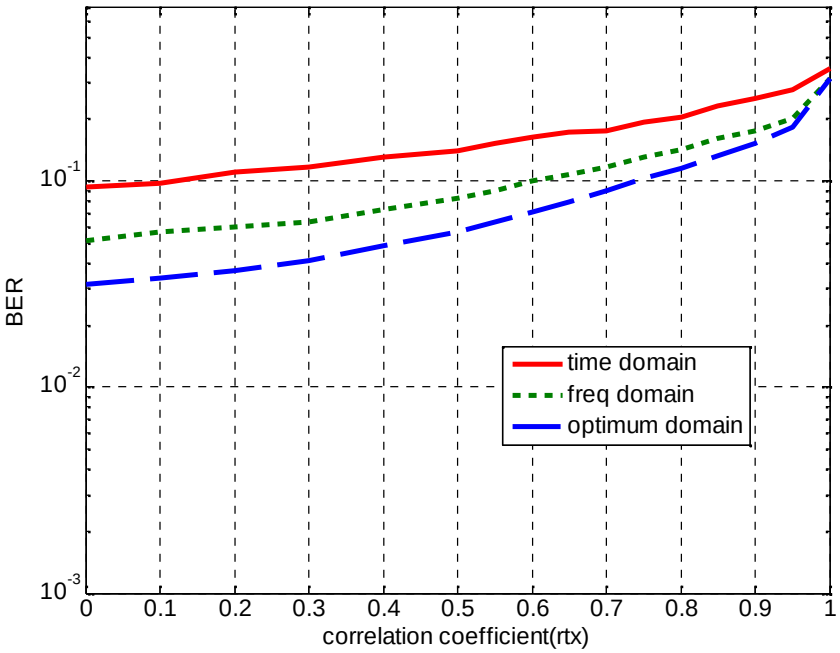

Figure 3.35: BER vs. transmit correlation (r_{TX}) for N_T=N_R=4 and a fixed SNR=10dB (r_{RX}=0) in flat Rayleigh fading channel

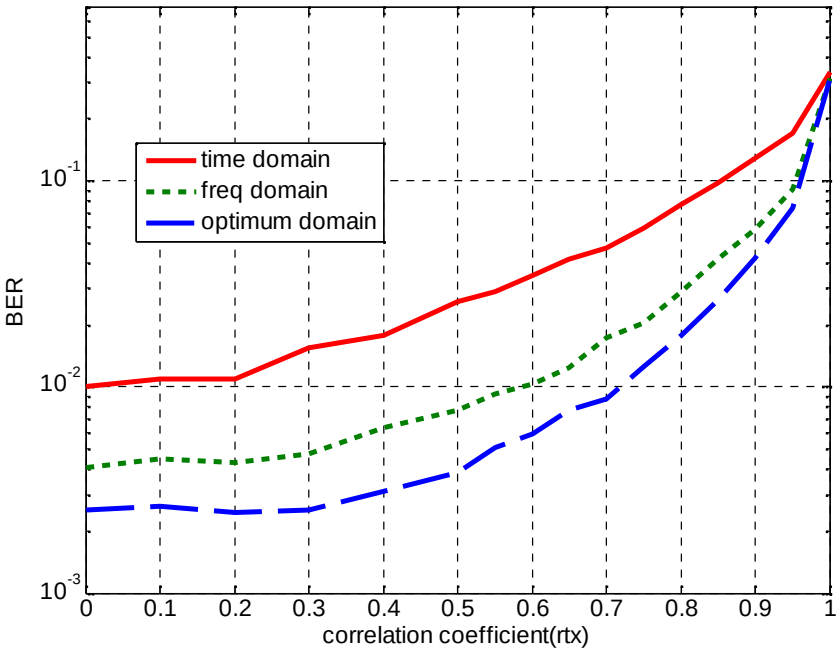

Figure 3.36: BER vs. transmit correlation (r_{TX}) for N_T=N_R=4 and a fixed SNR=20dB (r_{RX}=0) in flat Rayleigh fading channel

The results compare the BER of the three MMSE receivers in the presence of transmit correlation for 2×2 and 4×4 system. It is seen that the degradation of the error performance of all the receivers is less in the case of transmit correlation (no receive correlation) as compared to when correlation is present at both ends. Table 3.6 compares the BER of three receivers for r_{TX}=0.2, 0.5 and 0.8 at SNR=10 dB and 20 dB.

Table 3.6: Comparison of BER of proposed receiver with the time and frequency domain receivers for transmit correlation at a fixed SNR

r_{RX}=0	N_T=N_R=2			N_T=N_R=4		
r_{TX} / SNR	Time domain	Freq domain	Optimum domain	Time domain	Freq domain	Optimum domain
0.2 (10 dB)	0.0988	0.0638	0.0487	0.1100	0.0595	0.0364
0.5 (10 dB)	0.1234	0.0767	0.0597	0.1396	0.0829	0.0566
0.8 (10 dB)	0.1702	0.1023	0.0833	0.2048	0.1415	0.1146
0.2 (20 dB)	0.0129	0.0068	0.0054	0.0109	0.0042	0.0024
0.5 (20 dB)	0.0171	0.0076	0.0059	0.0258	0.0076	0.0038
0.8 (20 dB)	0.0343	0.0118	0.0090	0.0768	0.0290	0.0179

In previous results, correlation was only assumed to be on the transmitter side. In the following results, we consider the effect of receive correlation (r_{RX}) on the error performance of the three receivers. Transmit correlation (r_{TX}) is assumed to be zero. This is the case when the transmitter has enough spacing between the antenna elements and the receiver is small in size and has insufficient spacing between the antennas.

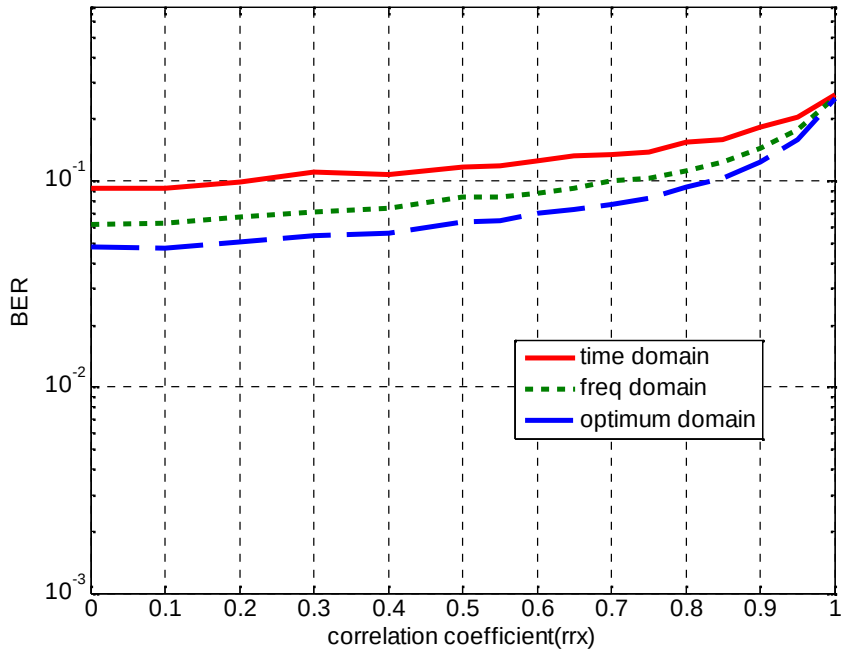

Figure 3.37: BER vs. receive correlation (r_{RX}) for N_T=N_R=2 and a fixed SNR=10dB (r_{TX}=0) in flat Rayleigh fading channel

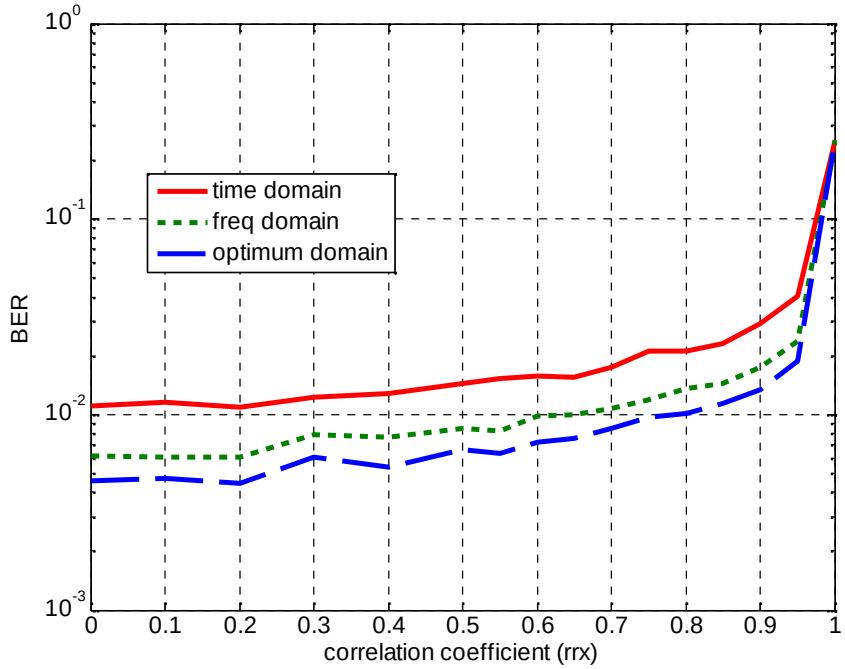

Figure 3.38: BER vs. receive correlation (r_{RX}) for N_T=N_R=2 and a fixed SNR=20dB (r_{TX}=0) in flat Rayleigh fading channel

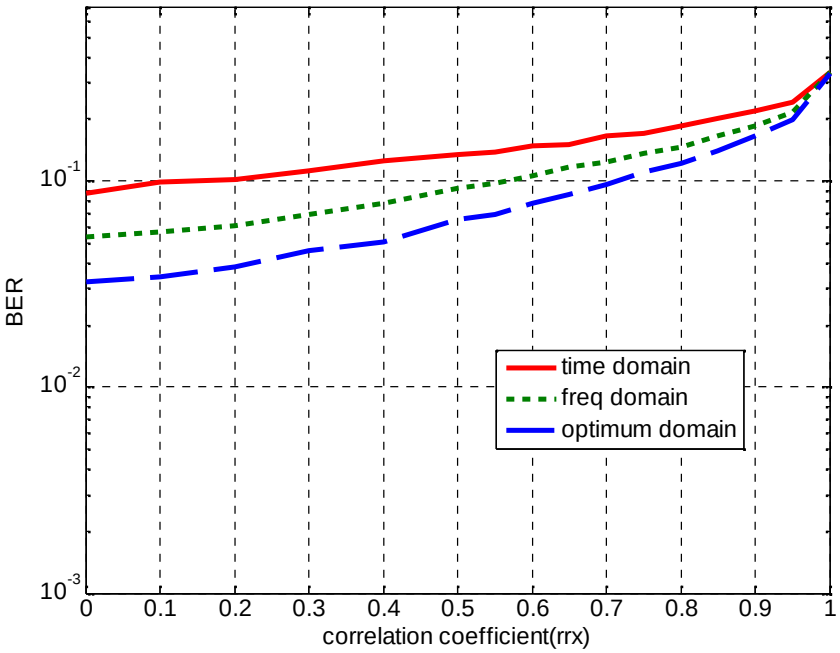

Figure 3.39: BER vs. receive correlation (r_{RX}) for N_T=N_R=4 and a fixed SNR=10dB (r_{TX}=0) in flat Rayleigh fading channel

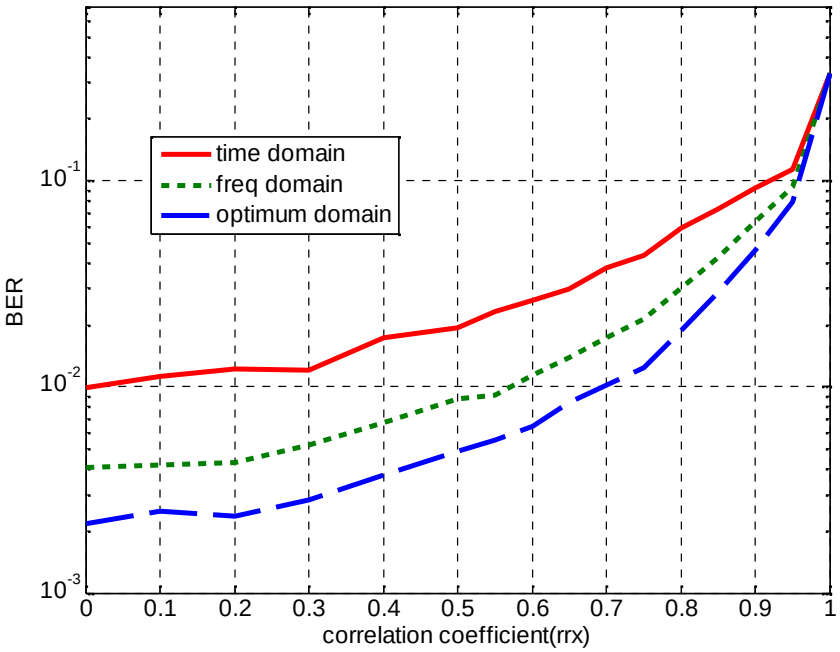

Figure 3.40: BER vs. receive correlation (r_{RX}) for N_T=N_R=4 and a fixed SNR=20dB (r_{TX}=0) in flat Rayleigh fading channel

Table 3.7: Comparison of BER of proposed receiver with the time and frequency domain receivers for receive correlation at a fixed SNR

r_{TX}=0	N_T=N_R=2			N_T=N_R=4		
r / SNR	Time domain	Freq domain	Optimum domain	Time domain	Freq domain	Optimum domain
0.2 (10 dB)	0.0981	0.0670	0.0509	0.1022	0.0604	0.0382
0.5 (10 dB)	0.1166	0.0836	0.0633	0.1338	0.0918	0.0647
0.8 (10 dB)	0.1533	0.1122	0.0938	0.1837	0.1456	0.1213
0.2 (20 dB)	0.0109	0.0060	0.0044	0.0121	0.0043	0.0024
0.5 (20 dB)	0.0144	0.0084	0.0065	0.0192	0.0087	0.0048
0.8 (20 dB)	0.0210	0.0135	0.0101	0.0589	0.0301	0.0188

Table 3.7 compares the BER for receive correlation at correlation values of r_{RX}=0.2, 0.5 and 0.8 at fixed SNR of 10 dB and 20 dB. It is observed that the degradation of BER is lesser as compared to the case of spatial correlation on both the ends.

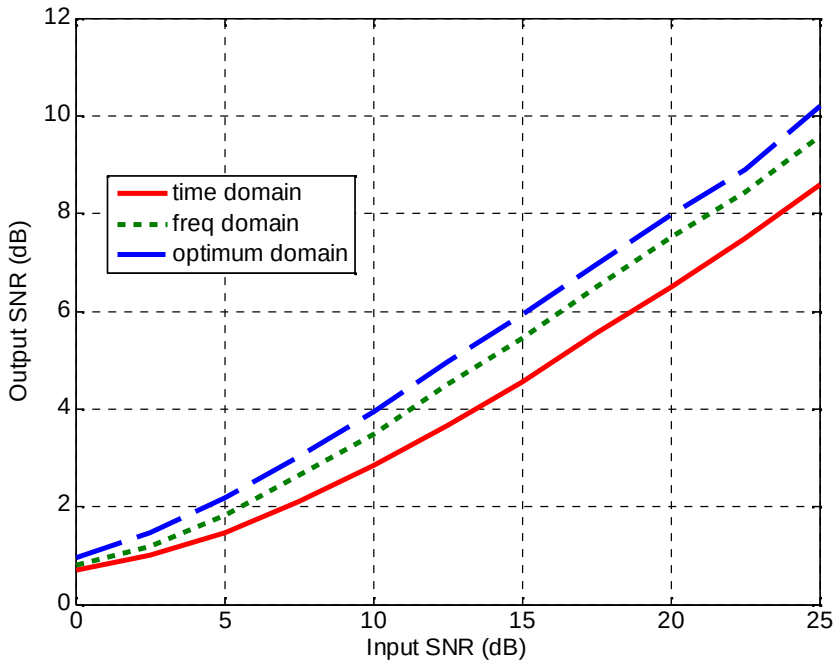

Figure 3.41: Output SNR vs. input SNR for N_T=N_R=2 in uncorrelated Rayleigh fading channel

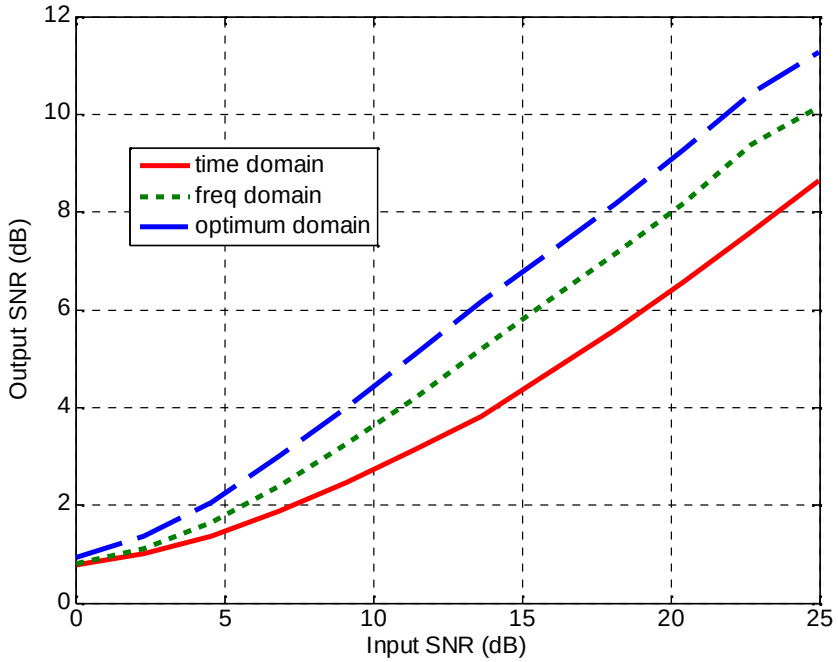

Figure 3.42: Output SNR vs. input SNR for N_T=N_R=4 in uncorrelated Rayleigh fading channel

Table 3.8: Comparison of output SNR of the time, freq and optimum domain receivers

	N_T=N_R=2			N_T=N_R=4		
Receiver domain	5 dB	15 dB	25 dB	5 dB	15 dB	25 dB
Time domain	1.464	4.569	8.579	1.471	4.350	8.649
Freq domain	1.827	5.443	9.594	1.80	5.8	10.13
Optimum domain	2.188	5.925	10.21	2.25	6.76	11.27

Table 3.8 shows the comparison of output SNR for fixed values of input SNR. It is observed that the proposed receiver gives the maximum output SNR for the same input SNR as compared to the time domain and frequency domain receivers. This is equivalent to giving lower BER for the same value of input SNR. The comparison of MSE vs. SNR for the three receivers in uncorrelated Rayleigh fading for N_T=N_R=2 and 4 is shown in Fig.3.43 and 3.44. The optimum domain MMSE receiver gives the lowest MSE at all values of SNR.

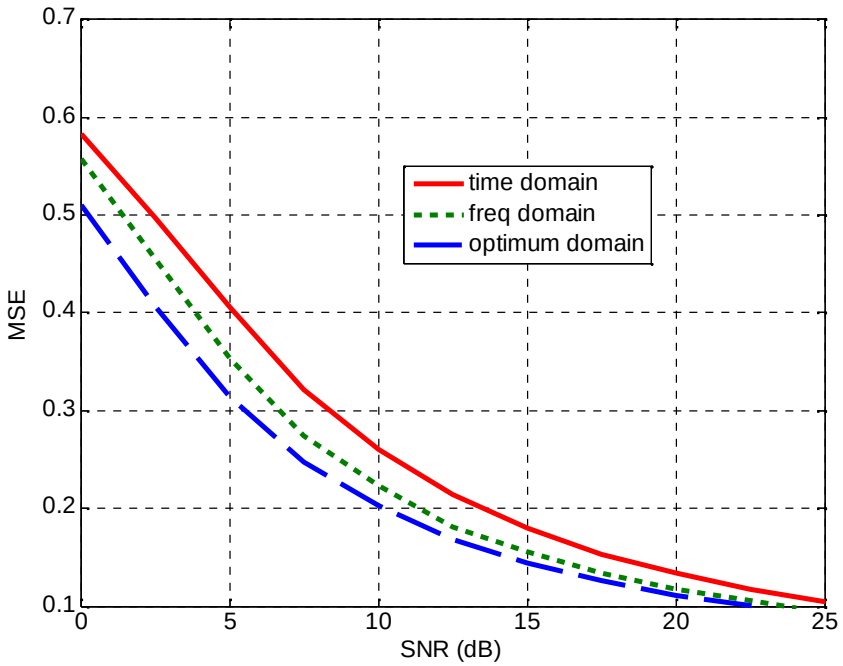

Figure 3.43: Comparison of MSE of FRFT domain MMSE receiver with time and frequency domain MMSE receivers for $N_T=N_R=2$ in uncorrelated Rayleigh fading

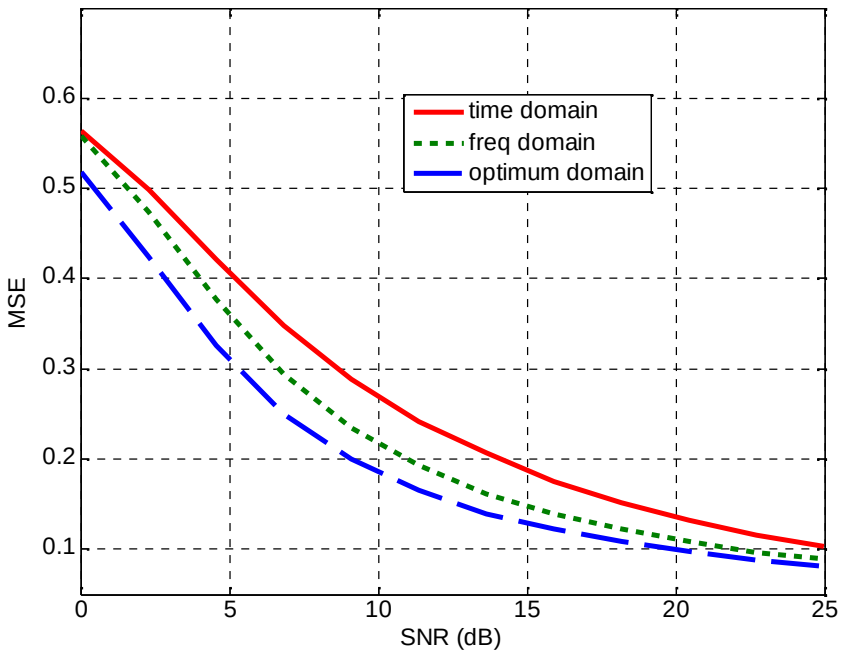

Figure 3.44: Comparison of MSE of FRFT domain MMSE receiver with time and frequency domain MMSE receivers for $N_T=N_R=4$ in uncorrelated Rayleigh fading

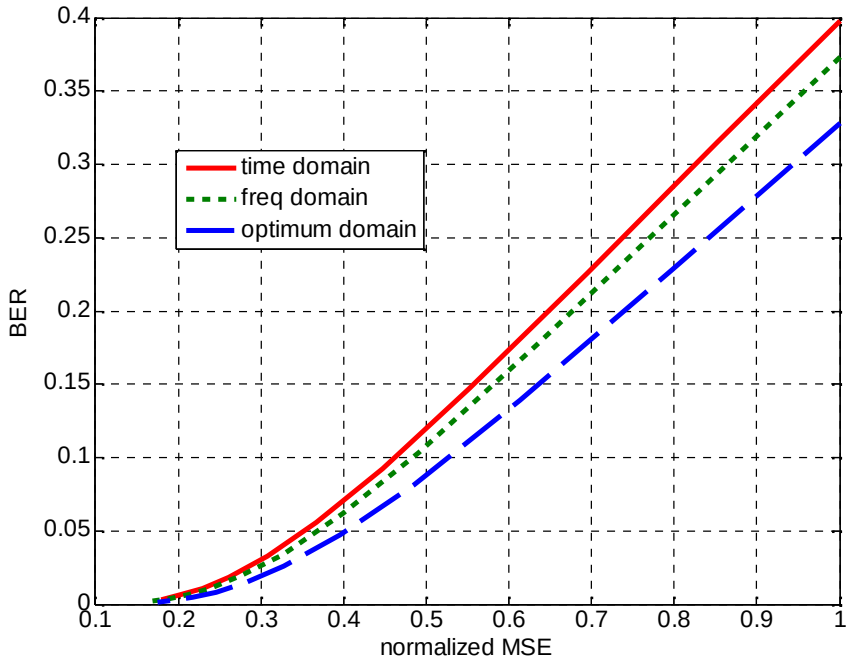

Figure 3.45: BER vs. normalized MSE comparison of time, frequency and FRFT domain MMSE receiver for $N_T=N_R=2$ in uncorrelated Rayleigh fading

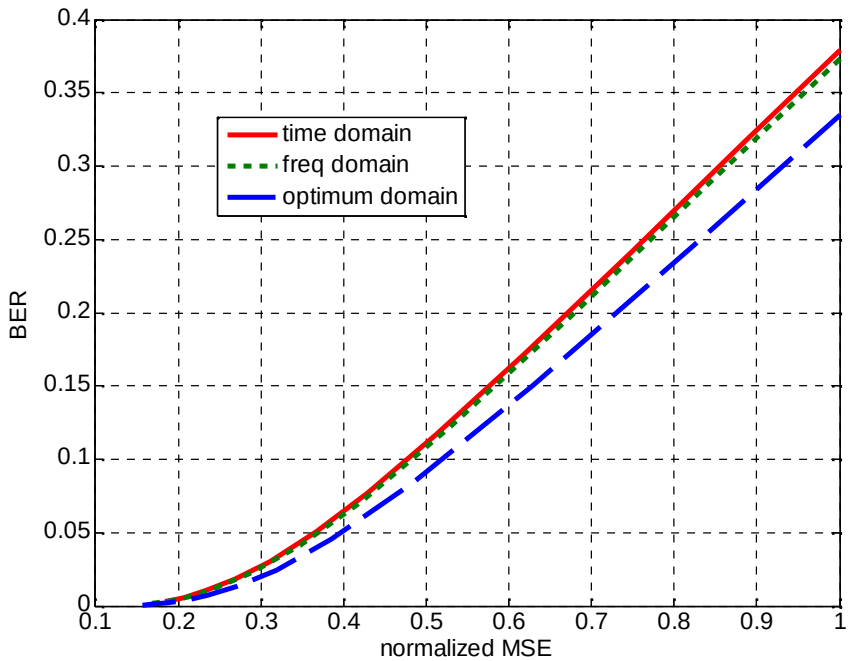

Figure 3.46: BER vs. normalized MSE comparison of time, frequency and FRFT domain MMSE receiver for $N_T=N_R=4$ in uncorrelated Rayleigh fading

Fig. 3.45 and 3.46 show the BER vs. normalized MSE comparison of the three receivers for $N_T=N_R=2$ and 4 in uncorrelated Rayleigh fading. It is seen that the optimum domain receiver has the lowest BER for the same value of normalized MSE. All the results presented above are for Rayleigh fading. In the following results, the three receivers are compared when the channel is considered to be Rician distributed, i.e. having a dominant LOS path. In Fig.3.47 and 3.48, the BER vs. SNR results over a Rician fading channel with a *K*-factor of 10 dB are presented for $N_T=N_R=2$ and 4 respectively. It is seen that the proposed optimum domain receiver gives the lowest BER for both the cases in Rician fading channel.

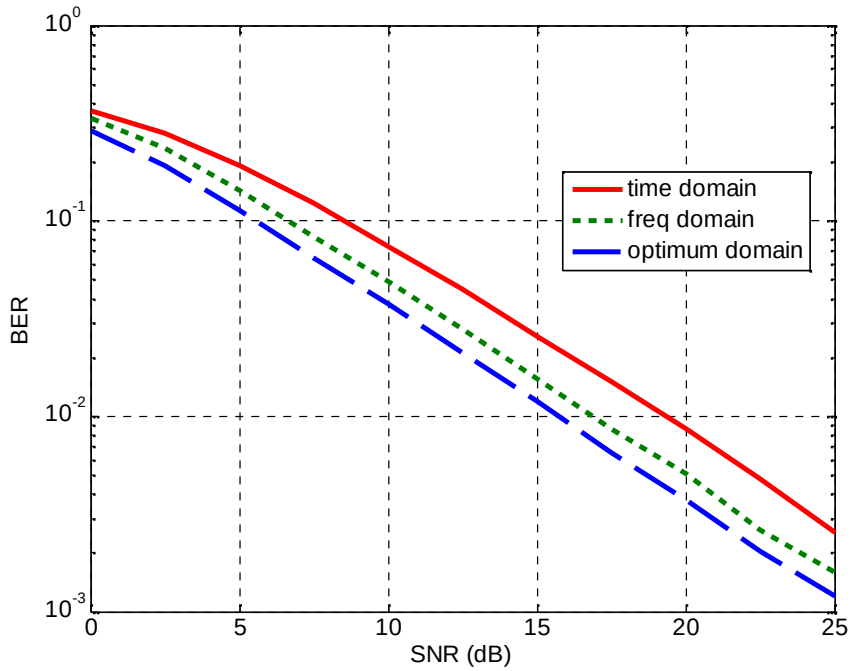

Figure 3.47: Comparison of BER of FRFT domain MMSE receiver with time and frequency domain MMSE receiver for $N_T=N_R=2$ in Rician fading channel with K (dB) =10

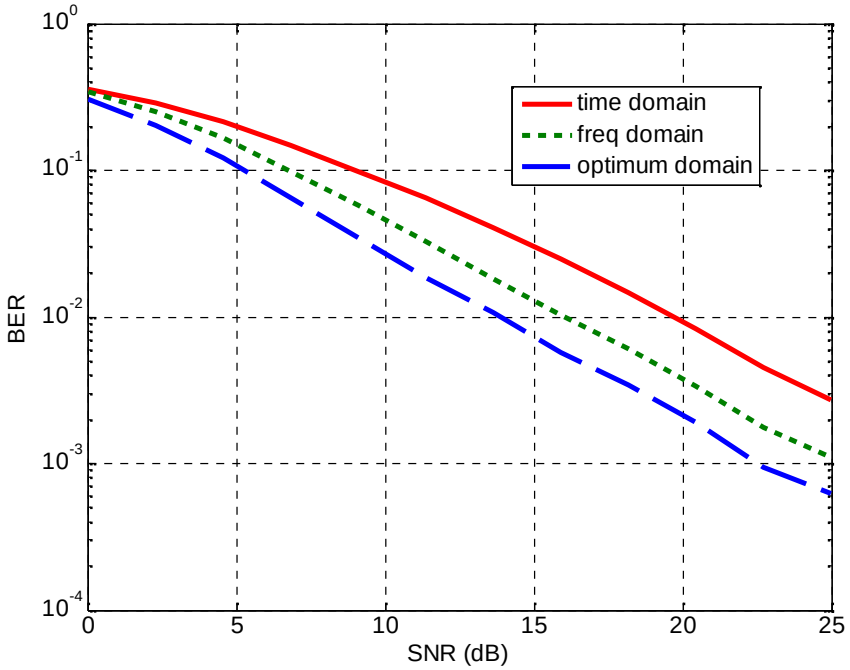

Figure 3.48: Comparison of BER of FRFT domain MMSE receiver with time and frequency domain MMSE receiver for $N_T=N_R=4$ in Rician fading channel with K (dB) =10

Table 3.9: SNR improvement of proposed MMSE receiver over the time and frequency domain MMSE receivers for a BER=10^{-2} and $N_T=N_R=2$ and 4

Rician K=10	Time domain (dB)	Freq domain (dB)	Optimum domain (dB)	SNR Advantage over Time domain MMSE	SNR Advantage over Freq domain MMSE
$N_T=N_R=2$	19.32	16.85	15.73	3.59 dB	1.12 dB
$N_T=N_R=4$	19.73	16.07	13.91	5.82 dB	2.16 dB

The table 3.9 shows the SNR advantage achieved by the proposed receiver over the existing receivers to achieve a fixed BER of 10^{-2}. It is seen that the proposed receiver gives SNR advantage of 3.59 dB and 1.12 dB over time and frequency domain receivers respectively for $N_T=N_R=2$ and 5.82 dB and 2.16 dB for $N_T=N_R=4$. MSE vs. SNR comparison for the three receivers for NT=NR=2 and 4 in Rician fading (*K*-factor=10) is shown in Fig. 3.49 and 3.50.

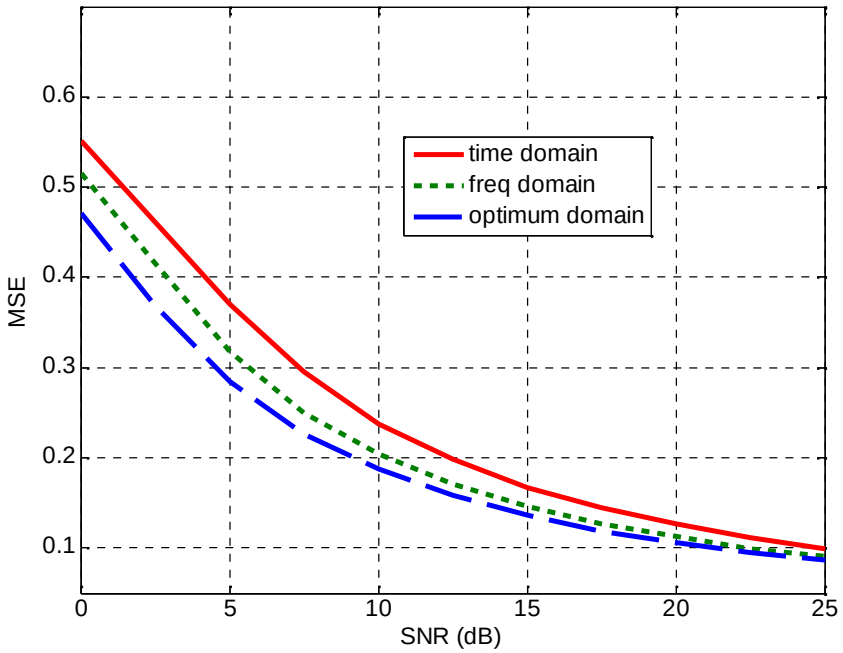

Figure 3.49: Comparison of MSE of FRFT domain MMSE receiver with time and frequency domain MMSE receivers for $N_T=N_R=2$ in Rician fading for K (dB) =10

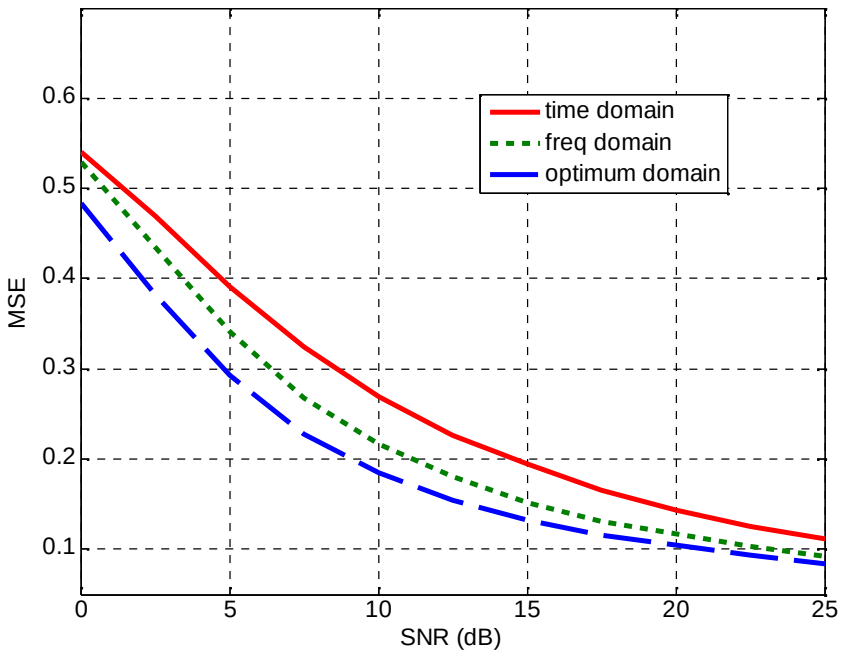

Figure 3.50: Comparison of MSE of FRFT domain MMSE receiver with time and frequency domain MMSE receivers for $N_T=N_R=4$ in Rician fading for K (dB) =10

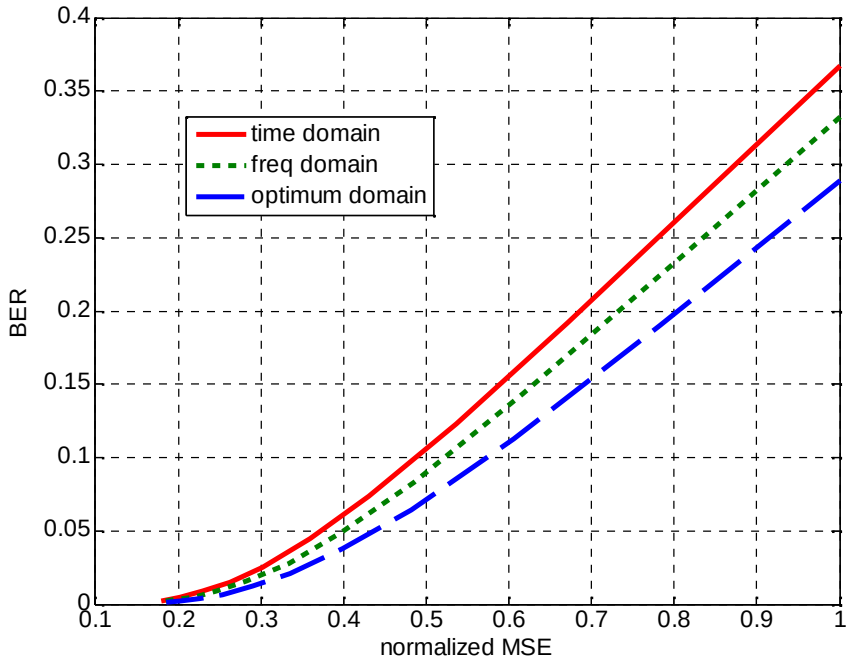

Figure 3.51: BER vs. normalized MSE comparison of time, frequency and FRFT domain MMSE receiver for N_T=N_R=2 in Rician fading with K (dB) =10

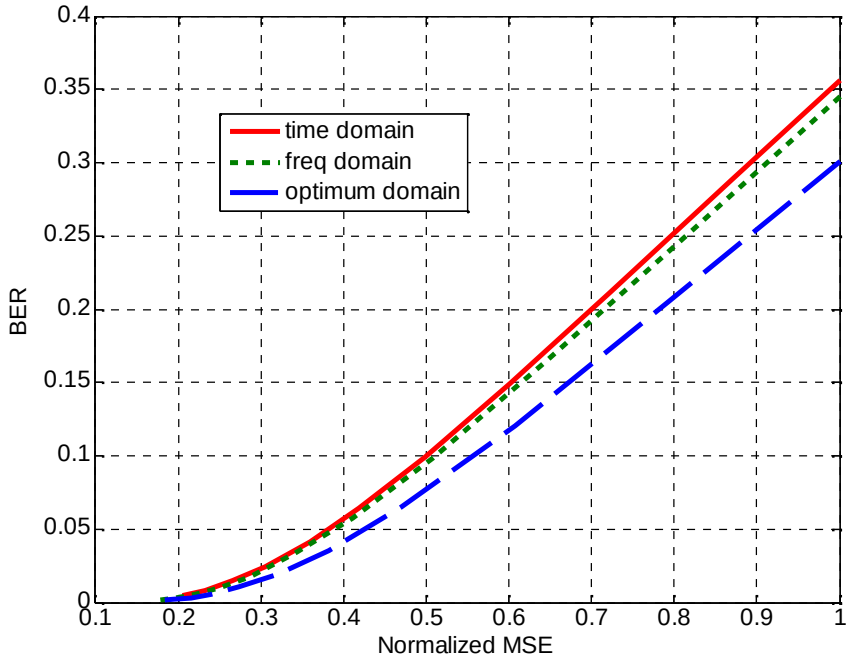

Figure 3.52: Comparison of BER of FRFT domain MMSE receiver with time and frequency domain MMSE receiver for N_T=N_R=4 in Rician fading channel with K (dB) =10

The method of calculating BER from MSE and SINR is discussed in the preceding sections. Now, using this method we obtain the analytical BER and compare it with simulated BER. From (3.55), the equation for finding the MMSE is given by:

$$\mathrm{MMSE}(\mathbf{W}_{opt}) = E\left\{\left\|\boldsymbol{x} - \boldsymbol{F}^{-aopt}\mathbf{W}^{H}\boldsymbol{F}^{aopt}\boldsymbol{y}\right\|^{2}\right\}$$

Once the MMSE is obtained, the BER can be calculated from it using eq. (3.24):

$$\mathrm{P}_e \cong 0.49\alpha e^{-\frac{8\left(\sqrt{\beta(\mathrm{MSE}^{-1}-1)}\right)}{13}} e^{-\frac{\beta(\mathrm{MSE}^{-1}-1)}{2}}$$

Therefore, the BER obtained by simulation and the BER obtained analytically can be compared and the correctness of the simulation results can be verified. In Fig. 3.53 and 3.54, the analytical BER vs. SNR is plotted for all the three receivers in 2×2 and 4×4 system respectively. It is observed that the optimum receiver outperforms the other two receivers. The simulation and analytical BER results are compared in Fig. 3.55-3.60. Fig. 3.55-3.57 show the comparison of simulated and analytical BER for time, frequency and optimum domain receivers for N_T=N_R=2. Fig. 3.58-3.60 show similar results for a N_T=N_R=4 system. The analytical results are in agreement with the simulation results.

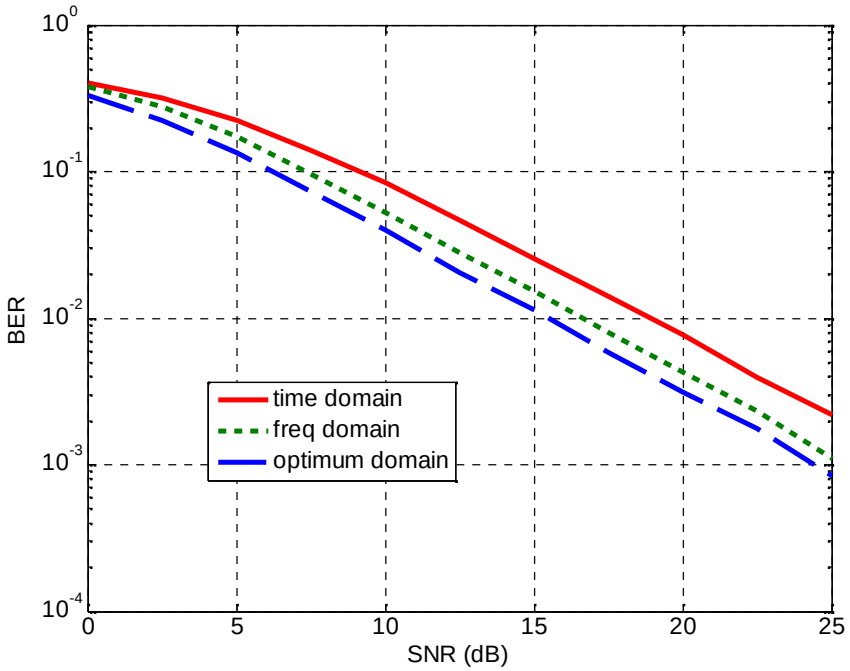

Figure 3.53: Analytical BER performance comparison of time, frequency and FRFT domain MMSE receivers for N_T=N_R=2 in uncorrelated Rayleigh fading

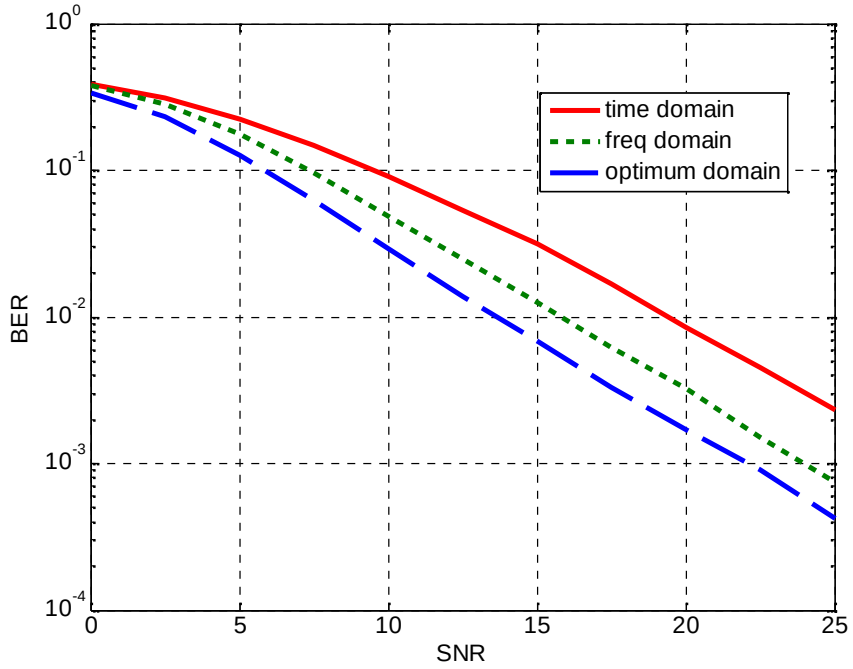

Figure 3.54: Analytical BER performance comparison of time, frequency and FRFT domain MMSE receivers for $N_T=N_R=4$ in uncorrelated Rayleigh fading

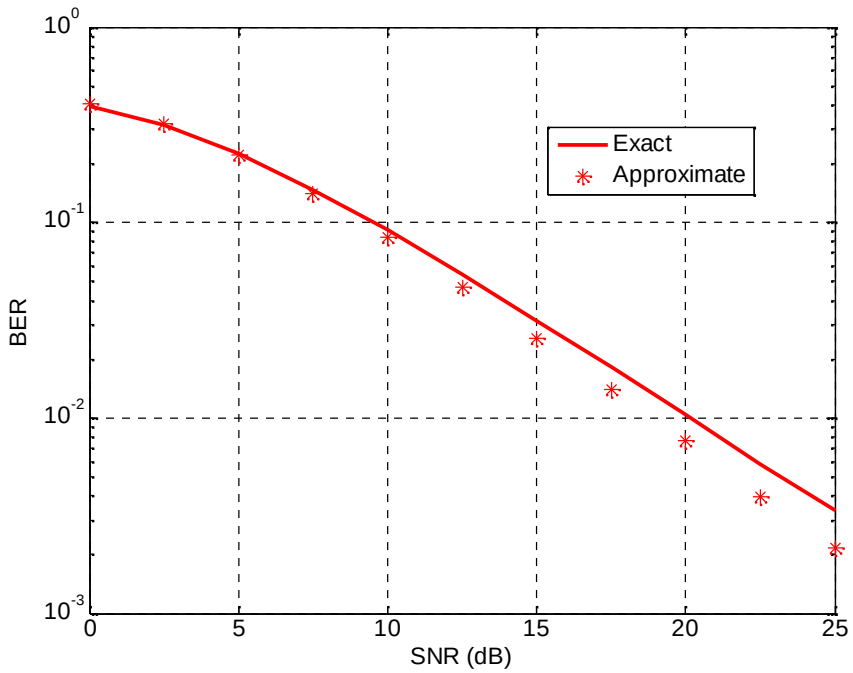

Figure 3.55: Comparison of analytical BER calculation of time domain MMSE using the exact Q-function and its approximation for $N_T=N_R=2$ in uncorrelated Rayleigh fading

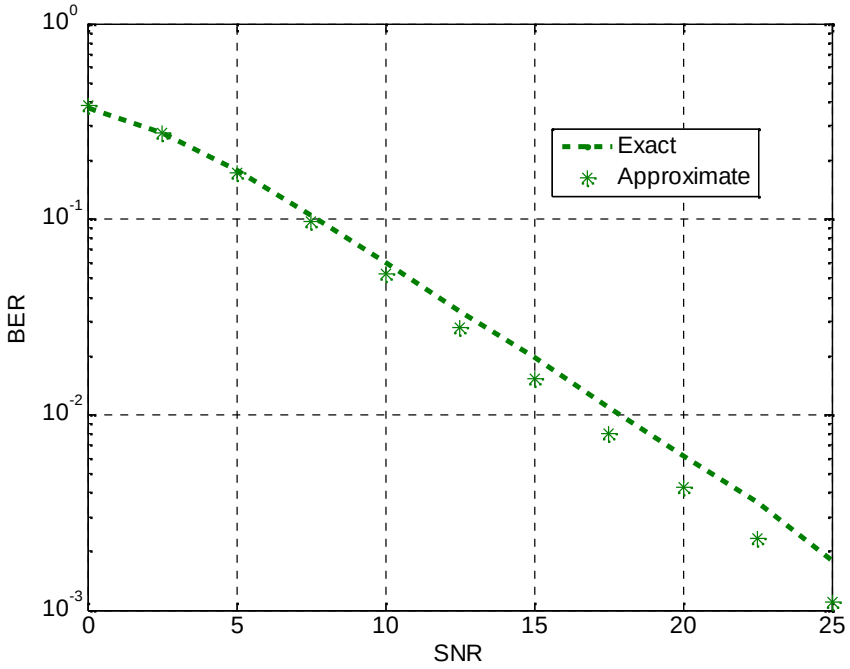

Figure 3.56: Comparison of analytical BER calculation of frequency domain MMSE using the exact Q-function and its approximation for $N_T=N_R=2$ in uncorrelated Rayleigh fading

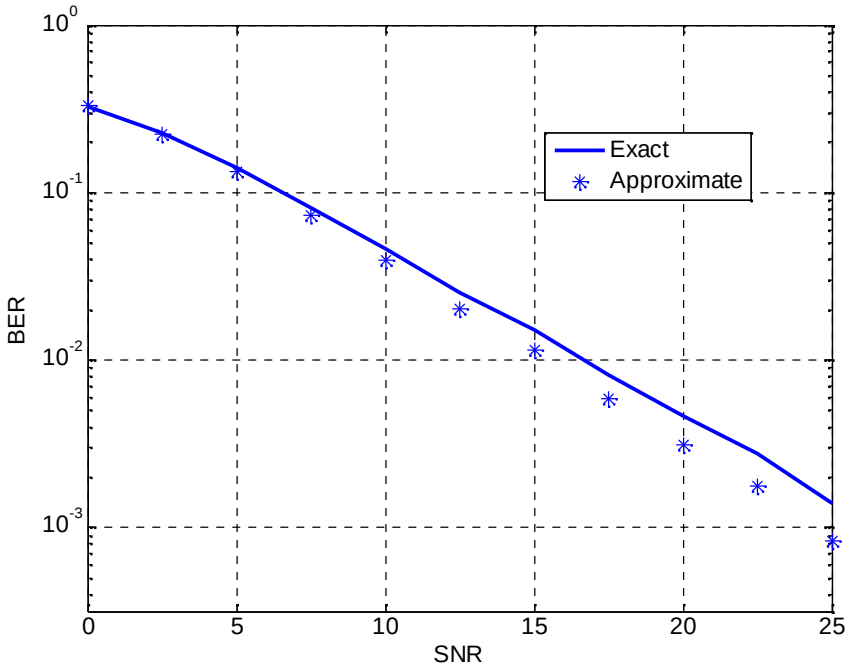

Figure 3.57: Comparison of analytical BER calculation of FRFT domain MMSE using the exact Q-function and its approximation for $N_T=N_R=2$ in uncorrelated Rayleigh fading

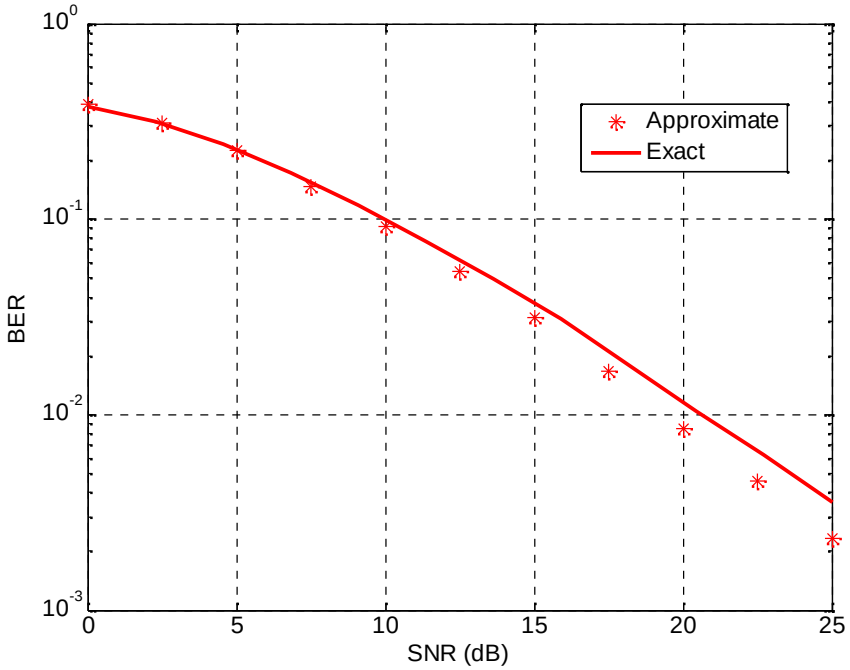

Figure 3.58: Comparison of analytical BER calculation of time domain MMSE using the exact Q-function and its approximation for $N_T=N_R=4$ in uncorrelated Rayleigh fading

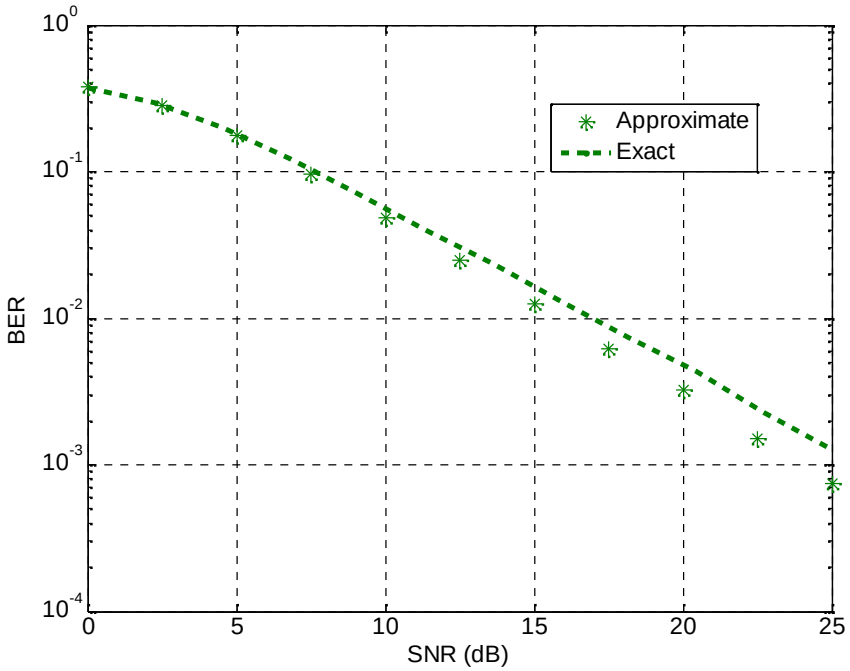

Figure 3.59: Comparison of analytical BER calculation of frequency domain MMSE using the exact Q-function and its approximation for $N_T=N_R=4$ in uncorrelated Rayleigh fading

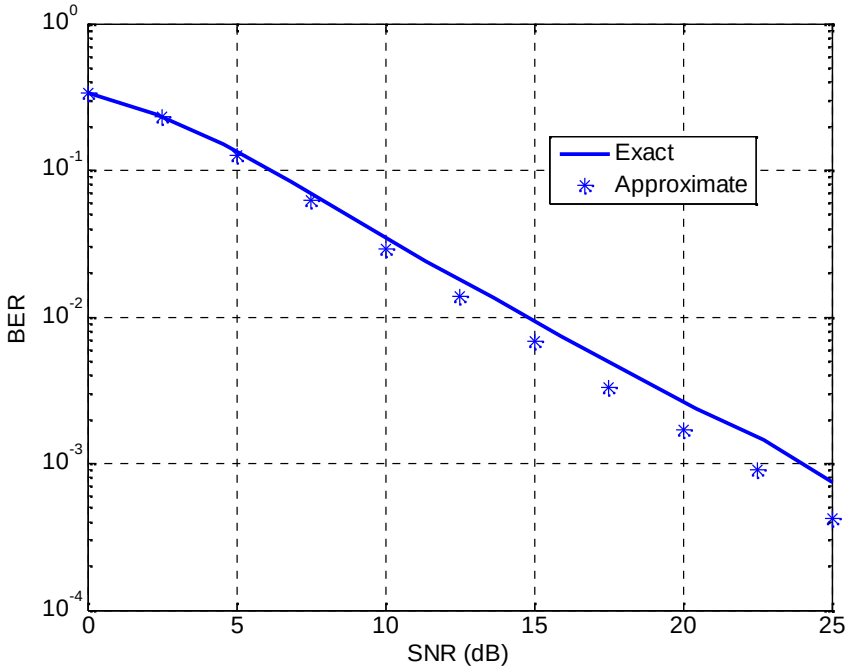

Figure 3.60: Comparison of analytical BER calculation of FRFT domain MMSE using the exact Q-function and its approximation for $N_T=N_R=4$ in uncorrelated Rayleigh fading

Table 3.10: SNR required for achieving a BER of 10^{-2} using exact and approximate cases

Analytical	Exact (in dB)	Approximate (in dB)
Time domain, $N_T=N_R=2$	20.2	18.9
Freq domain, $N_T=N_R=2$	17.86	16.63
Optimum domain, $N_T=N_R=2$	16.69	15.5
Time domain, $N_T=N_R=4$	20.64	19.41
Freq domain, $N_T=N_R=4$	16.95	15.81
Optimum domain, $N_T=N_R=4$	14.76	13.64

From the above results, it is seen that the simulation results match very closely analytical results for all the three receivers verifying the correctness of the simulation results.

3.6 Conclusions

In this chapter, we proposed a novel MMSE receiver based on fractional Fourier domain filtering for multiple antenna systems. From the results it is observed that the proposed FRFT MMSE receiver outperforms the time and frequency domain MMSE receivers in terms of error performance. The performance of the proposed receiver is then further analyzed in the presence of spatial correlation at the transmitter and/or receiver. Finally, analytical BER is derived from the MSE using a tight approximation of the Q-function and it is seen that the analytical results agree with the simulation results.

Chapter 4

Channel Estimation for MIMO Systems

4.1 Introduction

The theory of all the gains available from MIMO system is based on the assumption that the channel state information is known at the transmitter/receiver or both. The CSI describes how a signal propagates from the transmitter to the receiver and represents the combined effect of, for example, scattering, fading, and power decay with distance. Also, the severe amplitude and phase fluctuations inherent to wireless channels inhibits the use of multilevel Quadrature Amplitude Modulation (QAM) schemes because the demodulator has to scale the received signal to normalize the channel gain so that its decision regions correspond to the transmitted signal constellation. This process is called Automatic Gain Control (AGC) [80-81]. Therefore, training and channel estimation are key factors in the performance of MIMO systems. Practically, CSI is never known apriori and some form of channel estimation technique to estimate the CSI has to be employed with MIMO systems. Based on the same concept as the receiver proposed in chapter 3, we propose improved channel estimation techniques in this chapter. Generally, we can classify the wireless channel as fast fading and slow fading. Depending upon the type of wireless channel, different estimation techniques have to be used. To estimate a rapidly fading channel, known training symbols are inserted into the data at specific intervals from which the CSI can be calculated at training symbol positions. The CSI at unknown positions can be estimated using interpolation techniques and the CSI at pilot positions [82-83]. Although the interpolation technique would also work for a block fading channel (the channel remains constant for the entire block length), it would lead to a loss of data rate due to unnecessary overhead. For a block fading channel, transmitting known training symbols at the start of the transmission block would suffice [84]. Although, CSI can also be obtained by using blind channel estimation or decision directed techniques which do not require any form of training symbols, their performance is inferior to techniques using training symbols [85]. In the following sections, improved channel estimation techniques for block fading and rapidly fading channels are presented.

4.2 Channel Estimation for Block Fading Channels

When the channel remains constant for a transmission block and then changes completely and independently for the next transmission block, it is known as a block fading channel. Due to the property of the block fading channel, it can be estimated using pilot symbols that are prefixed with the data. At the receiver, the pilot symbols are obtained and the channel information is extracted from them. As the channel remains constant throughout the transmission block, after the channel response is obtained from the prefixed pilots, it does not need to be updated until the next transmission block. If the length of transmission block is assumed to be L, the received signal matrix **Y** is given by:

$$\mathbf{Y} = \mathbf{H}\mathbf{X} + \mathbf{N}, \tag{4.1}$$

where **X** denotes the $L \times N_T$ transmit signal matrix. **H** is the $N_R \times N_T$ channel transfer matrix and represents the scattering medium. The elements h_{ij} represent the fading coefficient from the ith transmit antenna to the jth receive antenna. **Y** is the L x N_R receive signal matrix where the column index of this matrix corresponds to the receive antenna and the row index to the time index [84]. N is the complex Gaussian noise matrix having independent identically distributed (i.i.d) entries with zero mean and unit variance ($\sigma_n^2 = 1$).

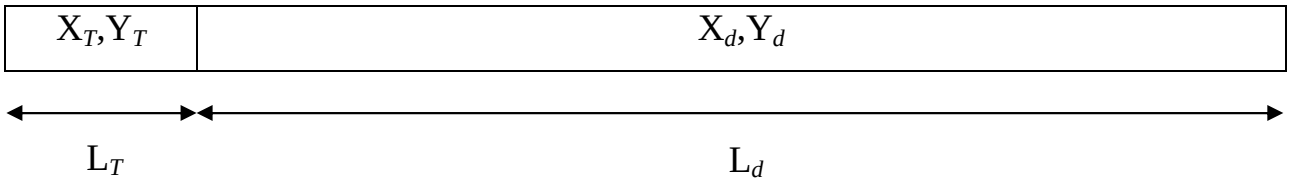

The transmit symbol matrix **X** can be decomposed into

$$\mathbf{X} = \mathbf{X}_T + \mathbf{X}_d \tag{4.2}$$

and the receive symbol matrix Y into

$$\mathbf{Y} = \mathbf{Y}_T + \mathbf{Y}_d, \tag{4.3}$$

where $\mathbf{X}_T$, $\mathbf{Y}_T$ and $\mathbf{X}_d$, $\mathbf{Y}_d$ are the training symbols and data symbols respectively. The block length L can be further decomposed into

$$L = L_T + L_d \tag{4.4}$$

where L_T is the length of training symbols in a block and L_d is the length of data symbols in a block. Let us consider normalized matrix $\overline{\mathbf{X}}_T$ which contains the training symbols only. The optimum training symbol design is based on the orthogonality condition, where the training symbols have to be orthogonal to each other in time and space. The orthogonality condition is given by

$$\overline{\mathbf{X}}_T \overline{\mathbf{X}}_T^H = const.\mathbf{I}_{L_T}, \tag{4.5}$$

where *const* denotes an arbitrary, real, non zero factor. The orthogonality condition minimizes the variance of estimation error. Once the training symbols are received at the receiver, the CSI can be extracted from them in various methods. Two common techniques used for obtaining channel estimates are Least-Square (LS) and MMSE estimation.

$$\hat{\mathbf{H}}_{LS} = (\mathbf{X}_T^H \mathbf{X}_T)^{-1} \mathbf{X}_T^H \mathbf{Y}_T \tag{4.6}$$

$$\hat{\mathbf{H}}_{MMSE} = (\mathbf{X}_T^H \mathbf{X}_T + \sigma_n^2 \mathbf{I}_{N_T})^{-1} \mathbf{X}_T^H \mathbf{Y}_T \tag{4.7}$$

where $\hat{\mathbf{H}}_{LS}$ is the least squares estimate and $\hat{\mathbf{H}}_{MMSE}$ are the channel estimates obtained by MMSE method. After estimation the channel matrix can be decomposed into:

$$\mathbf{H} = \hat{\mathbf{H}} + \tilde{\mathbf{H}} \tag{4.8}$$

Since capacity is the measure of the information that can be reliably transmitted, it is an effective parameter to access the quality of channel estimation. From [84] the channel capacity bound of a block flat fading channel with variable block length and power allocation is given by

$$C_T \geq E\left\{ \frac{L - L_T}{L} \log\det\left(\mathbf{I}_{\mathrm{N_R}} + \frac{\rho_{eff}}{\mathrm{N_T}} \overline{\mathbf{H}}.\overline{\mathbf{H}}^H \right) \right\}, \tag{4.9}$$

where C_T is the channel capacity and $\overline{\mathbf{H}} = \hat{\mathbf{H}} / \sigma_{\hat{\mathbf{H}}}$ is the normalized channel estimate. The above equation is based on optimum power allocation where optimum training power and optimum data power is incorporated into the system through ρ_{eff} which is the effective SNR.

$$\rho_{eff} = \frac{\rho_d \rho_T L_T}{N_T(1+\rho_d) + \rho_T L_T} \tag{4.10}$$

In communication systems one often does not have the luxury of varying the power during training and data phases; therefore, in this work we consider the data and training power to be equal. For equal training and data power, the capacity becomes:

$$C_T \geq E\left\{\frac{L-L_T}{L}\log\det\left(\mathbf{I}_{\mathrm{N_R}}+\frac{\rho^2 L_T/N_T}{1+\left(1+\frac{L_T}{N_T}\right)\rho}\frac{\bar{\mathbf{H}}.\bar{\mathbf{H}}^H}{N_T}\right)\right\}, \tag{4.11}$$

where $\rho_{eff}=\dfrac{\rho^2 L_T/N_T}{1+\left(1+\frac{L_T}{N_T}\right)\rho}$ is the effective SNR when $\rho_d=\rho_T=\rho$.

The transformed received ($\mathbf{Y}_a$) and transmitted ($\mathbf{X}_a$) vectors are given by:

$$\left.\begin{aligned}\mathbf{Y}_a &= F^a\{\mathbf{Y}\}\\ \mathbf{X}_a &= F^a\{\mathbf{X}\}\end{aligned}\right\}, \tag{4.12}$$

where F^a denotes the a[th] order FRFT. (4.12) can be written as:

$$\left.\begin{aligned}\mathbf{Y}_a &= \mathbf{Y}_{T_a}+\mathbf{Y}_{d_a}\\ \mathbf{X}_a &= \mathbf{X}_{T_a}+\mathbf{X}_{d_a}\end{aligned}\right\} \tag{4.13}$$

In the training phase we consider $\mathbf{X}_{T_a}$ and $\mathbf{Y}_{T_a}$, and during the information phase we consider $\mathbf{X}_{d_a}$ and $\mathbf{Y}_{d_a}$. The channel estimation in this work is done using the MMSE method given by eq. (4.7). Channel estimation in the a[th] domain is given by:

$$\hat{\mathbf{H}}_a = \mathbf{W}_a^H\mathbf{Y}_{T_a} \tag{4.14}$$

where $\hat{\mathbf{H}}_a$ is the channel gain estimate in the a[th] fractional domain. For this process, the optimum domain is not calculated in the same way as the proposed received in chapter 3. The parameter 'a' for the fractional Fourier domain is selected to minimize the following cost function [87]:

$$\tilde{J}(\alpha) = \sum_i E\left\{[\mathbf{X}_{T_a}]_i[\mathbf{X}_{T_a}^H]_i\right\} - 2\,\mathrm{Re}\left\{[w_\alpha]_i^H E\left\{[\mathbf{X}_{T_a}]_i[\mathbf{Y}_{T_a}^H]_i\right\}\right\} + [w_\alpha]_i[w_\alpha^H]_i E\left\{[\mathbf{Y}_{T_a}]_i[\mathbf{Y}_{T_a}^H]_i\right\} \tag{4.15}$$

$$[w_\alpha]_i = \frac{E\left\{[\mathbf{X}_{T_a}]_i[\mathbf{Y}_{T_a}^H]_i\right\}}{E\left\{[\mathbf{Y}_{T_a}]_i,[\mathbf{Y}_{T_a}^H]_i\right\}} \tag{4.16}$$

The domain in which the cost function *J* is the optimum domain 'aopt' and the channel estimate in the optimum domain can be obtained using eq. (4.15)

$$[w_{\alpha opt}]_i = \frac{E\left\{[\mathbf{X}_{T_{aopt}}]_i[\mathbf{Y}_{T_{aopt}}^H]_i\right\}}{E\left\{[\mathbf{Y}_{T_{aopt}}]_i,[\mathbf{Y}_{T_{aopt}}^H]_i\right\}} \tag{4.17}$$

$$\hat{\mathbf{H}}_{aopt} = \mathbf{W}_{aopt}^H \mathbf{Y}_{T_{aopt}} \tag{4.18}$$

After obtaining the channel estimate in the optimum fractional Fourier domain according to the MMSE criteria, it is converted back to time domain by using the inverse FRFT operator (F^{-a}).

$$\hat{\mathbf{H}}_{opt} = F^{-aopt}(\hat{\mathbf{H}}_{aopt}) \tag{4.19}$$

The overall process to obtain the channel estimate in the optimum domain can be summarized as:

1. Find the optimum domain 'aopt' using the transmitted and received training symbols by inserting them into eq. (4.15).
2. Find the weight matrix in the optimum domain 'aopt' by using eq. (4.17).
3. Calculate the channel estimate $\hat{\mathbf{H}}_{aopt}$ in the 'aopt' domain and then transform it back to the time domain.

$$\hat{\mathbf{H}}_{opt} = F^{-aopt}\mathbf{W}_{aopt}^H F^{aopt}\mathbf{Y}_T \tag{4.20}$$

Now, the capacity using $\hat{\mathbf{H}}_{opt}$ is given by:

$$C_T \geq E\left\{\frac{L-L_T}{L}\log\det\left(\mathbf{I}_{\mathrm{N_R}}+\frac{\rho^2 L_T/N_T}{1+\left(1+\frac{L_T}{N_T}\right)\rho}\frac{\bar{\mathbf{H}}_{opt}.\bar{\mathbf{H}}_{opt}^{H}}{N_T}\right)\right\} \tag{4.21}$$

To compare the channel estimate obtained in the time domain and optimum domain, the MSE is calculated between the original channel and the estimated channel.

$$\mathrm{MSE}(time)=E\left\{\left\|\mathbf{H}-\hat{\mathbf{H}}\right\|^2\right\} \tag{4.22}$$

$$\mathrm{MSE}(opt)=E\left\{\left\|\mathbf{H}-\hat{\mathbf{H}}_{opt}\right\|^2\right\} \tag{4.23}$$

4.2.1 Simulation Details and Performance Assessment

In this section, firstly we study the performance of the proposed scheme in the low SNR regime. The total number of transmit and receive antennas is taken to be 4. The block length is taken to be 101 and the total number of blocks is 2000. The training symbols are designed according to the orthogonality condition. The channel is assumed to obey the block fading law in which the channel remains constant over the full duration of a transmission block and changes completely and independently for the next block. The fading is considered to be frequency flat and is assumed to follow Rayleigh distribution. Both the fading channel and noise are comprised of i.i.d complex Gaussian random variables CN **(0, 1)**.The value of 'a' is varied from -1 to +1 with a step size of 0.1 and 0.01. The results have been taken for four different values of SNR in the low SNR regime, i.e. -15dB, -10dB, -5dB and 0dB. The step size 0.01 gives better performance but higher computational complexity as compared to step size of 0.1 as step size of 0.01 requires 101 iterations as compared to 0.1 which requires only 21 iterations. The results are presented in the form of MSE vs. 'a'.

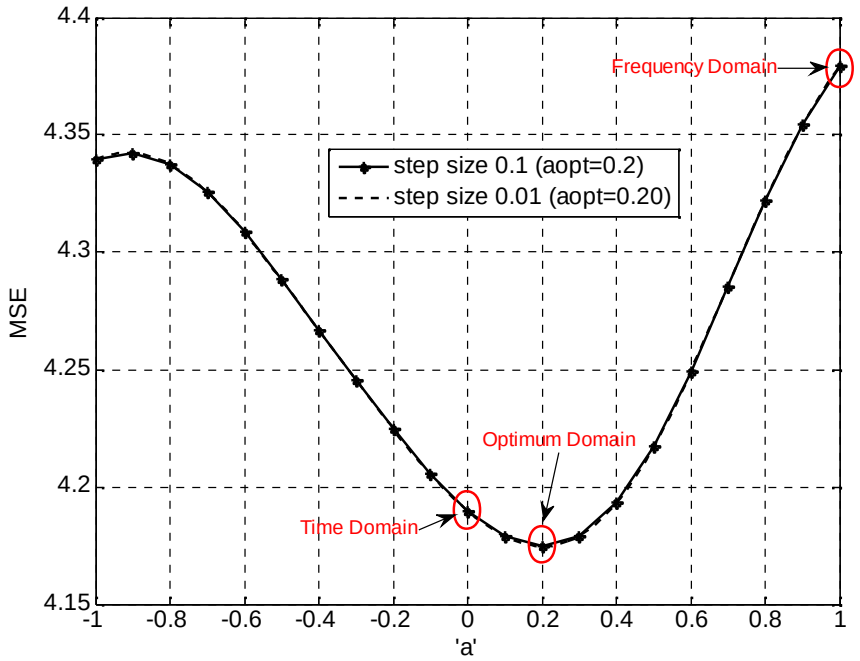

Figure 4.1: MSE vs. 'a' for a fixed SNR of -15dB

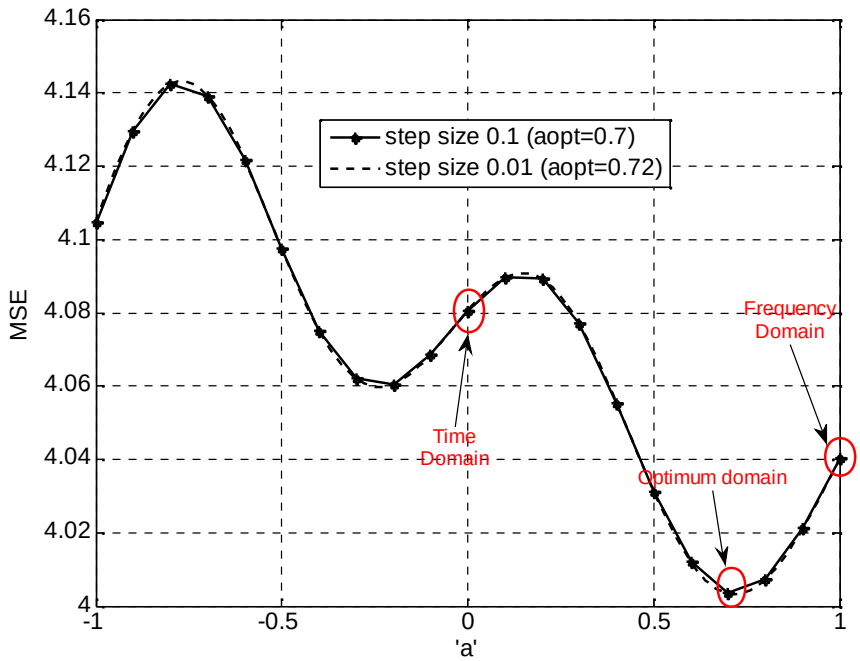

Figure 4.2: MSE vs. 'a' for a fixed SNR of -10dB

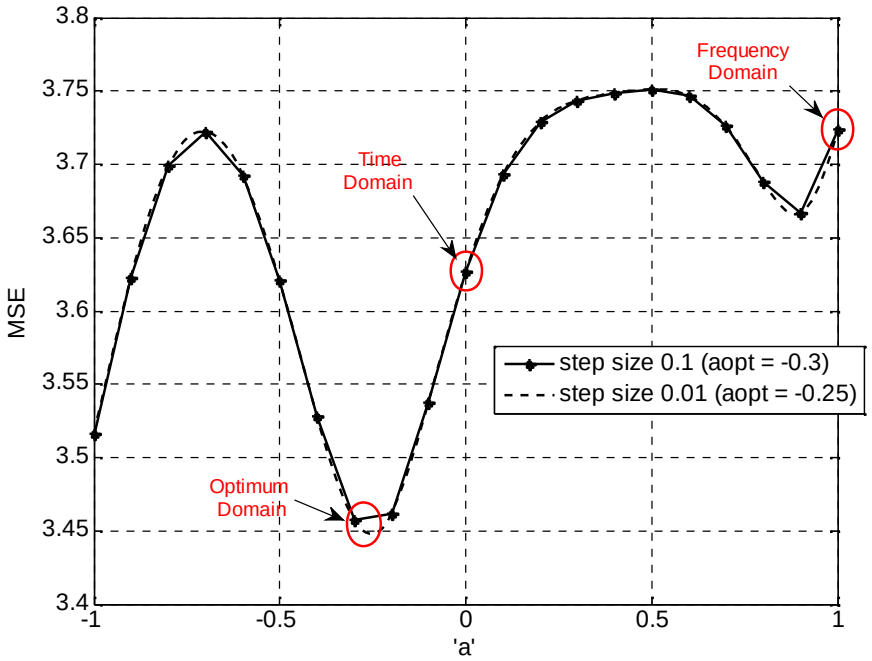

Figure 4.3: MSE vs. 'a' comparison of existing and proposed receiver for 4x4 MIMO system at a fixed SNR of -5dB

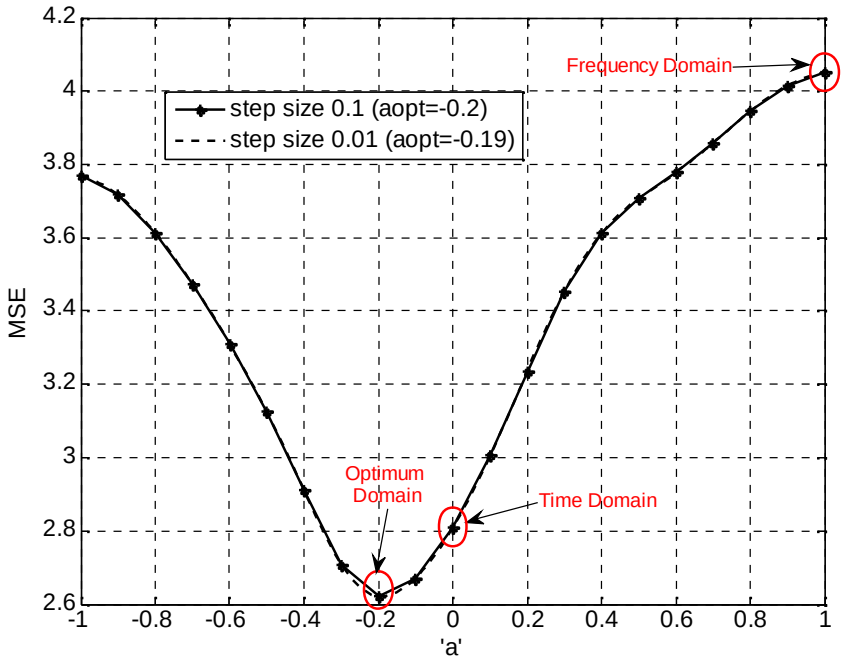

Figure 4.4: MSE vs. 'a' for a fixed SNR of 0dB

It is clear from the above results that the channel estimation in the optimum FRFT domain gives the minimum mean square error and is therefore better than the conventional time domain channel estimation at ‘a’=0. In this work, we have considered channel estimation in the low SNR regime. Due to high level of distortion and noise at low SNR, estimation in the fractional domain effectively helps to reduce the effects of noise. In the optimum domain, the signal appears compact which is otherwise scattered by the presence of noise. After channel estimation, the obtained estimates are used for the equalization process; therefore, the quality of equalization depends on the quality of estimation. Fig. 4.5 shows the BER vs. SNR for 2x2 MIMO system for MMSE equalization using existing CE method, proposed CE method and perfect CSIR with time domain equalization. The MMSE equalization has lower BER when the proposed CE method is used as compared to the existing CE method. BER with perfect CSIR and time domain equalization is also plotted as a reference. Similar results are shown in Fig. 4.6 for a 4x4 system.

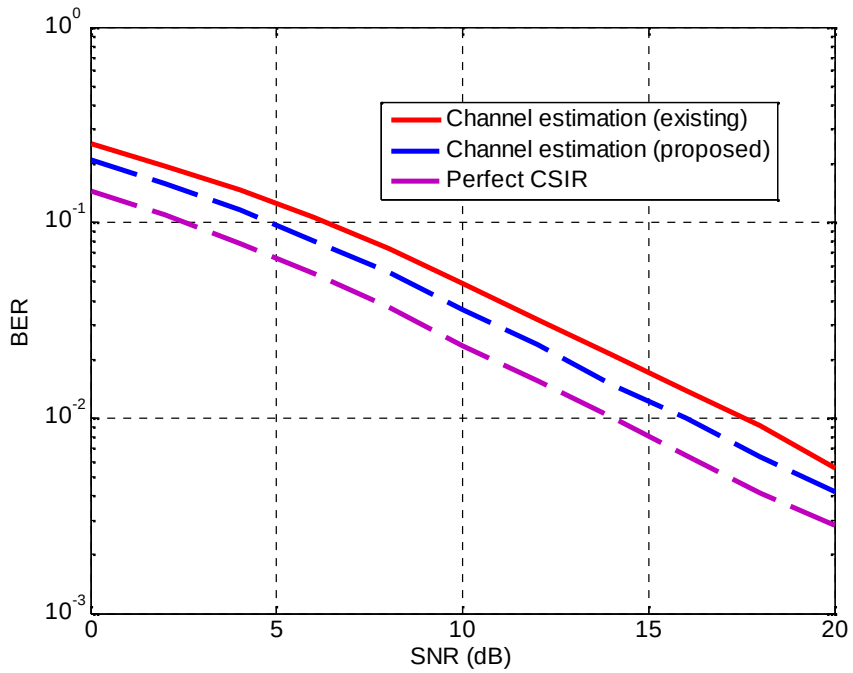

Figure 4.5: BER vs. SNR for MMSE equalization with existing and proposed channel estimation techniques for 2x2 MIMO system in block fading

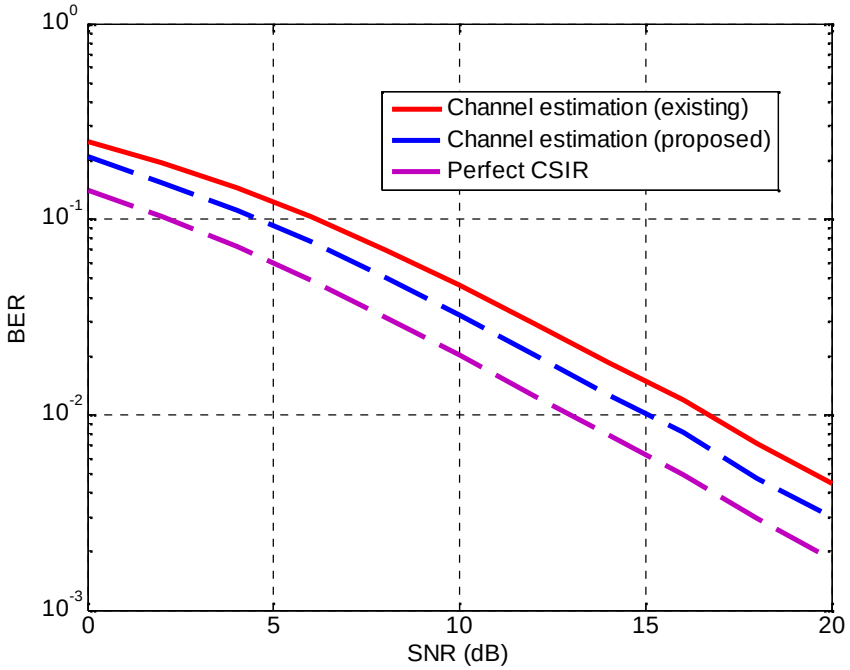

Figure 4.6: BER vs. SNR for MMSE equalization with existing and proposed channel estimation techniques for 4x4 MIMO system in block Rayleigh fading

Table 4.1: Comparison of SNR required by time domain estimation and proposed estimation techniques post MMSE equalization to achieve a fixed BER of 10^{-2}

No. of Antennas	Time Domain (dB)	FRFT (dB)	SNR Advantage (dB)
$N_T=N_R=2$	17.55	16.02	1.53
$N_T=N_R=4$	16.67	15.07	1.6

Fig. 4.7 shows comparison of MSE between the actual channel and the channel estimated by existing and proposed CE schemes in block Rayleigh fading for 2x2 MIMO system. It is observed MSE of the proposed CE schemes is lower than the existing scheme, i.e. the proposed scheme gives better channel estimates as compared to the existing scheme. Fig. 4.8 shows similar results for a 4x4 system.

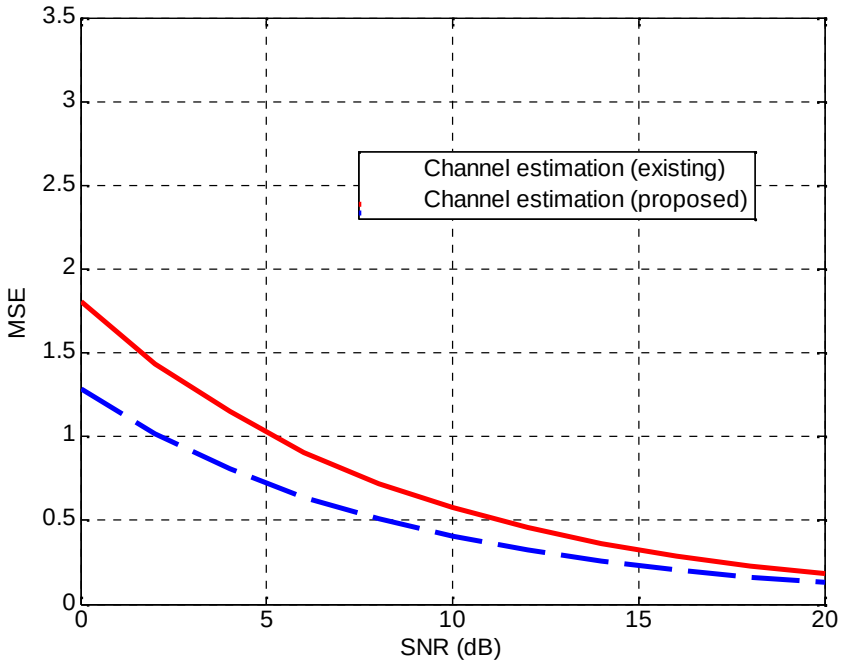

Figure 4.7: Comparison of MSE between the actual channel and estimated channel for $N_T=N_R=2$ in block fading

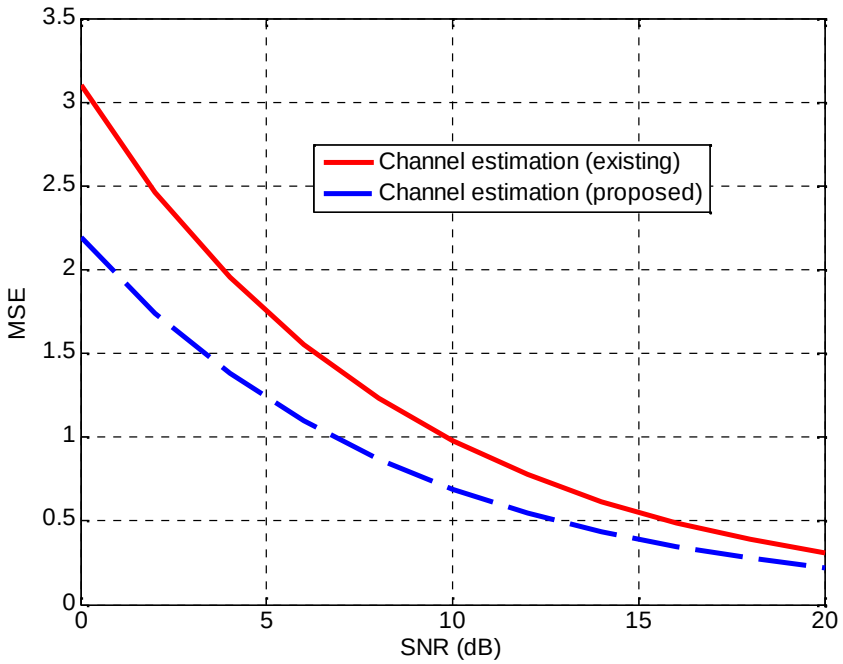

Figure 4.8: Comparison of MSE between the actual channel and estimated channel for $N_T=N_R=4$ in block Rayleigh fading

4.3 Joint Channel Estimation and Equalization in the Fractional Domain

In the previous section, improved channel estimation of block fading channels was proposed. Due, to the property of fractional filtering, that given the statistics of noise and transmitted signal, the optimum domain is calculated only once and can be used arbitrary many times until these statistics change, we propose a Joint Channel Estimation and Equalization process (JCEE). First, the Conventional Joint Estimation and Equalization (CJEE) process in time domain is presented and then it is extended for Optimum Joint Estimation and Equalization (OJEE). We recall the equations from the previous section:

$$\mathbf{X}=\mathbf{X}_T+\mathbf{X}_d$$

$$\mathbf{Y}=\mathbf{Y}_T+\mathbf{Y}_d$$

$$\hat{\mathbf{H}}_{LS}=(\mathbf{X}_T^H\mathbf{X}_T)^{-1}\mathbf{X}_T^H\mathbf{Y}_T$$

$$\hat{\mathbf{H}}_{MMSE}=(\mathbf{X}_T^H\mathbf{X}_T+\sigma_n^2\mathbf{I}_{N_T})^{-1}\mathbf{X}_T^H\mathbf{Y}_T$$

After obtaining the channel estimate $\hat{\mathbf{H}}$, it is used for equalization process:

$$\mathbf{W}=\mathbf{R}_{\mathrm{Y}_d\mathrm{Y}_d}^{-1}\mathbf{R}_{\mathrm{Y}_d\mathrm{X}_d} \tag{4.24}$$

$$\mathbf{R}_{\mathrm{Y}_d\mathrm{Y}_d}=E[\mathbf{Y}_d\mathbf{Y}_d^H]=\hat{\mathbf{H}}\mathbf{R}_{\mathrm{X}_d\mathrm{X}_d}\hat{\mathbf{H}}^H+\mathbf{R}_{\mathrm{NN}} \tag{4.25}$$

$$\mathbf{R}_{\mathrm{Y}_d\mathrm{X}_d}=\mathbf{R}_{\mathrm{X}_d\mathrm{X}_d}\hat{\mathbf{H}}^H \tag{4.26}$$

where $\mathbf{R}_{\mathrm{NN}}=E[\mathbf{N}\mathbf{N}^H]=\sigma_{\mathrm{N}}^2.\mathbf{I}$ and $\mathbf{R}_{\mathrm{XX}}=E[\mathbf{X}\mathbf{X}^H]=\sigma_{\mathrm{X}}^2.\mathbf{I}$

$$\hat{\mathbf{X}}_d=\mathbf{W}^H\mathbf{Y}_d \tag{4.27}$$

$$\mathrm{MSE}=E\left\{\left\|\mathbf{X}_d-\hat{\mathbf{X}}_d\right\|\right\} \tag{4.28}$$

To extend this process for optimum domain filtering, we first obtain the MMSE estimate in the ath domain:

$$\hat{\mathbf{H}}_a=\left(\mathbf{X}_{T_a}^H\mathbf{X}_{T_a}+\sigma_n^2\mathbf{I}_{N_t}\right)^{-1}\mathbf{X}_{T_a}^H\mathbf{Y}_{T_a} \tag{4.29}$$

$$\mathbf{W}_a=\boldsymbol{R}_{\mathbf{Y}_{d_a}\mathbf{Y}_{d_a}}^{-1}\boldsymbol{R}_{\mathbf{Y}_{d_a}\mathbf{Y}_{d_a}} \tag{4.30}$$

$$\boldsymbol{R}_{\mathbf{Y}_{d_a}\mathbf{X}_{d_a}}=\boldsymbol{R}_{\mathbf{X}_{d_a}\mathbf{X}_{d_a}}\hat{\mathbf{H}}_a^H \tag{4.31}$$

$$\boldsymbol{R}_{\mathbf{Y}_{d_a}\mathbf{Y}_{d_a}} = \hat{\mathbf{H}}_a \boldsymbol{R}_{\mathbf{X}_{d_a}\mathbf{X}_{d_a}} \hat{\mathbf{H}}_a^H + \boldsymbol{R}_{\mathbf{N}_{d_a}\mathbf{N}_{d_a}} \tag{4.32}$$

$$\hat{\mathbf{X}}_{d_a} = F^{-a}\left\{\mathbf{W}_a^H \mathbf{Y}_{d_a}\right\} \tag{4.33}$$

$$MSE(\mathbf{W}_a) = E\left\{\left\|\mathbf{X}_d - F^{-a}\left\{\mathbf{W}_a^H \mathbf{Y}_{d_a}\right\}\right\|^2\right\} \tag{4.34}$$

Once the optimum value 'a_{opt}' is calculated, it can be used for arbitrary many realizations of that signal and noise statistics. After the initial calculation, 'a' in all the equations will be replaced by 'a_{opt}'. The comparison of BER for CJEE, OJEE and MMSE equalization with perfect CSIR for 2x2 and 4x4 system is shown in Fig. 4.9 and 4.10 respectively. The OJEE clearly outperforms the CJEE technique. The BER of OJEE technique is very close to the JEE with perfect CSIR which is indicative of the advantages of filtering in the optimum fractional domain.

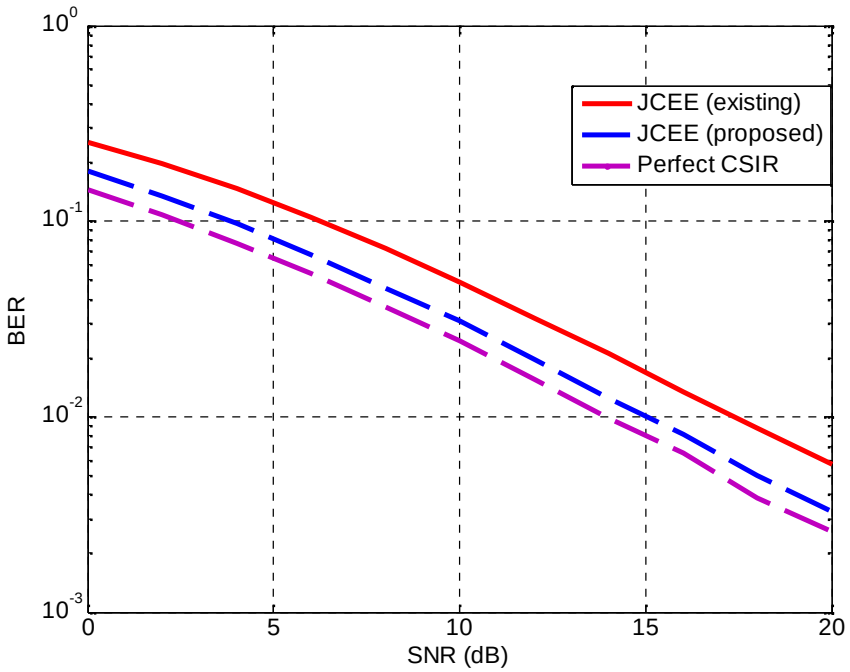

Figure 4.9: BER vs. SNR for joint channel estimation and equalization with existing and proposed techniques for N_T=N_R=2 in Rayleigh fading

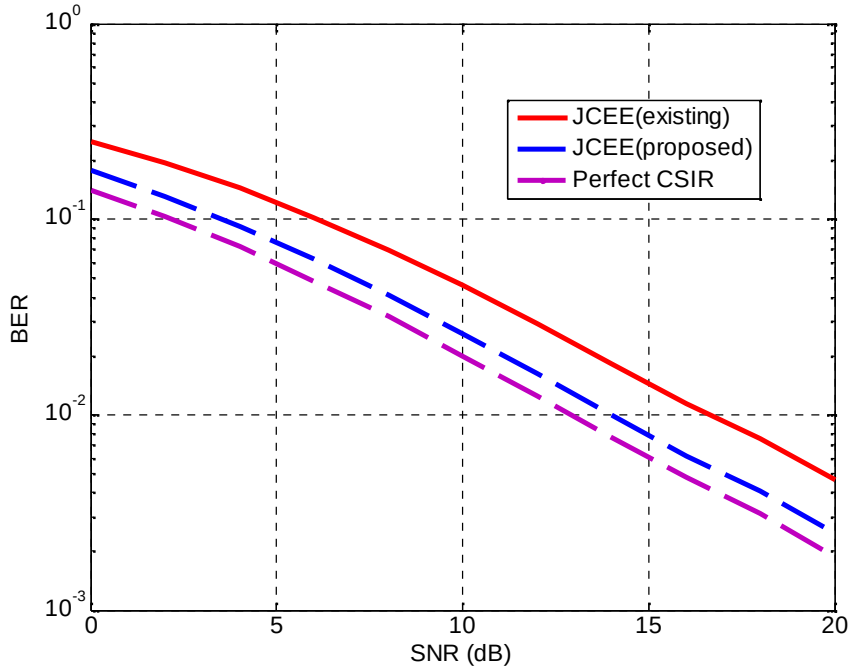

Figure 4.10: BER vs. SNR for joint channel estimation and equalization with existing and proposed techniques for $N_T=N_R=4$ in Rayleigh fading

Table 4.2: Comparison of SNR of JCEE (existing) and JCEE (proposed) to achieve a fixed BER=10^{-2}

No. of Antennas	Time Domain (dB)	FRFT (dB)	SNR Advantage (dB)
$N_T=N_R=2$	17.36	15.03	2.33
$N_T=N_R=4$	16.64	14	2.64

4.4 Channel Estimation for Fast Fading Channels

In the previous section, channel estimation for block fading channels was considered. Estimation of block fading requires less training as the fading channel remains constant for a complete transmission block. However, estimating a channel which is fading rapidly is a more difficult proposition because it requires constant monitoring. The channel response can be obtained at the receiver by using Pilot Symbol Assisted Modulation (PSAM), in which the transmitter periodically inserts pilots (known symbols) into the information stream. These pilot symbols can be recovered and used at the receiver to obtain an estimate of the channel response. The channel may have changed from the pilot symbol time instant to the data symbol time instant, therefore, the channel gain at the data symbol is estimated using multiple pilot symbols and an

interpolation filter. The interpolation filter helps to construct the channel response at data points with the help of discrete set of known channel response at the pilot points. The estimates obtained by interpolation are valid because of the time correlation of the fading channel. In practice, the channel estimation is never perfect and errors due to noise are always present in the estimated channel response. If a technique can be found to reduce these errors, the overall quality of the interpolated channel estimates can be improved. The basics of existing PSAM technique are discussed in the following section.

4.4.1 Pilot Symbol Assisted Modulation (PSAM)

The block diagram of a conventional PSAM system is shown in Fig. 4.11. The symbols are transmitted in frames of length N. Without loss of generality, assume that, in each frame, the first symbol is a pilot symbol $b(0)$, and the remaining $N-1$ symbols are the data symbols $b(1), b(2) \ldots b(N-1)$.

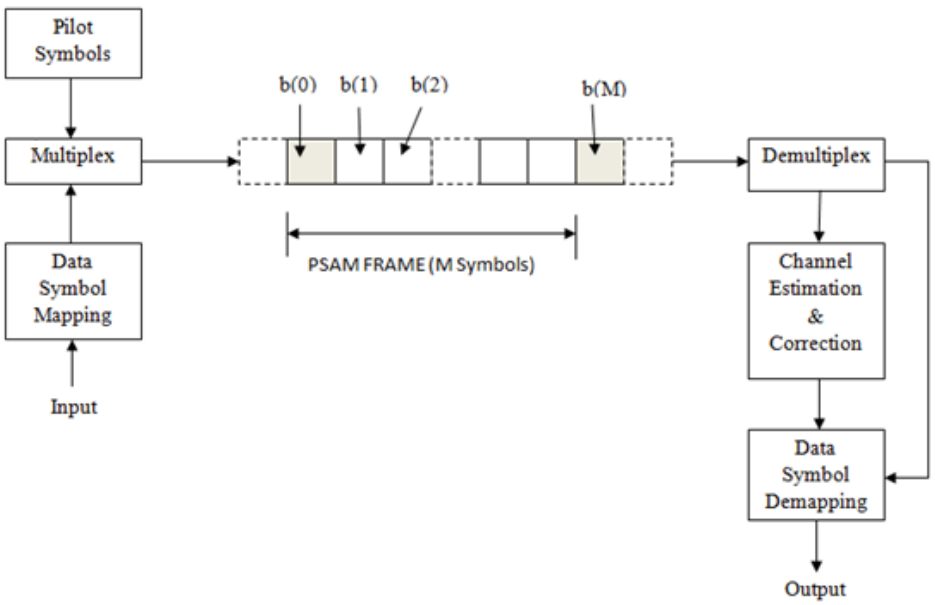

Figure 4.11: Schematic of conventional PSAM System showing the frame structure [83]

The data symbols are modulated by Gray coded 16-QAM; therefore, the data symbol belongs to the set of 16 possible signals. The pilot symbols have a fixed value $\tilde{b}$ which is known to the receiver. The transmitted signal has a complex envelope given by:

$$x(t) = \sum_{k=-\infty}^{\infty} b(k)\, p(t - kT) \tag{4.35}$$

where T is the symbol duration, $b(k)$ represents the In-phase or Quadrature components of the symbols to be transmitted and $p(t)$ is a band limited unit energy signaling pulse, for which we have:

$$\int_{-\infty}^{\infty} |p(t)|^2 \, dt = 1 \tag{4.36}$$

The received signal for a narrowband Rayleigh channel is given by:

$$y(t) = h(t)x(t) + n(t), \tag{4.37}$$

where n(t) is AWGN with variance $\sigma_n^2 = N_0 / 2$ and c(t) is the complex channel gain.

$$h(t) = \alpha(t)e^{j\theta(t)}, \tag{4.38}$$

where $\alpha(t)$ is the Rayleigh fading envelope and $\theta(t)$ is the uniformly distributed phase. The output of the matched filter at sampling instant kT is given by:

$$y(k) = h(k).x(k) + n(k) \tag{4.39}$$

The pilot symbols are inserted at times $i = kN$, therefore, the pilot symbols are represented by $y(iN)$ and the estimated channel response $\hat{h}(iN)$ at the pilot positions is calculated by:

$$\hat{h}(iN) = y(iN) / \tilde{b} \tag{4.40}$$

$$\hat{h}(iN) = h(iN) + \frac{n(iN)}{\tilde{b}} \tag{4.41}$$

$$\hat{h}(iN) = \hat{\alpha}(iN)e^{j\hat{\theta}(iN)}, \tag{4.42}$$

where $\hat{\alpha}(iN)$ is the estimated fading channel envelope and $\hat{\theta}(iN)$ is the estimated phase. From the above expression, it is clear that the channel estimate at pilot positions is affected by noise errors i.e. $n(iN) / \tilde{b}$. The channel response at the data symbol positions is obtained by interpolating the

sequence $\hat{h}(iN)$. The channel state estimator prepares an estimate of $\hat{h}(k)$ using the K nearest pilot symbols:

$$\hat{h}(k) = \sum_{i=-\lfloor K/2 \rfloor}^{\lfloor K/2 \rfloor} g^{*}(i,k)\hat{h}(iN) \tag{4.43}$$

where $g(i,k)$ are the interpolation coefficients which explicitly depend on position k within the frame. The estimation error $e(k)$ is given by:

$$e(k) = h(k) - \hat{h}(k) \tag{4.44}$$

From eq. (4.43) we can see that the accurate estimation of $\hat{h}(k)$ depends on the quality of $\hat{h}(iN)$. The noise component in eq. (4.41) contributes a large percentage of the estimation error especially at low SNR. Hence, any reasonable system that can improve $\hat{h}(iN)$ and reduce $e(k)$ will improve $h(k)$. One such system is the FRFT based PSAM (FPSAM) in which the received pilot symbols $y(iN)$ are processed in the fractional Fourier domain before channel estimation is performed. By processing $y(iN)$ in the fractional domain, the effect of noise on the pilot symbols is minimized and therefore the estimation error $e(k)$ is reduced. The motivation behind the proposed method is the ability of FRFT to reduce the effect of noise on the received symbols. A detailed description of FPSAM is given in the following section.

4.4.2 Fractional Fourier Transform based PSAM (FPSAM)

Define the length K column vectors $\boldsymbol{y}$ and $\boldsymbol{x}$ as the set of received pilot samples $y(iN)$ and transmitted pilot samples $x(iN)$. Also, define the length K column vector $\boldsymbol{h}$ as the set of channel coefficients at pilot positions. Fig. 4.12(a) shows the block diagram of FPSAM and Fig. 4.12(b) shows the internal diagram of the fractional domain processing block.

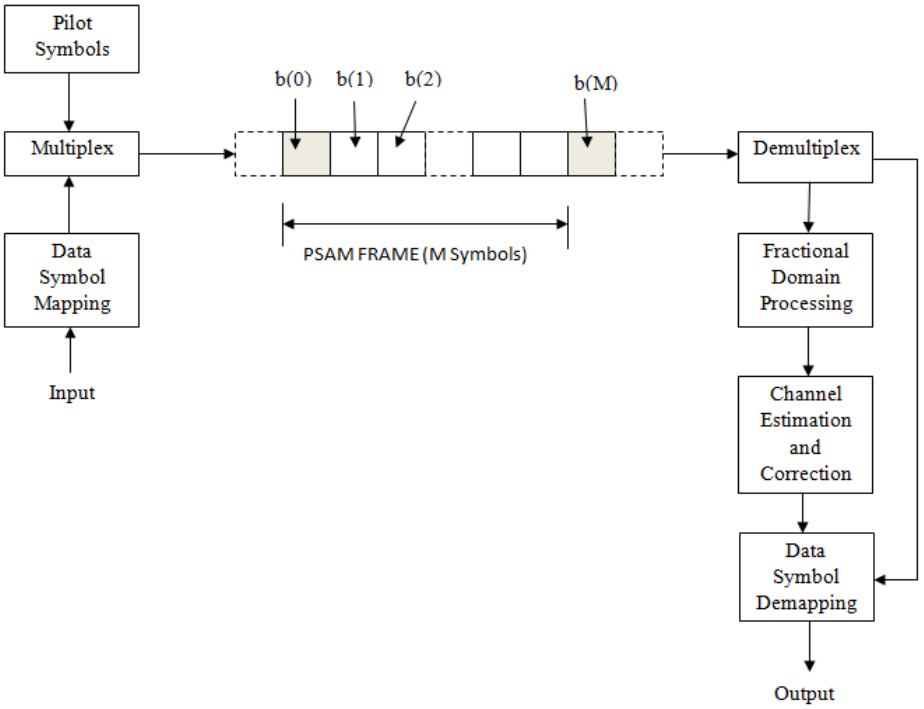

Figure 4.12(a): Schematic of FPSAM system showing the frame structure

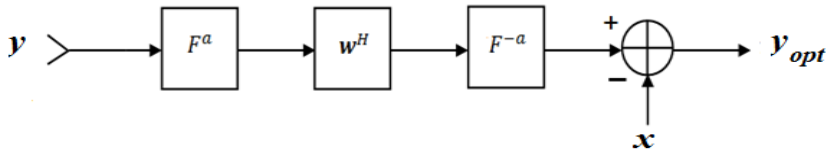

Figure 4.12(b): Internal diagram of fractional domain processing block

The transmitted and received pilot symbol vectors $\boldsymbol{x}$ and $\boldsymbol{y}$ are transformed from time domain to the fractional Fourier domain by using the transformation operator F^a

$$\boldsymbol{y}_a = F^a\{\boldsymbol{y}\} \tag{4.45}$$

$$\boldsymbol{x}_a = F^a\{\boldsymbol{x}\} \tag{4.46}$$

After $\boldsymbol{y}_a$ is obtained, the filtering process is performed using the Wiener filtering technique already discussed in chapter 2.

$$\boldsymbol{w}_a = \boldsymbol{R}_{y_a y_a}^{-1} \boldsymbol{R}_{y_a x_a} \tag{4.47}$$

where $\boldsymbol{w}_a$ is the weight vector in the ath domain, $\boldsymbol{R}_{y_a y_a}$ is the auto covariance of the vector $\boldsymbol{y}$ in the ath domain and $\boldsymbol{R}_{y_a x_a}$ is the cross covariance of $\boldsymbol{y}$ and $\boldsymbol{x}$ in the ath domain.

The optimum value of 'a' is found by minimizing the MSE for 'a' $\in [-1,1]$. The MSE is calculated by:

$$MSE(\boldsymbol{w}_a) = E\left\{\left\|\boldsymbol{x} - \boldsymbol{F}^{-a}\boldsymbol{w}_a^H \boldsymbol{F}^a \boldsymbol{y}\right\|^2\right\} \tag{4.48}$$

where E {*} denotes the expectation operator and $\|*\|$ is the L_2 norm. After the optimum order is calculated, the weight vector is calculated in the optimum domain using eq. (4.47). The weight vector calculated in the optimum domain (a_{opt}) is called optimum weight vector $(\boldsymbol{w}_{opt})$.

$$\boldsymbol{w}_{opt} = \boldsymbol{R}^{-1}_{y_{aopt}y_{aopt}} \boldsymbol{R}_{y_{aopt}x_{aopt}} \tag{4.49}$$

After Wiener filtering in the optimum domain, the signal is converted back to its original domain by using inverse FrFT. After optimum domain filtering, the effect of AWGN on $\boldsymbol{y}$ is minimized, therefore, it is denoted by $\boldsymbol{y}_{opt}$.

$$\boldsymbol{y}_{opt} = \boldsymbol{F}^{-a}\left\{\boldsymbol{w}_{opt}^H \left(F^a\left\{\boldsymbol{y}\right\}\right)\right\} \tag{4.50}$$

The MSE given by eq. (4.48) is minimum for $\boldsymbol{w}_a = \boldsymbol{w}_{opt}$. As discussed above, the value of 'a' which minimizes the MSE is chosen to be optimum. Also, the accuracy of 'a_{opt}' depends on the step size of the discrete values of 'a', e.g. in this study the step size is taken to be 0.1. After $\boldsymbol{y}_{opt}$ is obtained, the CSI at the pilot positions can be calculated for $\boldsymbol{y}_{opt}$ using eq. (4.40).

$$\hat{h}_{opt}(iN) = \frac{y_{opt}(iN)}{\tilde{b}}, \tag{4.51}$$

where $\hat{h}_{opt}(iN)$ is the optimum CSI at pilot positions. In terms of optimum estimated envelope $(\hat{\alpha}_{opt})$ and phase $(\hat{\theta}_{opt})$, $\hat{h}_{opt}(iN)$ is given by

$$\hat{h}_{opt}(iN) = \hat{\alpha}_{opt}(iN)e^{j\hat{\theta}_{opt}(iN)} \tag{4.52}$$

Channel Interpolation: After the estimation of the channel response at the pilot positions, the channel response at data positions can be obtained by interpolating $\hat{h}_{opt}(iN)$ using eq. (4.43).

$$\hat{h}_{opt}(k) = \sum_{i=-\lfloor K/2 \rfloor}^{\lfloor K/2 \rfloor} g^*(i,k)\hat{h}_{opt}(iN) \tag{4.53}$$

where $\hat{h}_{opt}(k)$ is the optimum estimated channel with estimated envelope $\hat{\alpha}_{opt}$ and phase $\hat{\theta}_{opt}$. In terms of $\hat{\alpha}_{opt}$ and $\hat{\theta}_{opt}$, $\hat{h}_{opt}(k)$ is given by

$$\hat{h}_{opt}(k) = \hat{\alpha}_{opt}(k) e^{j\hat{\theta}_{opt}(k)} \tag{4.54}$$

In eq. (4.53) the term $g^*(i,k)$ denotes the interpolation coefficients. These coefficients explicitly depend on the position of k within the frame. The interpolation techniques which have been used in this study to obtain $g^*(i,k)$ are listed below:

1. Linear Interpolation
2. Spline Interpolation
3. FFT interpolation

4.4.3 Results and Discussion

The details of simulation and the performance comparison of the proposed channel estimation technique with the existing estimation techniques are done in this section.

4.4.3.1 Simulation Details

The number of information bits is taken as 1593. The frame length (*N*) is 10 and the first symbol in each frame is a known pilot symbol. The number of pilot symbols is 177 and the total number of transmitted symbols (data symbols + pilot symbols) is 1770. The modulation scheme used is Gray-coded 16-QAM. The channel is considered to be flat Rayleigh faded and noise is modeled as additive white Gaussian noise. Both the fading channel and noise are comprised of i.i.d complex Gaussian random variables $\mathcal{CN}(\mathbf{0}, \mathbf{1})$. The value of FRFT order 'a' is varied from $-1$to $+1$ with a step size of 0.1. A total of 21 values of 'a' are investigated, selecting the one which gives the minimum MSE. For finding the BER, the SNR is varied from 0 to 40 dB in a step of 1 dB with 500 iterations done on each value of SNR to give statistically justified results. Three interpolation techniques, namely, linear, spline and FFT interpolation have been used for simulations. All the simulations have been done using *MATLAB*.

4.4.3.2 Performance Comparison

In this section, a method to improve channel estimation of fast fading channels by filtering the received pilot symbols in optimum fractional Fourier domain has been presented. In conventional PSAM, the received pilots are used for channel estimation without any kind of processing, which results in inaccurate channel estimation. This inaccurate channel estimation is due to the errors in the pilot signals due to noise in the channel. Hence, if the errors due to noise can be reduced, the quality of channel estimation can be improved. Fig. 4.13 shows the BER vs. SNR performance of PSAM and FPSAM for spline interpolation technique. In the figure, the PSAM technique is indicated by the solid red line and the FPSAM technique is represented by the dashed blue line. It is seen that the proposed method gives lower BER at all SNRs as compared to PSAM. Fig. 4.14 and 4.15 show similar results for FFT and linear interpolation techniques respectively.

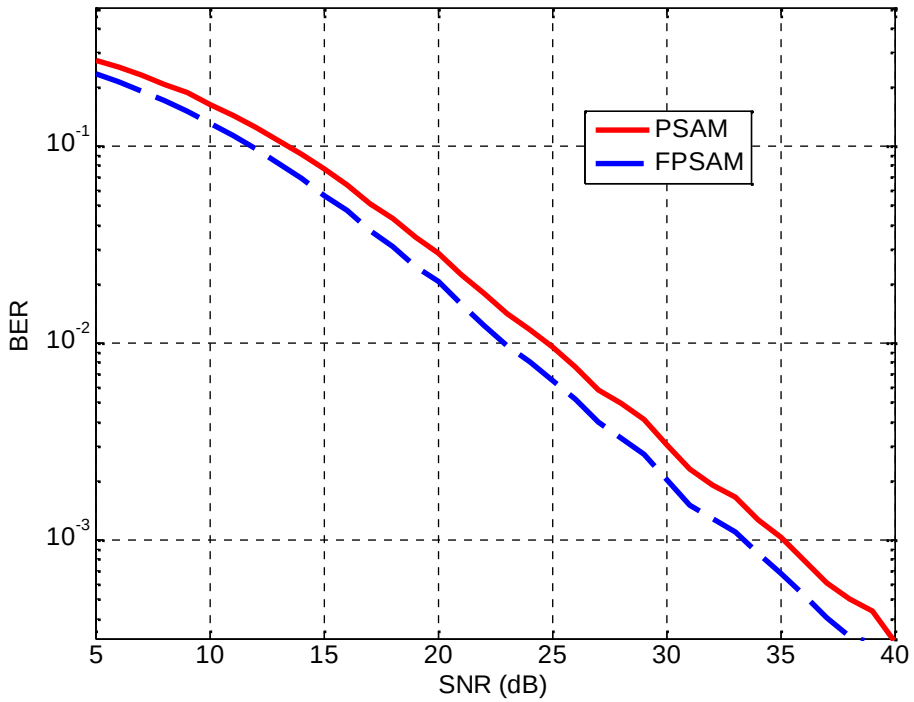

Figure 4.13: BER vs. SNR for PSAM and FPSAM using spline interpolation

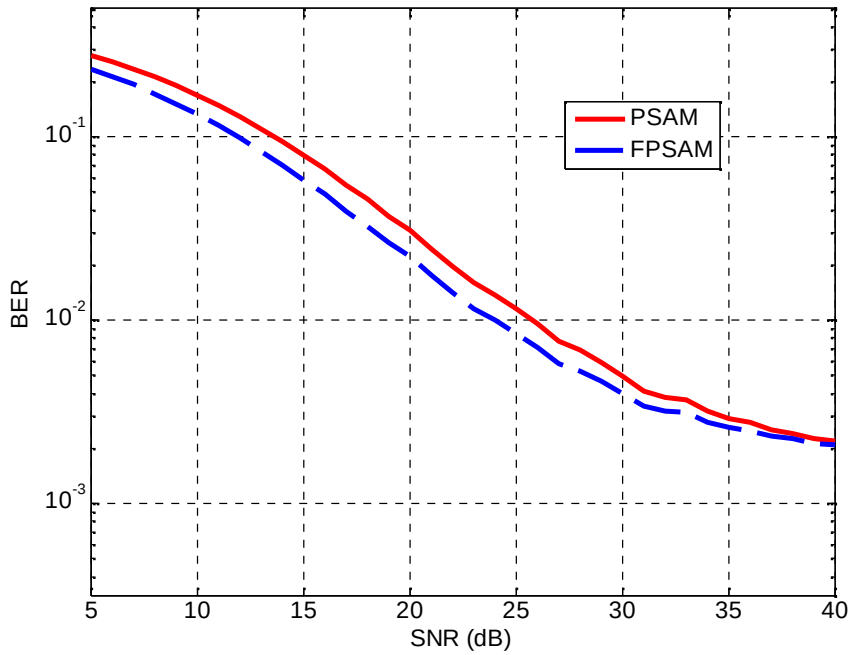

Figure 4.14: BER vs. SNR for PSAM and FPSAM using FFT interpolation

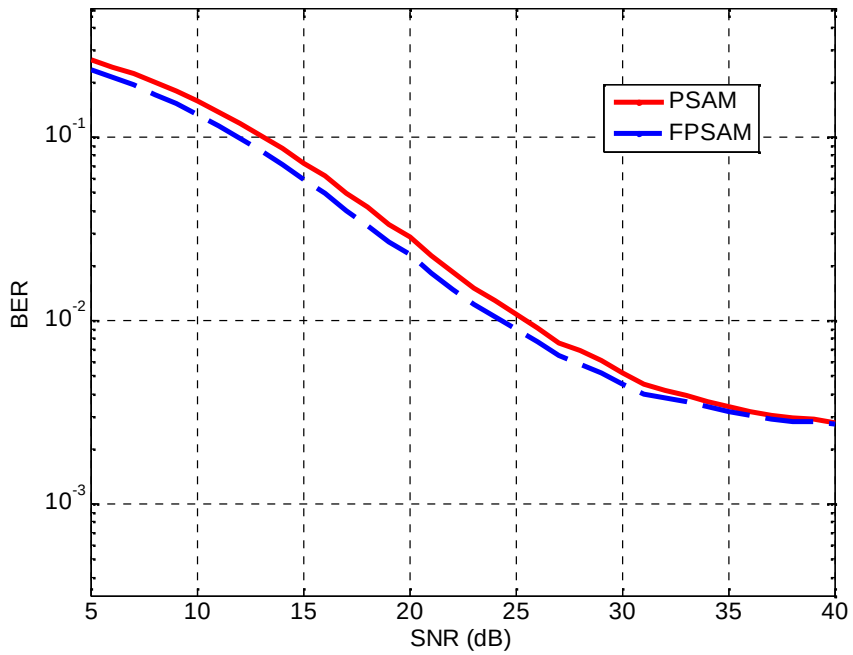

Figure 4.15: BER vs. SNR for PSAM and FPSAM using linear interpolation

The results shown in Fig. 4.13, 4.14 and 4.15 are summarized in Tables 4.1, 4.2 and 4.3. Tables 4.1 and 4.2 compare the BER of two techniques for fixed SNRs of 10 and 15 dB. It is seen that as compared to PSAM, lower BER can be achieved by using FPSAM for same SNR. Also, Table 4.3 compares the SNR for a fixed BER of 10^{-2} and it is shown that the proposed technique gives an SNR advantage in all the three cases.

Table 4.1: BER improvement of FPSAM over PSAM for a fixed SNR of 10 dB

Technique	Linear (BER)	FFT (BER)	Spline (BER)
CPSAM	0.1571	0.1682	0.1642
FPSAM ($a = 0.3$)	0.1330	0.1322	0.1312

Table 4.2: BER improvement of FPSAM over PSAM for a fixed SNR of 15 dB

Technique	Linear (BER)	FFT (BER)	Spline (BER)
CPSAM	0.0726	0.0796	0.0764
FPSAM ($a = -0.2$)	0.0587	0.0581	0.0566

Table 4.3: SNR improvement of FPSAM over PSAM for a fixed BER of 10^{-2}

Technique	Linear (SNR)	FFT (SNR)	Spline (SNR)
CPSAM	25.49	25.73	24.79
FPSAM	24.32	23.99	22.89

The effect of AWGN and fading on the transmitted signal is shown in Fig. 4.16. The signal appears to be completely scattered and the information carried by it is unintelligible in this form. This scattering of the received signal is due to presence of fading and noise. To demodulate this signal properly, accurate channel estimates at the data positions are required. These estimates are obtained by interpolating the channel response at pilot positions. The quality of the demodulation depends on the accuracy of the channel estimation. Fig. 4.17 compares the PSAM demodulated signal with the FPSAM demodulated signal. The results in Fig. 4.17 are obtained for linear interpolation at a fixed SNR of 30 dB. The signal demodulated using the estimates obtained by FPSAM appears to be compact whereas the signal obtained by using channel estimates obtained for PSAM appears to be scattered.

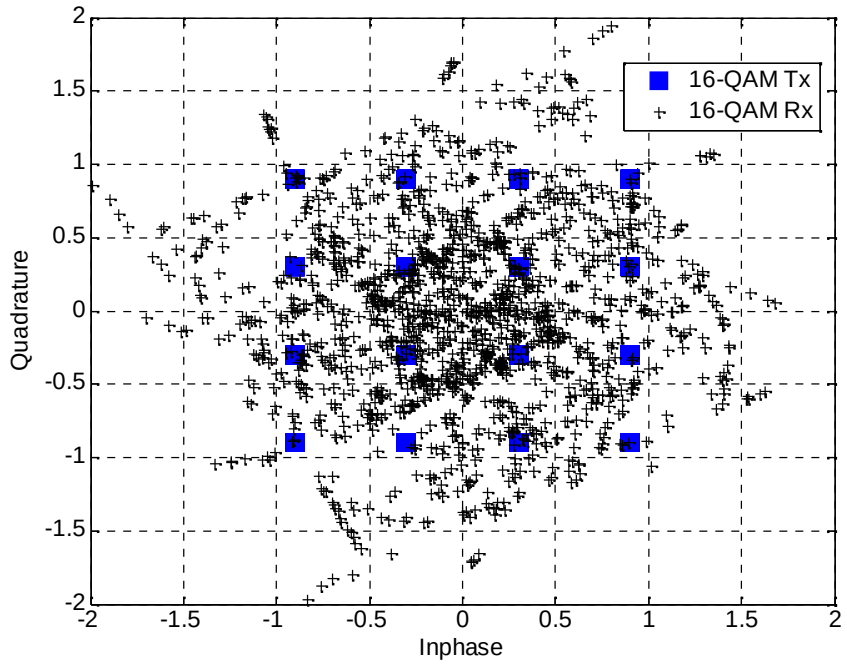

Figure 4.16: Comparison of transmitted 16-QAM signal with received 16-QAM signal (before demodulation) distorted by noise and fading at a fixed SNR of 20dB

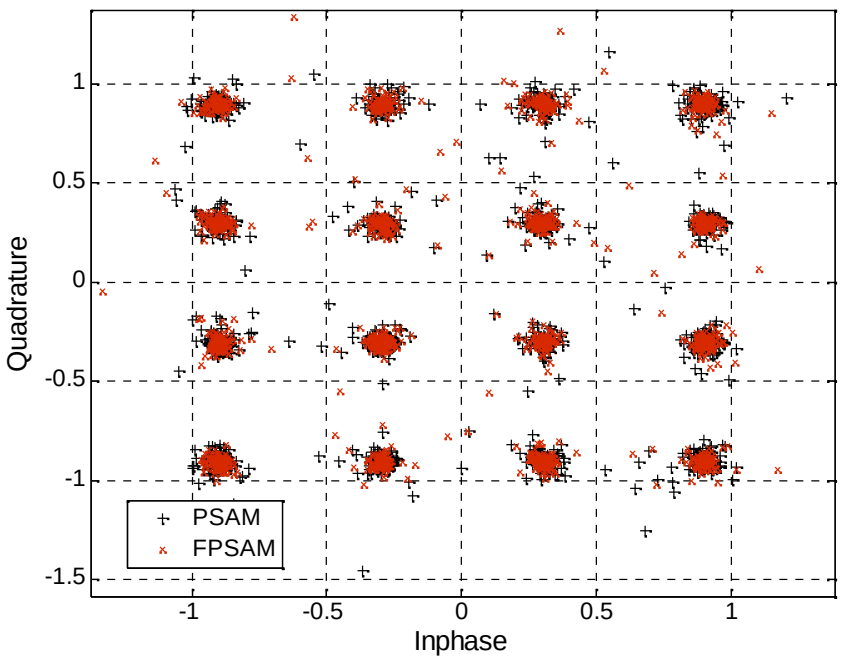

Figure 4.17: Demodulated 16-QAM for PSAM and FPSAM using linear interpolation

4.4.4 Extension of FPSAM to MIMO systems

Since, the PSAM technique is valid due to the temporal correlation of the fading channels; the proposed technique is valid for both single and multiple antenna systems. For simplicity and loss of generality, we take an example of a 2×2 MIMO system to explain the concept of PSAM. This can be generalized for any number of transmit or receive antennas. At any time t, the channel **H** can be represented as:

$$\mathbf{H}(\mathrm{t}) = \begin{bmatrix} h_{11}(t) & h_{12}(t) \\ h_{21}(t) & h_{22}(t) \end{bmatrix} \tag{4.55}$$

Due to fast fading, the elements of **H** change rapidly and independently. Therefore, it is hard to predict the elements of **H** together as a matrix by using interpolation. After receiving the pilot symbols which are time multiplexed with the data, each element of **H** has to be estimated independently as a vector by using interpolation. Fig. 16-21 show the actual and estimated values of vector $\boldsymbol{h}_{12}$ of **H** matrix.

$$\boldsymbol{h}_{11} = \begin{bmatrix} h_{11}(1) & h_{11}(2) & h_{11}(3) & \cdots & h_{11}(\mathrm{N}) \end{bmatrix} \tag{4.56}$$

$$\boldsymbol{h}_{12} = \begin{bmatrix} h_{12}(1) & h_{12}(2) & h_{12}(3) & \cdots & h_{12}(\mathrm{N}) \end{bmatrix} \tag{4.57}$$

$$\boldsymbol{h}_{21} = \begin{bmatrix} h_{21}(1) & h_{21}(2) & h_{21}(3) & \cdots & h_{21}(\mathrm{N}) \end{bmatrix} \tag{4.58}$$

$$\boldsymbol{h}_{22} = \begin{bmatrix} h_{22}(1) & h_{22}(2) & h_{22}(3) & \cdots & h_{22}(\mathrm{N}) \end{bmatrix} \tag{4.59}$$

$$\mathbf{H}(1) = \begin{bmatrix} h_{11}(1) & h_{12}(1) \\ h_{21}(1) & h_{22}(1) \end{bmatrix} \tag{4.60}$$

$$\mathbf{H}(2) = \begin{bmatrix} h_{11}(2) & h_{12}(2) \\ h_{21}(2) & h_{22}(2) \end{bmatrix} \tag{4.61}$$

$$\vdots$$

$$\mathbf{H}(\mathrm{N}) = \begin{bmatrix} h_{11}(\mathrm{N}) & h_{12}(\mathrm{N}) \\ h_{21}(\mathrm{N}) & h_{22}(\mathrm{N}) \end{bmatrix} \tag{4.62}$$

From the above discussion it is clear that the elements $\boldsymbol{h}_{11}$, $\boldsymbol{h}_{12}$, $\boldsymbol{h}_{21}$ and $\boldsymbol{h}_{22}$ have to be estimated

independently as vectors just as if we are estimating a SISO channel. After interpolation, they can be recombined to form a channel matrix and used for equalization. Therefore, the proposed FPSAM technique can be easily implemented to any wireless system that uses PSAM and is valid for both single and multiple antenna systems. To verify the quality of channel estimation, the estimates obtained by conventional PSAM (CPSAM) and FPSAM using different interpolation techniques are compared for a fixed SNR of 20 dB in Fig. 4.18-4.23. From the results it is observed that the fading envelope estimated by FPSAM is closer to the actual channel envelope than the envelope estimated by CPSAM. This indicates that the quality of channel estimates obtained by using the proposed FPSAM technique is better than the quality of channel estimates obtained by using the existing PSAM technique.

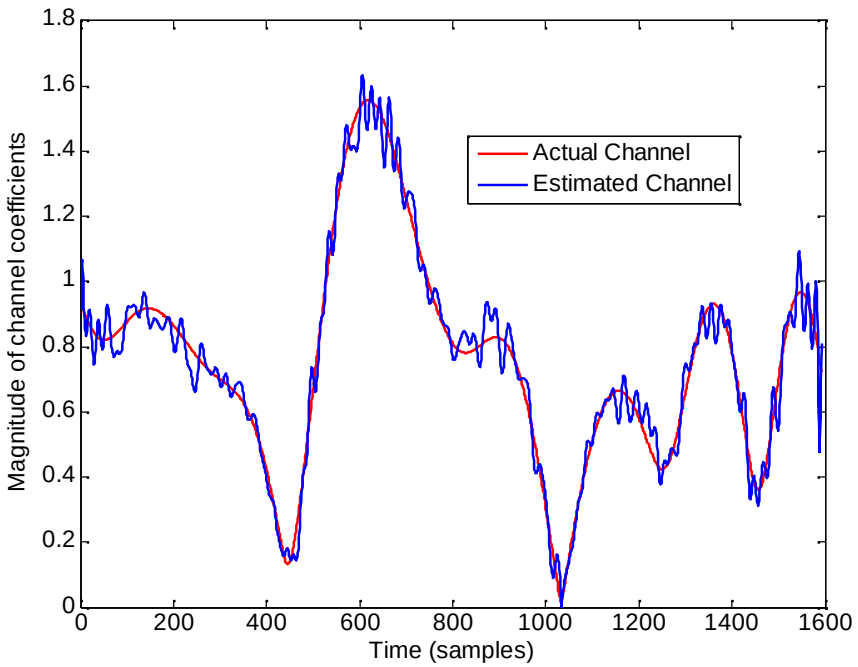

Figure 4.18: Actual channel vs. estimated channel using FFT interpolation for CPSAM at a fixed SNR of 20 dB

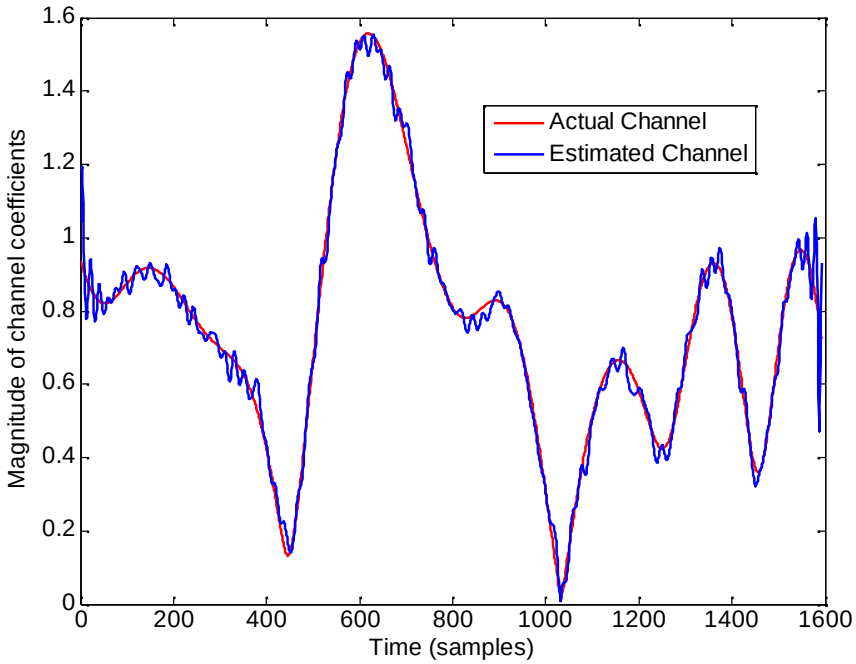

Figure 4.19: Actual channel vs. estimated channel using FFT interpolation for FPSAM at a fixed SNR of 20 dB

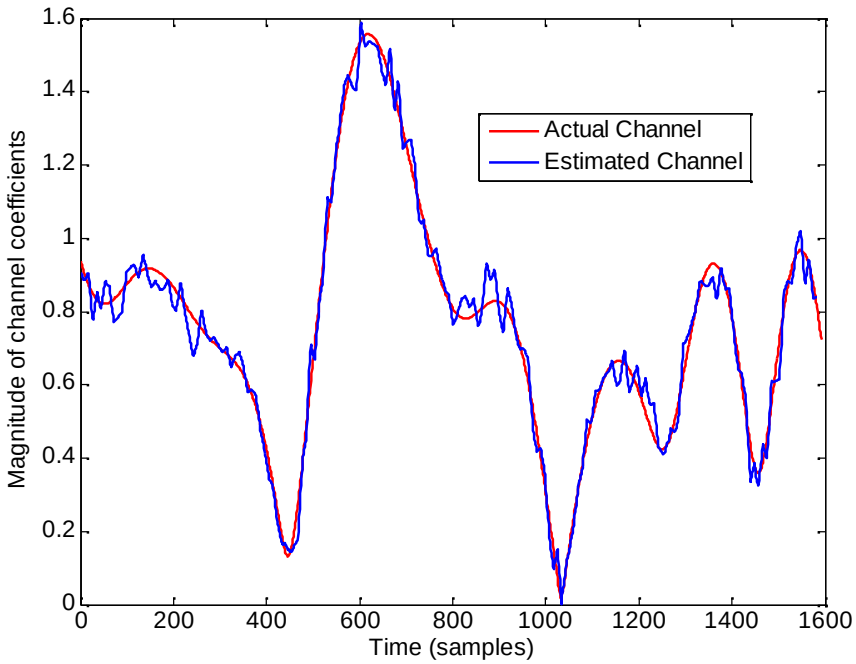

Figure 4.20: Actual channel vs. estimated channel using linear interpolation for CPSAM at a fixed SNR of 20 dB

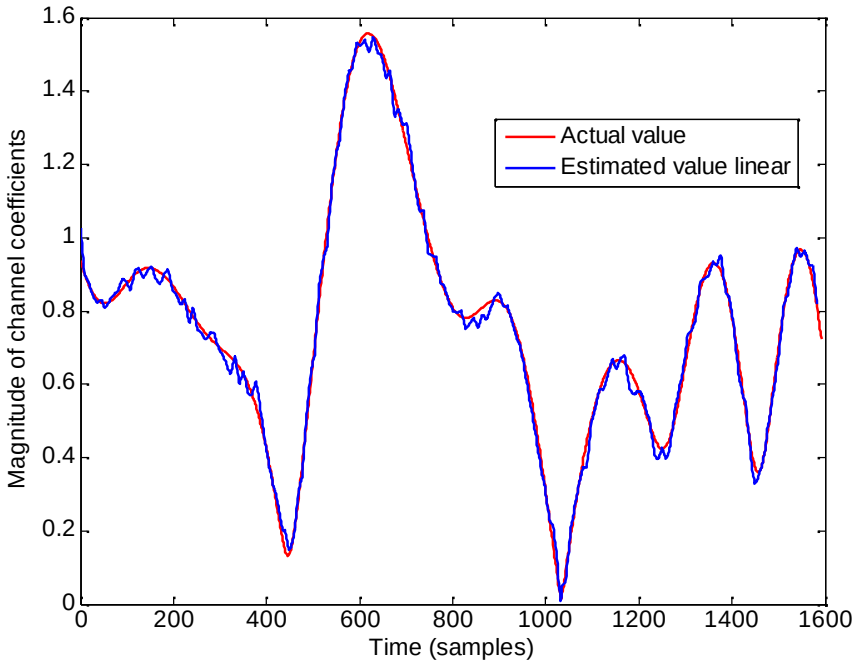

Figure 4.21: Actual channel vs. estimated channel using linear interpolation for FPSAM at a fixed SNR of 20 dB

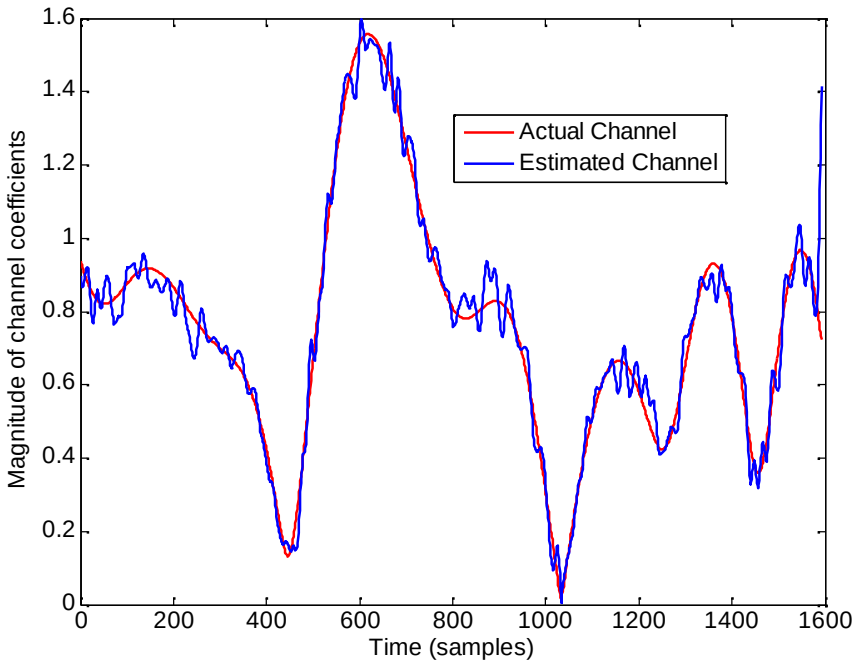

Figure 4.22: Actual channel vs. estimated channel using spline interpolation for CPSAM at a fixed SNR of 20 dB

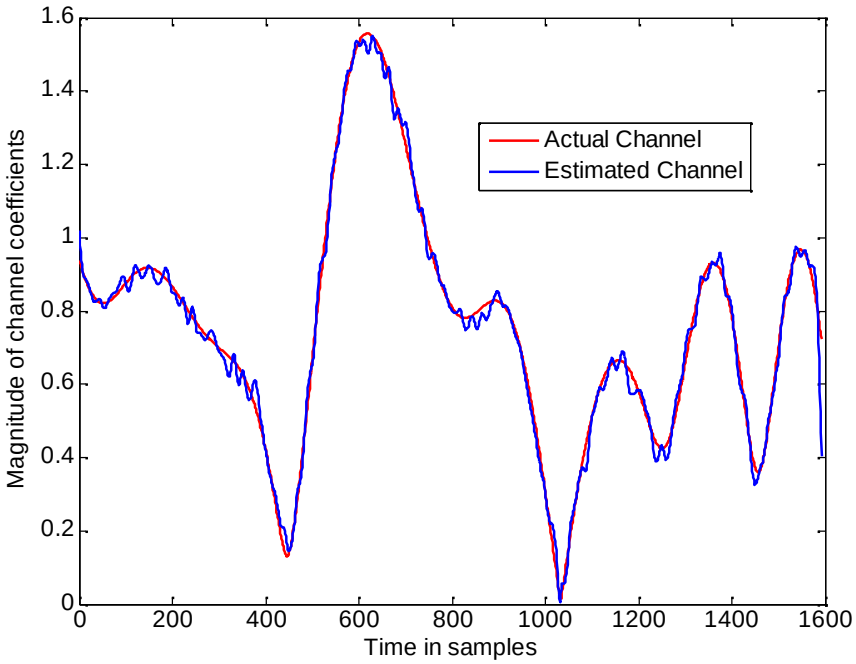

Figure 4.23: Actual channel vs. estimated channel using spline interpolation for FPSAM at a fixed SNR of 20 dB

For all the three interpolation techniques, the FPSAM technique gives a closer fading envelope to the actual channel than the CPSAM technique. Therefore, it can be concluded that for the estimation of fast fading channels, the FPSAM technique outperforms the CPSAM technique.

4.5 Conclusions

In this chapter, improved channel estimation techniques are proposed for block and rapidly fading channels. The improvement in the quality of channel estimates is achieved by filtering the pilot symbols in the optimum fractional Fourier domain. It is observed that the BER obtained by using channel estimates obtained in the optimum domain is lower than the BER obtained by using the channel estimates in time domain.

Chapter 5
Fractional MMSE Receiver with LDPC Coding

5.1 Introduction

The fractional MMSE receiver proposed in chapter 3 is shown to outperform the time and frequency domain MMSE receivers. In chapter 3, no error correction coding was used. As the name suggests, error correction coding increases the reliability of a system by detecting and correcting errors. For certain applications, if the required BER is lower than what can be achieved by the proposed receiver, error correction coding can be used with FRFT MMSE. In this chapter, the error rate performance of proposed MMSE receiver is studied with channel coding. A basic block diagram of a wireless system with channel coding is shown in Fig. 5.1.

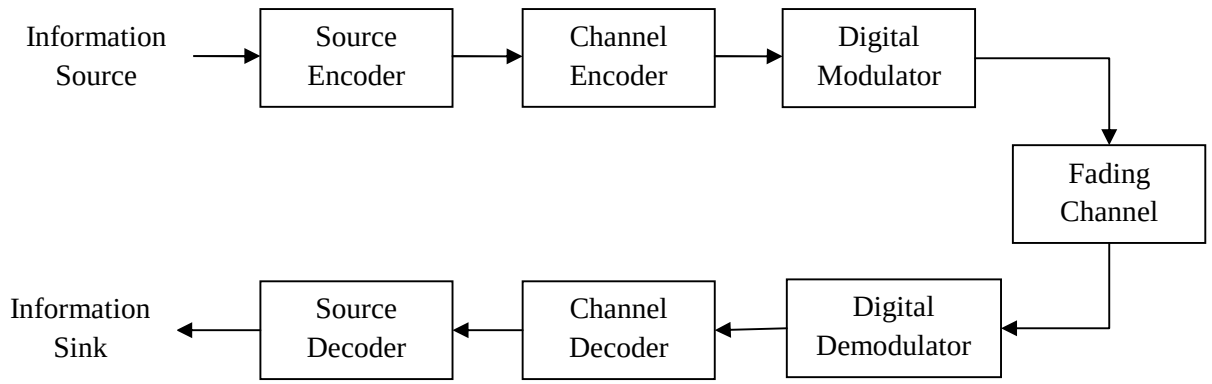

Figure 5.1: Block diagram of a wireless system with channel coding

Since, low density parity check codes have been proven to be the best error correcting codes and are currently being used in various wireless standards (see chapter 1, section 1.4); we study the performance of proposed FRFT based MMSE receiver with LDPC coding. A brief introduction of LDPC encoding/decoding process is presented in the following section.

5.2 Low Density Parity Check (LDPC) Codes

LDPC codes previously called Gallager codes are a class of linear block codes proposed by Robert Gallager in his PhD dissertation [86]. The name LDPC comes from the characteristic of

their parity-check matrix which contains only a few 1's in comparison to the amount of 0's. These codes were ignored for a long time due to their high computational complexity and lack of hardware support, especially if long codes are considered. Nowadays, however, with the increasing popularity of DSP processors, LDPC codes are one of the most commonly used error correcting codes [89]. In 1993, C. Berrou et. al. invented the turbo codes and their associated iterative decoding algorithm [48]. Although these codes were complex to work with they attracted a lot of attention towards iterative codes. In the year 1995, LDPC codes were rediscovered by Mackay and Neal [90] and they set up a link between their iterative algorithms to the Pearl's belief algorithm [91], from the artificial intelligence community (Bayesian networks). Gallager's LDPC codes were not originally described in the language of graphical theory. R.M Tanner [92], in 1981 introduced a recursive approach to the construction of codes which generalized the LDPC code construction and suggested that the design of algorithms for encoding and decoding is amenable to the basic techniques of graph theory. In this work, a method is described for constructing long error-correcting codes from one or more shorter error-correcting codes, referred to as sub codes, and a bipartite graph. Also, a lot of work was done by Wiberg [93] in the field of graphical theory of LDPC codes. Hence, LDPC codes are at the confluence of two major revolutions in the channel coding community: the graph-based code-description, and the iterative decoding techniques. LDPC codes are now used in many recent high-speed communication standards, such as DVB-S2 (Digital video broadcasting), Wi-MAX (IEEE 802.16e standard for microwave communications), High-Speed Wireless LAN (IEEE 802.11n), 10GBase-T Ethernet (802.3an) and G.hn/G.9960 (ITU-T Standard).

5.3 Encoding

LDPC codes are defined by a sparse parity check matrix. In the example given below for a low density matrix of dimension $n \times m$ for a (6, 3) code, we can define two parameters, w_r is the number of ones in each row and w_c is the number of ones in each column. For a matrix to be called low density, there are two conditions: $w_r << m$ and $w_c << n$. An example matrix is given below:

$$\mathbf{H}_p = \begin{bmatrix} 1 & 1 & 0 & 1 & 1 & 0 & 1 & 1 & 0 & 0 \\ 0 & 1 & 0 & 1 & 1 & 0 & 1 & 0 & 1 & 1 \\ 1 & 0 & 1 & 0 & 1 & 1 & 0 & 1 & 0 & 1 \\ 1 & 1 & 1 & 0 & 0 & 1 & 0 & 0 & 1 & 1 \\ 0 & 0 & 1 & 1 & 0 & 1 & 1 & 1 & 1 & 0 \end{bmatrix} \quad (5.1)$$

In order to meet the two conditions given above, the parity check matrix should be very large in size; therefore, the matrix given above cannot be truly called a low density matrix.

Tanner introduced an effective graphical representation for LDPC codes. These graphs provide a complete representation of the code and also help to describe the decoding algorithm. These graphs called Tanner graphs are bipartite graphs in which the nodes of the graph are separated into two distinctive sets and edges are only connecting nodes of two different types. The two types of nodes in a Tanner graph are called variable nodes (v-nodes) and check nodes -nodes). The graph gives rise to a linear code of block length n and dimension at least n-r in the following way: The 'n' coordinates of the codewords are associated with the n message nodes. The codewords are those vectors $(c_1 \ldots c_n)$ such that for all check nodes the sum of the neighboring positions among the message nodes is zero. Fig. 5.2 is an example for such a Tanner graph and represents the same code as the matrix in (5.1). The graphical representation is analogous to a matrix representation by looking at the adjacency matrix of the graph: let $\mathbf{H}_p$ be a binary $r \times n$ matrix in which the entry (i, j) is 1 if and only if the i^{th} check node is connected to the j^{th} message node in the graph. Then the LDPC code defined by the graph is the set of vectors $(c_1 \ldots c_n)$ such that $\mathbf{H}_p.c^T = 0$. The matrix $\mathbf{H}_p$ is called a parity check matrix for the code. The sparseness of the graph structure is key property that allows for the algorithmic efficiency of LDPC codes. For a good decoding performance the Tanner graph should be cycle free as in Fig. 5.2. In a Tanner graph, short cycles shown in Fig. 5.3 should be avoided as they are bad for decoding performance. The following tanner graph represents the parity check matrix completely.

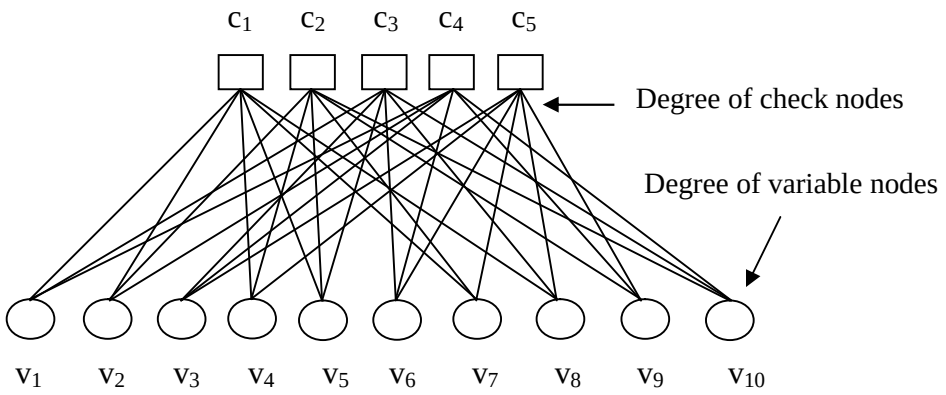

Figure 5.2: Tanner graph of the parity check matrix $\mathbf{H}_p$ from (5.1)

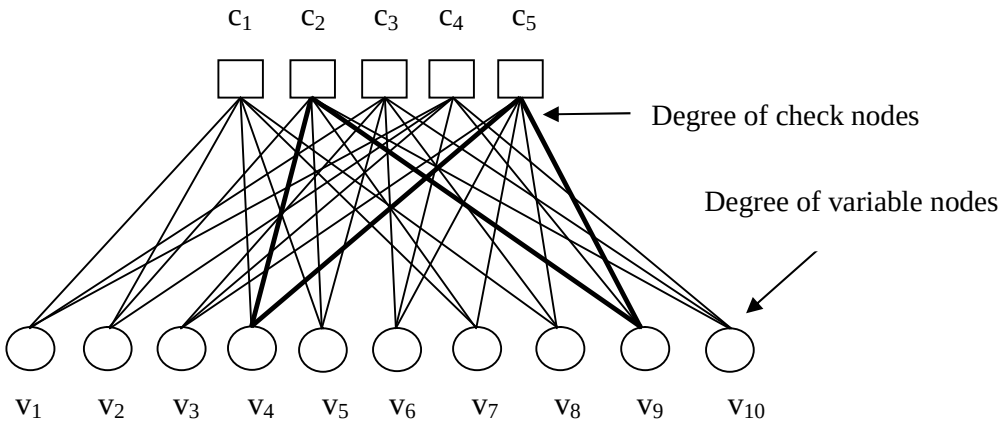

Figure 5.3: Tanner graph with a short cycle of length 4

A LDPC code is called regular if w_c is constant for every column and $w_r = w_c.(n/m)$ is constant for every row. According to this criteria, the parity check matrix in the example is regular with $w_c = 3 \text{and} \, w_r = 6$. It is also possible to tell if the matrix is regular or irregular by looking at the Tanner graph. If the number of incoming edges for all v-nodes are same and number of incoming edges for all c-nodes are also the same, the matrix is regular, and otherwise it is irregular. If the number of edges emanating from a variable node is called variable node degree d_v and the number of edges emanating from a check node is called check node degree d_c, then the rate of (d_v, d_c) regular LDPC code is $R=1-d_v/d_c$. The number of 1's in the parity check matrix $\mathbf{H}_p$ is $N.d_v$, while the total number of elements in $\mathbf{H}_p$ is $N^2.R_c$, where N is the length of the code. When N increases linearly, the total number of elements in $\mathbf{H}_p$ quadratically, therefore, the parity check

matrix is sparse with large N. The sparse characteristic of the parity check matrix is essential because the number of 1's presents the relations between a variable node and a check node. As the number of 1's increase, the tanner graph becomes more complex and in turn the decoder becomes more complex. So the sparseness of the parity check matrix directly controls the complexity of the decoder.

$$\mathbf{H}_p \cdot c^T = 0 \tag{5.2}$$

The generator matrix **G** can be found from the parity check matrix $\mathbf{H}_p$ by:

1. Covert $\mathbf{H}_p$ into the form of $\left[\mathbf{P}^T \quad \boldsymbol{I}\right]$ by using Gaussian elimination method.
2. **G** is simply $\left[\boldsymbol{I} \quad \mathbf{P}\right]$

Since the LDPC codes are characterized by the parity check matrix $\mathbf{H}_p$, the receiver uses the same condition to check for errors.

If $\mathbf{H}_p \cdot y^T = 0$, there are no errors in the received signal.

If $\mathbf{H}_p \cdot y^T \neq 0$, there are errors in the received signal.

Although the $\mathbf{H}_p$ matrix is sparse but the **P** of generator matrix **G** is dense. To store **G**, $k(N_c - k) = N_c^2\left(\frac{1}{R} - 1\right)$ bits of memory are needed. Therefore, the encoding complexity of LDPC codes is very high.

5.4 Decoding Algorithms

The traditional channel codes use ML or MAP detection where the errors are corrected by comparing the received signal with all the possible combinations given the constellation size of the modulation scheme. Practically, it is possible only if the number of message bits and the constellation size is small. With the increase in the number of message bits and/or constellation size, the computational complexity increases greatly. However, to exploit the sparseness of the parity check matrix of LDPC codes, Gallager introduced a class of iterative decoding algorithms. The iterative algorithms to decode LDPC codes are called message passing algorithms since they can be completely characterized by passing the messages along the edges of a tanner graph [94]. The nodes in Tanner graph are isolated as in each node only has access to the information contained in the messages on the edges connected to it. The message passing algorithms are also

denoted as iterative because the messages are moved a number of times between the two sets of nodes before the decision is made. Bit-flipping algorithm is a relatively lower complexity message passing decoding algorithm in which the messages are binary and decisions are hard. The most commonly used decoding algorithm is the sum product algorithm/belief propagation decoding algorithm [47, 95] in which the messages are in the form of probabilities which indicate a level of belief about the value of the codeword bits. Often, the probabilities are represented as log likelihood ratios and the message passing algorithm is called as sum product algorithm since the calculations at the variable and check nodes are in the form of sum and product operations.

5.4.1 Bit Flipping Algorithm

The bit flipping algorithm is a hard decision message passing algorithm for LDPC codes. It was proposed by Gallager as a message passing algorithm with hard decision inputs [88, 96]. A binary (hard) decision is made for each received bit by the detector and passed on to the decoder. The working of this algorithm is described by the following steps:

Let **t**, be the binary hard decision vector obtained from **y**, i.e. $t_i = \text{sign}(y_i)$, where sign(y) =1, if $y \geq 0$ and sign(y) =0 if $y < 0$.

Iterative Decoding Steps:

1. Compute the parity-check sums (syndrome bits) $\mathbf{s} = \mathbf{t}\mathbf{H}_p^T$. If all the parity-check equations are satisfied, i.e. no errors in the received bits and **s**=0, stop the decoding process.
2. If not, then count the number of unsatisfied parity checks for each code bit position given by: $\mathbf{u} = \mathbf{s}\mathbf{H}_p$
3. Identify the set of bits for which u_j is largest and flip the bits in this set.
4. Go back to step 1 and repeat steps 1 to 3 until all the parity-check equations are satisfied or the maximum number of predefined iterations is reached.

5.4.2 Sum Product/Belief Propagation Algorithm

The sum-product algorithm is a soft decision message-passing algorithm. In this algorithm, the messages representing each decision are in the form of probabilities or log likelihood ratios. The sum-product algorithm is a soft decision algorithm which accepts the probability of each

received bit as input. Also, the advantage of using logarithmic probabilities is that the product of several messages will be converted to sum in the log domain. Implementing this algorithm will reduce the complexity of the decoding process.

The input probabilities are known to the receiver even before it is operated so they are termed as *a priori* probabilities. The log likelihood ratios used to represent for a binary variable by a single value are given as:

$$L(x) = \log \frac{p(x=0)}{p(x=1)} \tag{5.3}$$

If $p(x=0) > p(x=1)$ then L(x) is positive and greater the difference between $p(x=0)$ and $p(x=1)$ greater is the positive value of L(x). Similarly, if $p(x=1) > p(x=0)$ then L(x) is negative and greater the difference between $p(x=0)$ and $p(x=1)$ greater is the negative value of L(x). Therefore, the sign of L(x) clearly provides a hard decision on x. The LLR's can be translated back to probabilities as:

$$p(x=1) = \frac{e^{-L(x)}}{1+e^{-L(x)}} \text{ and } p(x=0) = \frac{e^{L(x)}}{1+e^{L(x)}} \tag{5.4}$$

If $\mathbf{x} = (\mathrm{x}_1, \mathrm{x}_2 \cdots \mathrm{x}_\mathrm{n})$ is the transmitted codeword after modulation and $\mathbf{y} = (y_1, y_2 \cdots y_\mathrm{n})$ is the received codeword, then the system model can be described as:

$$y_\mathrm{g} = \mathrm{h_g x_g} + \mathrm{n_g} \tag{5.5}$$

where $g = 1, 2 \ldots \mathrm{n}$, $\mathrm{n_g}$ is the additive Gaussian noise with zero mean and σ_n^2 variance and hg is the Rayleigh fading channel with zero mean and unit variance. The pdf of the Rayleigh distribution can be given as:

$$p(\mathrm{h_g}) = 2\mathrm{h_g} \exp(-\mathrm{h_g^2}) \tag{5.6}$$

The conditional pdf for uncorrelated Rayleigh fading channel, of the $\mathrm{g^{th}}$ output $\mathrm{y_d}$ is:

$$P_r(\mathrm{y_g} / \mathrm{n_g}, \mathrm{h_g}) = \frac{1}{\sqrt{2\pi\sigma_n^2}} \exp\left(-\frac{(\mathrm{y_g} - \mathrm{n_g}.\mathrm{h_g})}{2\sigma_n^2} \right) \tag{5.7}$$

As shown in Fig. 5.4, the output message at a given variable node to be passed to the check node is the summation of the initial message q and the incoming edge LLRs $L_{c \to v,l}{}^{p-1}(\mathrm{x_g})$ for $l = 1, 2, \ldots d_{v-1}$ along each of the variable node edges.

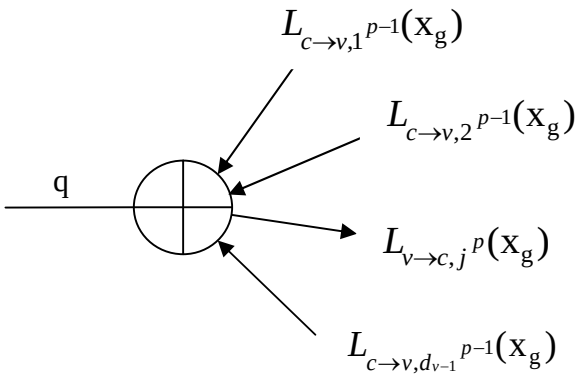

Figure 5.4: Variable node computation

The incoming LLRs at the variable node x_g are assumed to be zero, i.e.

$$q_{(c\to v,l)}{}^{0}(\mathrm{x_g}) = 0, \text{ where } l = 1,2,\ldots d_v - 1 \tag{5.8}$$

As shown in Fig. 5.5, the j[th] outgoing LLR of a given variable node x_g at the p[th] iteration is given as:

$$L_{v\to c,j}{}^{p}(\mathrm{x_g}) = q + \sum_{l=1}^{d_{v-1}} L_{c\to v,l}{}^{p-1}(\mathrm{x_g}) \tag{5.9}$$

The output message given by (5.9) is transferred to the check node c. The j[th] output message at the check node is given by [96]:

$$L_{c\to v,l}{}^{p}(\mathrm{y_g}) = 2\tanh^{-1}\prod_{j=1}^{d_{c-1}}\tanh(L_{v\to c,l}{}^{p}(\mathrm{y_g})) \tag{5.10}$$

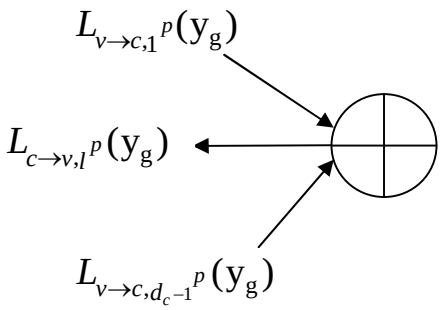

Figure 5.5: Check node computation

The message computed at the check node is now transferred to the variables nodes. At the end of the decoding process each variable node computes an output reliability value as follows:

$$L(\mathrm{x_g}) = q + \sum_{l=0}^{d_{v-1}} L_{c\to v,l}^{p}(\mathrm{x_g}) \tag{5.11}$$

Hard decision is obtained as follows:

$$\begin{aligned} \hat{\mathrm{x}}(\mathrm{y}) &= 1 \quad \text{if } L(x_g) < 0 \\ \hat{\mathrm{x}}(\mathrm{y}) &= 0 \quad \text{if } L(\mathrm{x_g}) < 1 \end{aligned} \tag{5.12}$$

5.5 Results and Discussion

In this section, the simulation details are given and the performance comparison of the three receivers in the presence of LDPC coding is coding. First, we present the simulation details.

5.5.1 Simulation Details

In this chapter, the performance of the fractional MMSE receiver proposed in chapter 3 is evaluated with LDPC coding. The LDPC codes considered in this chapter are irregular with a mean column weight of 3. The information signal consisting of random 0's and 1's is encoded using the generator matrix and then modulated into -1's and +1's using BPSK modulation. The length of each coded frame is taken to be 256 bits. The number of iterations for each frame has been taken to be 1000 and the total number of frames is taken to be 100. Two different fading channels are considered, i.e. Rayleigh and Rician. The noise is modeled as AWGN. The received signal that is corrupted by fading and noise is first filtered in the optimum domain by the proposed receiver. After that, the filtered signal is fed into the LDPC decoder for further error detection and correction.

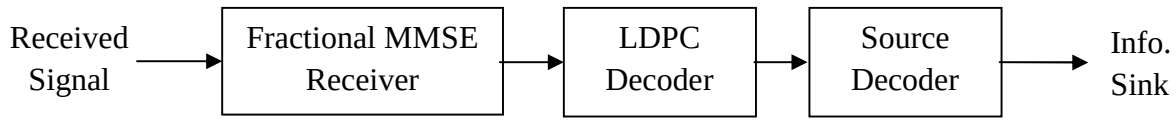

Figure 5.6: Block diagram of the receiver side with LDPC and Source decoder

5.5.2 Performance Comparison

The comparison of BER for uncoded and LDPC coded receiver for a 2×2 MIMO system in uncorrelated Rayleigh fading is shown in Fig. 5.7. It is observed that the LDPC coded system has fewer errors as compared to the uncoded system. For a BER of 10^{-2}, the LDPC coded system gives a SNR advantage of 5.47 dB, i.e. it achieves the same BER at 5.47 dB less than the uncoded system. Similar results are obtained for a 4×4 system in Fig. 5.8 with the LDPC coded system giving a SNR advantage of 4.69 dB. In Fig. 5.9 and 5.10, the BER of the uncoded and coded system is obtained in Rician fading with K-factor=10 for 2×2 and 4×4 systems respectively. For a BER of 10^{-2}, the LDPC coded system gives a SNR advantage of 6.2 dB in the case of 2x2 antennas and a SNR advantage of 4.4dB in the case of 4x4 antennas. The SNR advantage obtained by the coded system over the uncoded system for 2x2 and 4x4 systems in Rayleigh and Rician fading is summarized in tables 5.1 and 5.2 respectively.

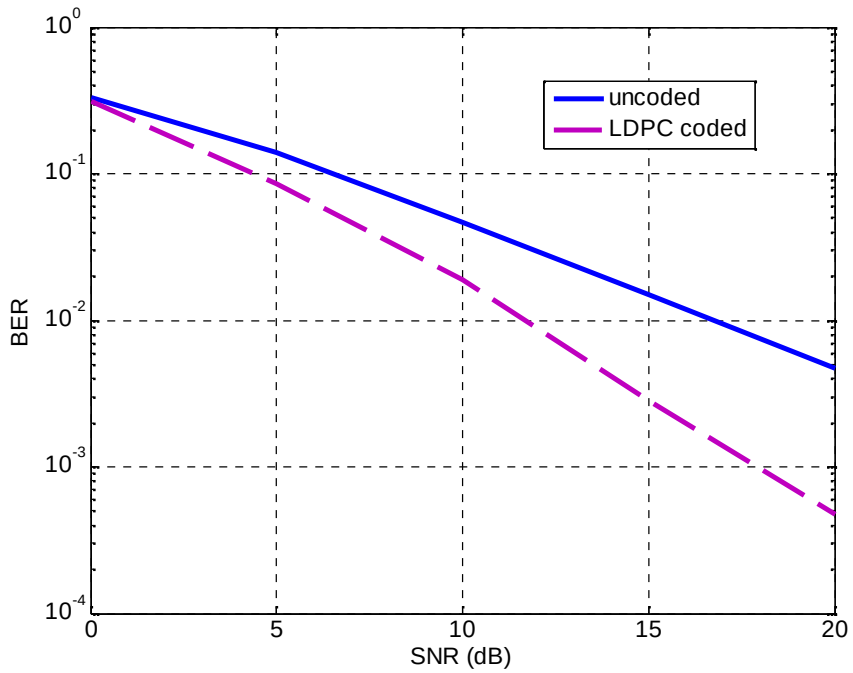

Figure 5.7: BER vs. SNR comparison of the uncoded and LDPC coded FRFT MMSE receiver for a 2×2 system in Rayleigh fading

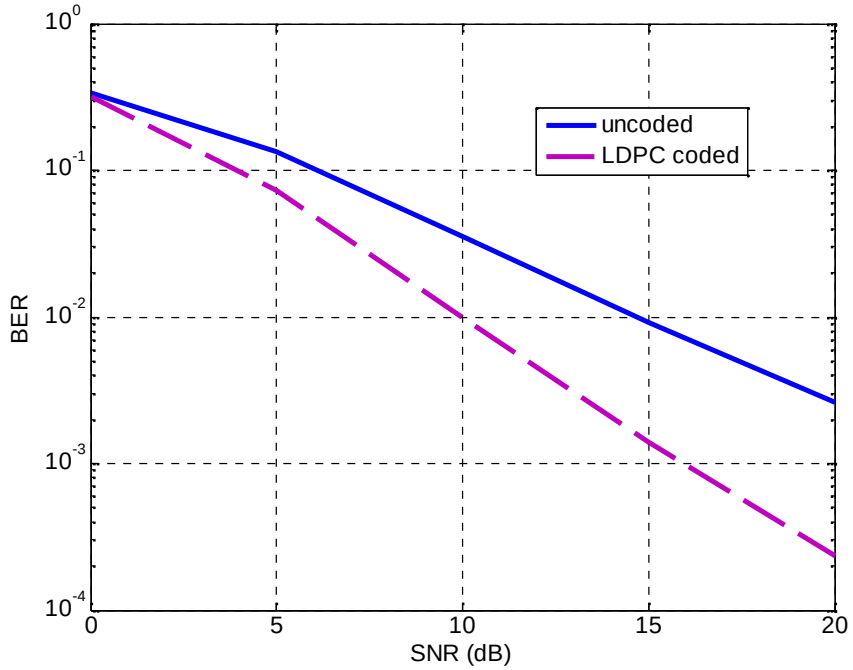

Figure 5.8: BER vs. SNR comparison of the uncoded and LDPC coded FRFT MMSE receiver for a 4×4 system in Rayleigh fading

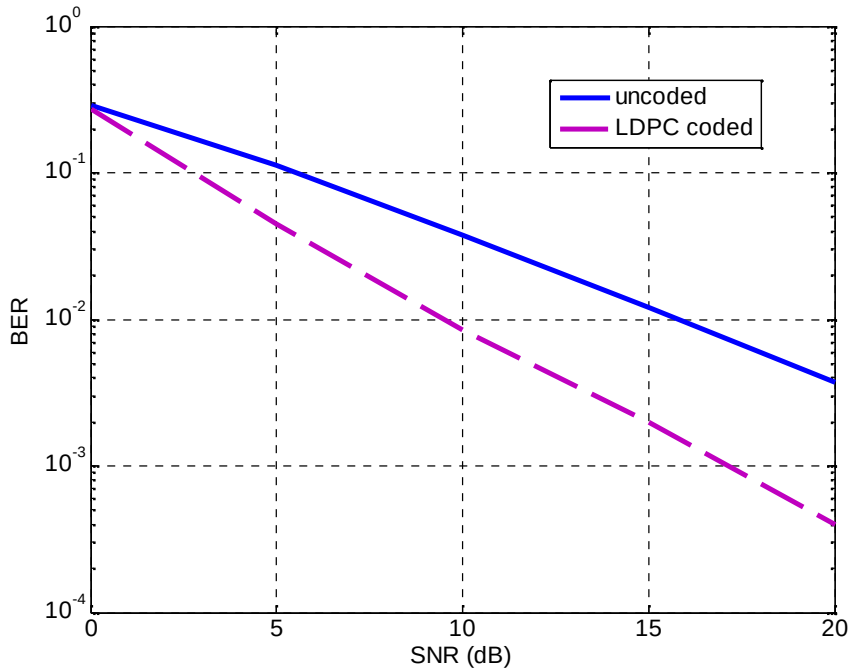

Figure 5.9: BER vs. SNR comparison of the uncoded and LDPC coded FRFT MMSE receiver for a 2×2 system in Rician fading with *K*-factor=10dB

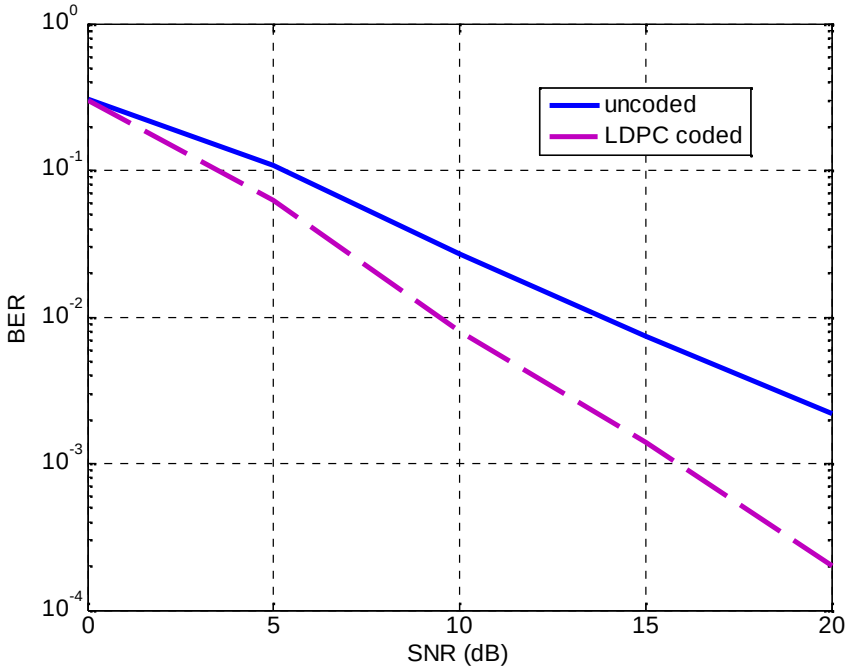

Figure 5.10: BER vs. SNR comparison of the uncoded and LDPC coded FRFT MMSE receiver for a 4×4 system in Rician fading with *K*-factor=10dB

Table 5.1: SNR improvement of LDPC coded system over the uncoded system for a BER of 10^{-2} in Rayleigh fading

No. of antennas	Uncoded	LDPC coded	SNR Advantage (dB)
$N_T=N_R=2$	17.27	11.8	5.47
$N_T=N_R=4$	14.69	10	4.69

Table 5.2: SNR improvement of LDPC coded system over the uncoded system for a BER of 10^{-2} in Rician fading with a K-factor of 10

No. of antennas	Uncoded	LDPC coded	SNR Advantage (dB)
$N_T=N_R=2$	15.7	9.5	6.2
$N_T=N_R=4$	13.8	9.4	4.4

5.6 Conclusions

In this chapter, the FRFT MMSE receiver proposed in chapter 3 was considered in the presence of LDPC coding. Tables 5.1 and 5.2 show the improvement of the BER of FRFT MMSE with LDPC coding as compared to the uncoded case. The coded system gives a marked SNR improvement over the uncoded system and in systems where lower BER is required channel coding can be used with the proposed receiver to achieve the desired result.

Chapter 6
Conclusions and Future Scope

With the rapid advancement in wireless communications, there is a demand for higher data rates to support high speed services such as high definition mobile TV, 3-D television etc. Therefore, one of the most important goals of next generation systems is to design techniques for achieving higher data rate. MIMO is seen as the solution to the demand for higher data rates due to its capability to provide increased data rate without imposing any bandwidth penalty. One of the factors which influences data rate is the number of errors in the transmission. If a receiver achieves lower BER for the same value of received SNR, it leads to an increase in the capacity of a wireless system. In this work, a fractional MMSE receiver is proposed for multiple antenna systems which gives an improved error rate performance as compared to the existing time and frequency domain receivers without much increase in the computational complexity. In section 6.1, the proposed objectives are reviewed and the work done towards the achievement of each objective is addressed. In section 6.2, several topics are listed which might be of interest for future research.

6.1 Conclusions

Objective 1: To study some of the existing reception schemes for MIMO systems.

The existing MIMO receivers whose performance is reviewed are: ZF, MMSE, VBLAST and ML. The fading channels in which the performance of these receivers is simulated are taken to be both correlated and uncorrelated. Two different fading channels are considered, i.e. Rayleigh and Rician fading. The results obtained for observing the error performance of these receivers are in the form of BER vs. SNR, BER vs. *K*-factor (for Rician fading) and BER vs. correlation coefficient (*r*). It is seen that both VBLAST and ML receivers have a superior error performance as compared to ZF and MMSE receivers. To give the complete picture, a complexity analysis of all the receivers is done which shows that both the VBLAST and ML receivers are more computationally complex than ZF and MMSE. Also, the complexity of the ML receiver increases considerably with increase in the modulation constellation. It is also observed that although MMSE has a better error performance than the ZF receiver, both the receivers have the

same complexity. Therefore, the MMSE receiver is selected as optimum based on its linear nature, low complexity and good error performance. Below, Table 6.1 shows the comparison of computational complexity of various receivers in terms of equivalent ADDs/s.

Table 6.1: Comparison of Complexity (Eq. ADDs/s) for various MIMO receivers

$N_T=N_R=N$	ZF	MMSE	VBLAST	ML
2	1.74×10^7	1.74×10^7	3.5×10^7	1.91×10^7
4	7.001×10^7	7.001×10^7	1.404×10^8	1.535×10^8
8	2.809×10^8	2.809×10^8	5.626×10^8	4.915×10^9

Objective 2: To propose an improved reception scheme for MIMO systems.

Under this objective, an improved reception scheme is proposed for multiple antenna systems. This improved reception is based on fractional domain filtering process where the filtering is done in the optimum fractional domain rather than time or frequency domains. First, an improved receive diversity technique is proposed for single input multiple output systems. In this improved diversity scheme, the performance of optimum combining (which is based on Wiener filtering) is enhanced by fractional domain filtering. Filtering in optimum fractional domain enables the effective removal of noise and distortion due to signal compactness in the optimum domain which is not possible in conventional time and frequency domains. It is seen that the fractional optimum combiner gives lower BER than time and frequency domain optimum combiners. Table 6.2 shows the SNR advantage achieved by the fractional optimum combiner over the other two combiners.

Table 6.2: SNR improvement of FOC over the time and freq. domain OCs for a BER of 10^{-2}

N_T, N_R	At a BER of 10^{-2}, SNR improvement of optimum domain combiner over	
	time domain combiner	freq. domain combiner
1,2	7.2 dB	2.4 dB
1,4	7.5 dB	3.4 dB
1,8	7.3 dB	4.3 dB

The improved Wiener filtering is then extended for MIMO systems. As the MMSE receiver is based on Wiener filtering, the proposed fractional domain Wiener filtering based receiver is basically a fractional domain MMSE receiver. The results show that the BER of the proposed

receiver is lower than the time and frequency domain MMSE receivers. Table 6.3 presents the SNR improvement achieved by the proposed receiver over the other two receivers.

Table 6.3: SNR improvement (in dB) of proposed MMSE receiver over the time and frequency domain MMSE receivers for a fixed BER and $N_T=N_R=2$

N_T, N_R	At a BER of 10^{-2}, SNR improvement of optimum domain MMSE over	
	time domain MMSE	freq. domain MMSE
2,2	3.6 dB	1.132 dB
4,4	5.87 dB	2.25 dB

Objective 3: To analyze the performance of the proposed scheme with LDPC coding.

The fractional MMSE receiver proposed under the 2nd objective is considered with LDPC coding. Since LDPC codes are one of the best error correcting codes, their use has the effect of substantially decreasing the number of transmission errors, i.e. reducing the BER for the same value of received SNR. It is seen from the results that in a Rayleigh fading channel, the LDPC coded optimum fractional domain MMSE receiver gives a coding gain of 5.47 dB for 2×2 and 4.69dB for 4×4 MIMO system. Therefore, when the BER achieved by the proposed MMSE receiver needs to be reduced further, LDPC codes offer a smart solution with an excellent error performance but a low decoding complexity.

Objective 4: To analyze the effect of channel correlation on the performance of the proposed receiver.

The literature reveals that the multipath wireless channel is capable of enormous capacities, provided that the rich scattering is properly exploited with the use of independent multiple antennas. However, this is not always practically possible due to the size of wireless devices becoming smaller by the day. Minimum distance between the adjacent antennas for them to be independent is approximately 0.38λ. Therefore, insufficient distance $(d < 0.38\lambda)$ between antenna elements causes spatial correlation which degrades the capacity of the wireless system. In this thesis, we model the spatial correlation by using a single coefficient correlation model which considers equal correlation at the transmitter and receiver. The effect of spatial correlation on the performance of time, frequency and optimum domain MMSE receivers is considered for MIMO systems. The results are presented in the form of BER vs. SNR and BER vs. correlation

coefficient. It is seen that for values of spatial correlation up to 0.6, the optimum domain receiver has a lower BER than the other two receivers. When the spatial correlation is greater than 0.6, the BER of all the three receivers degrades severely. Table 6.4 shows the comparison of BER of proposed MMSE receiver with the other two receivers for different correlation coefficients and SNR=10dB and 20dB.

Table 6.4: Comparison of BER of proposed receiver with the time and frequency domain receivers for different correlation coefficients at a fixed SNR

	$N_T=N_R=2$			$N_T=N_R=4$		
Spatial Correlation / SNR	Time domain	Freq domain	Optimum domain	Time domain	Freq domain	Optimum domain
0.2 / 10 dB	0.1069	0.07252	0.05633	0.1174	0.07011	0.04511
0.5 / 10 dB	0.1503	0.1009	0.07952	0.1754	0.1219	0.09245
0.8 / 10 dB	0.2069	0.1553	0.1388	0.2451	0.2054	0.1829
0.2 / 20 dB	0.0133	0.0072	0.00519	0.0137	0.0055	0.0034
0.5 / 20 dB	0.02312	0.01043	0.0079	0.04364	0.01623	0.0089
0.8 / 20 dB	0.05883	0.02571	0.01805	0.137	0.08256	0.06686

It is also practical to assume that spatial correlation might be present at one end of the communication system only. This happens when one end of the communication system is large enough for incorporating multiple antennas while the other end is not. In that case, the system is subject to transmit/receive correlation only. Error performance of the three receivers has also been considered in transmit/receive correlation.

6.2 Future Scope

In this dissertation, a reception technique for multi antenna systems is proposed which is based on Wiener filtering of the received signal in optimum domain using fractional Fourier transform. It is seen that the proposed receiver outperforms the existing time and frequency domain receivers in terms of error rate performance. However, to find the optimum domain, an iterative approach is used where the MSE is calculated over closely spaced discrete values of $'a' \in (-1,1)$. Once the optimum domain is calculated, the iterations do no need to be performed again until the

statistics of signal and noise change. However, if the optimum domain can be calculated analytically without having to perform the iterations, it would make the receiver more suitable for real time applications. Therefore, finding a method for directly calculating the optimum domain is still an open area for further research.

Furthermore, very little work has been done on the hardware implementation of optimum domain filtering using FRFT. Therefore, the error rate measurements should be performed with experimental setup of MIMO systems and compared with the simulation results.

In this thesis, all analysis has been performed in frequency flat channels. The analysis can be extended for frequency selective channels.

References

1. C. Zhang, S. L. Ariyavisitakul and T. Meixia, “LTE-advanced and 4G wireless communications,” IEEE Communication Magazine, vol. 50, no. 2, pp. 102-103, Feb. 2012.
2. C. Zhang, S. L. Ariyavisitakul and T. Meixia, “LTE-advanced and 4G wireless communications: Part 2,” IEEE Communication Magazine, vol. 50, no. 6, pp. 26, June 2012.
3. E. Dahlman et al., “3G: HSPA and LTE for Mobile Broadband,” 2nd ed., Academic Press, 2008.
4. D. Astley, E. Dahlman, A. Furuskar, Y. Jading, M. Lindstrom and S. Parkvall, “LTE: the evolution of mobile broadband,” IEEE Communications Magazine, vol. 47, no. 4, pp. 44-51, April 2009.
5. J. Robson, “The LTE/SAE Trial Initiative: Taking LTE/SAE from specification to rollout,” IEEE Communication Magazine, vol. 47, no. 4, pp. 82–88, 2009.
6. R. Irmer et al., “Multisite Field Trial for LTE and Advanced Concepts,” IEEE Communication Magazine, vol. 47, no. 2, pp. 92–98, 2009.
7. E. Dahlman, “3G Evolution: HSPA and LTE for Mobile Broadband,” Academic Press, Edition 2008.
8. Rajender Kumar and Brahmjit Singh, “Comparison of vertical handover mechanisms using generic QOS trigger for next generation network,” International Journal of Next Generation Networks, vol. 2, no. 3, pp. 80-97, Sept. 2010.
9. V. K. Jain and S. N. Gupta, “Performance of binary baseband polar signals in white Gaussian and impulsive atmospheric radio noise with varying impulse rates and ISI,” Journal of Electrical & Electronics Engineers (Australia), vol.5, no.1, pp.65-68, March 1985.
10. V. K. Arora and E. Quershi, “Quantum theory of microwave conductivity,” Physica Status Solidi (b), vol. 77, pp. 77-84, 1976.

11. I. E. Telatar, “Capacity of multi-antenna Gaussian channels,” European Transactions on Telecommunications (ETT), vol. 10, no. 6, pp. 585–595, Nov.-Dec. 1999. (See also a previous version of the paper in AT&T Bell Labs Internal Tech. Memo, June 1995.).
12. G. J. Foschini, “Layered space-time architecture for wireless communication in a fading environment when using multi-element antennas,” Bell Labs Technical Journal, pp. 41-59, autumn 1996.
13. G. Foschini and M. Gans, “On limits of wireless communications in a fading environment when using multiple antennas,” Wireless Personal Communications, vol. 6, pp.311–335, 1998.
14. T. S. Rappaport, “Wireless Communications, Principles and Practice,” New Jersey, Prentice Hall, 1996.
15. A. Goldsmith, “Wireless Communications,” Cambridge University Press, Edition 2005.
16. M. K. Simon and M. S. Alouini, “Digital communication over fading channels: A unified approach to performance analysis,” John Wiley & Sons, Inc., Edition 2000.
17. A. Dixit, S. C. Sharma, R. P. Vats and A. K. Jain, “Bit error rate analysis of MRC diversity techniques in CDMA communication network,” International Journal of Computer Science and Knowledge Engineering, vol. 2, no. 2, pp. 143-147, Dec 2007
18. J. H. Winters, “Optimum combining in digital mobile radio with co-channel interference,” IEEE Transactions on Vehicular Technology, vol. 33, no. 3, pp. 144-155, 1984.
19. A. Shah and A. M. Haimovich, “Performance analysis of maximal ratio combining and comparison with optimum combining for mobile radio communications with co-channel Interference,” IEEE Transactions on Vehicular Technology, vol. 49, no. 4, pp. 1454-1463, 2000.
20. M. A. Kutay, H. M. Ozaktas, O. Arikan and L. Onural, “Optimal filtering in fractional Fourier domains,” IEEE Transactions on Signal Processing, vol. 45, no. 5, pp.1129–1143, 1997.
21. H. M. Ozaktas, Z. Zalevsky and M. A. Kutay, “The fractional Fourier transform with applications in optics and signal processing,” Wiley, New York, Inc., Edition 2000.

22. V. Tarokh, N. Seshadri, and A. R. Calderbank, “Space-time codes for high data rate wireless communication: Performance criterion,” Proceedings of IEEE International Conference on Communications, Montreal, Canada, vol. 1, pp. 299-303, Jun 1997.
23. N. Seshadri, V. Tarokh, and A. R. Calderbank, “Space-time codes for high data rate wireless communication: Code construction,” Proceedings of IEEE Vehicular Technology Conference, Phoenix, AZ, vol. 2, pp. 637-641, May 1997.
24. V. Tarokh, N. Seshadri, and A. R. Calderbank, “Space-time codes for high data rate wireless communication: Performance criterion and code construction,” IEEE Transactions on Information Theory, vol. 44, no. 2, pp. 744-765, Mar. 1998.
25. V. Tarokh, A. Naguib, N. Seshadri and A. R. Calderbank, “Space-time codes for high data rate wireless communication: Performance criteria in the presence of channel estimation errors, mobility, and multiple paths,” IEEE Transactions on Communications, vol. 47, no. 2, pp. 199-207, Feb. 1999.
26. S. M. Alamouti, “A simple transmit diversity technique for wireless communications,” IEEE Journal of Selected Areas in Communication, vol. 16, no. 8, pp. 1451–1458, Oct. 1998.
27. V. Tarokh, H. Jafarkhani and A. R. Calderbank, “Space-time block coding for wireless communications: performance results,” IEEE Journal of Selected Areas in Communications, vol. 17, no. 3, pp. 451-460, Mar. 1999.
28. G. G. Raleigh and J. M. Cioffi, “Spatial temporal coding for wireless communication,” IEEE Transactions on Communications, vol. 46, no. 3, pp. 357-366, Mar 1998.
29. E. Biglieri, R. Calderbank, A. Constantinides, A. Goldsmith, A. Paulraj and H. V. Poor, “MIMO wireless communications,” Cambridge University Press, Edition 2007.
30. G. Tsoulos, “MIMO system technology for wireless communication,” CRC Press, Taylor and Francis Group, FL, Edition 2006.
31. A. Goldsmith, S. Jafar, N. Jindal, and S. Vishwanath, “Capacity limits of MIMO channels,” IEEE Journal of Selected Areas in Communications, vol. 21, no. 3, pp. 684–702, June 2003.
32. A. J. Paulraj, R. U. Nabar and D. A. Gore, “Introduction to space-time wireless communications,” Cambridge University Press, UK, Edition 2003.

33. L. Zheng and D. Tse, “Diversity and multiplexing: A fundamental tradeoff in multiple antenna channels,” IEEE Transactions on Information Theory, vol. 49, no. 5, pp. 1073-1096, May 2003.
34. Ilhan Kim and Joohwan Chun, “MIMO structure which combines the spatial multiplexing and beamforming,” IEEE Vehicular Technology Conference (VTC 2004), vol. 1, pp. 108-112, May 2004.
35. Fang Shu, Li Lihua, Tao Xiaofeng and Zhang Ping, “A spatial multiplexing MIMO scheme with beamforming for downlink transmission,” IEEE Vehicular Technology Conference (VTC-2007), pp. 700-704, Oct 2007.
36. A. W. C. Lim and V. K. N. Lau, “On the fundamental tradeoff of spatial diversity and spatial multiplexing of MIMO links with imperfect CSIT,” IEEE International Symposium on Information Theory, 2006, pp. 2704-2708, July 2006.
37. Enis Akay, Ersin Sengul and Ender Ayanoglu, “Achieving full spatial multiplexing and full diversity in wireless communications,” IEEE Wireless Communications and Networking Conference (WCNC 2006), vol. 4, pp. 2046-2050, April 2006.
38. D.-S. Shiu, G. Foschini, M. Gans, and J. Kahn, “Fading correlation and its effect on the capacity of multielement antenna systems,” IEEE Transactions on Communications, vol. 48, no. 3, pp. 502–513, Mar. 2000.
39. I-METRA, D2, IST-1999-11729, MIMO channel characterization, Feb 1999.
40. W. Lee, “Effect on correlation between two mobile radio base-station antennas,” IEEE Transactions on Communications, vol. 21, no. 11, pp. 1214–1224, 1973.
41. IST-METRA project, [Online] Available: http://www.ist-imetra.org.
42. I-METRA, D2 v1.2, IST-2000-30148, Channel characterization, Oct. 2002.
43. I-METRA, IST-2000-30148, Final Report, Oct. 2003.
44. 3GPP TR 25.814, v1.2.2., 3rd Generation Partnership Project; Technical Specification Group Radio Access Network; Physical Layer Aspects for Evolved UTRA (Release 7), 2006.
45. 3GPP TR 25.996, v7.0.0., 3rd Generation Partnership Project; Technical Specification Group Radio Access Network; Spatial Channel Model for Multiple Input Multiple Output Simulations (Release 7), 2007.

46. T. J. Richardson, A. Shokrollahi, and R. Urbanke, “Design of capacity approaching irregular low-density parity-check codes,” IEEE Transactions on Information Theory, vol. 47, no. 2, pp. 619–637, Feb. 2001.
47. S. Y. Chung, G. D. Forney, T. J. Richardson and R. Urbanke “On the design of low-density parity-check codes within 0.0045 dB of the Shannon limit,” IEEE Communications Letters, vol. 47, no. 2, pp. 58-60, February 2001.
48. C. Berrou, A. Glavieux and P. Thitimajshima, "Near Shannon limit error correcting coding and decoding: Turbo codes," in Proceeding IEEE ICC '93, Geneva, Switzerland, pp. 1064-1070, May 1993.
49. http://www.dvb.org/technology/fact_sheets/
50. V. Oksman and S. Galli, “G.hn: The new ITU-T home networking standard,” IEEE Communications Magazine, vol. 47, no. 10, pp. 138-145, Oct. 2009.
51. IEEE Standard, section 20.3.11.6 "802.11n-2009", IEEE, October 29, 2009.
52. C. Oestges and B. Clerckx, “MIMO wireless communications: From real-world propagation to space-time code design,” Academic Press, Edition 2007.
53. M. Jankiraman, “Space-time codes and MIMO systems,” Artech House, Boston, London, Edition 2004.
54. A. Zelst and J. S. Hammerschmidt, “A single coefficient spatial correlation models for multiple-input multiple-output (MIMO) radio channels,” in Proc.URSI XXVIIth General Assembly, 2002.
55. A. Zelst, “MIMO OFDM for wireless LANs,” PhD Dissertation, Technische Universiteit Eindhoven, Netherlands, Chapter 4, 2004.
56. D. Tse, P. Viswanath, “Fundamentals of wireless communication,” Cambridge University Press, Inc., Edition 2005.
57. Christoph Windpassinger, Lutz Lampe, Robert F. H. Fischer and Thorsten Hehn, “A performance study of MIMO detectors,” IEEE Transactions on Wireless Communications, vol. 5, no. 8, pp. 2004-2008, August 2006.
58. Amaud Gueguen, “Comparison of suboptimal iterative space-time receivers,” IEEE Vehicular Technology Conference (VTC 2003), vol. 2, pp. 842-846, April 2003.
59. J. Mietzner, R. Schober, L. Lampe, W. H. Gerstacker and P. A. Hoeher, “Multiple-antenna techniques for wireless communications – A comprehensive literature survey,”

IEEE Communications Surveys & Tutorials, vol. 11, no. 2, pp. 87-105, 2009.

60. P. Wolniansky, G. J. Foschini, G. D. Golden, and R. A. Valenzuela, “V-BLAST: an architecture for realizing very high data rates over rich scattering wireless channel," International Symposium on Signals, Systems and Electronics URSI, pp. 295-300, 1998.
61. D. P Palomar, “A unified framework for communications through MIMO Channels,” PhD Dissertation, Universitat Politècnica De Catalunya, Barcelona, Spain.
62. D. P. Palomar and Y. Jiang, “MIMO transceiver design via majorization theory,” Foundations and Trends in Communications and Information Theory, Now Publishers, vol. 3, no. 4, 331-551, 2006.
63. P. C. Sofotasios, and S. Freear, “Novel expressions for the Marcum and one dimensional Q-functions,” 7th International Symposium on Wireless Communication Systems (ISWCS), UK, 2010.
64. H. M. Ozaktas, Z. Zalevsky and M. A. Kutay, “The fractional Fourier transform with applications in optics and signal processing” Wiley, New York, Edition 2000.
65. H. M. Ozaktas, B. Barshan, D. Mendlovic and L. Onural, “Convolution, filtering and multiplexing in fractional domains and their relation to chirp and wavelet transforms,” Journal of Optical Society of America-A, vol. 11, no. 2, 547–559, 1994.
66. I. S. Yetik, and A. Nehorai, “Beamforming using fractional Fourier transform,” IEEE Transactions on Signal Processing, vol. 51, no. 6, pp.1663–1668, 2003.
67. R. Khanna and R. Saxena, “A novel FRFT beamformer for Rayleigh faded channels,” Wireless Personal Communication, Springer Netherlands, vol. 52, no. 4, pp. 693-707, 2010.
68. R. Khanna, ‘Characterization and development of algorithms for array processing architectures of adaptive antennas in wireless communication’, PhD dissertation, Electronics and Communication Engineering Department, Thapar University, Patiala, Punjab, India, 2006.
69. C. Candan, M. A. Kutay and H. M. Ozaktas, "The discrete fractional Fourier transform," IEEE Transactions on Signal Processing, vol. 48, pp. 1329-1337, May 2000.
70. I. S. Yetik, M. A. Kutay, H. Ozaktas and H. M. Ozaktas, “Continuous and discrete fractional Fourier domain decomposition,” Proceedings of IEEE International Conference Acoustics Speech Signal Processing, pp: 93–96, 2000.

71. H. M. Ozaktas, O. Arikan, M.A. Kutay and G. Bozdagi, “Digital computation of the fractional Fourier transforms,” IEEE Transactions on Signal Processing, vol. 44, no. 9, pp. 2141–2150, 1996.
72. V. Namias, “The fractional order Fourier transform and its application to quantum mechanics,” IMA Journal of Applied Mathematics, vol. 25, pp. 241–265, 1980.
73. J. H. McClellan and T. W. Parks, “Eigenvalue and eigenvector decomposition of the discrete Fourier transform,” IEEE Transactions on Audio Electroacoustics, vol. AU-20, pp. 66–74, 1972.
74. R. Khanna and R. Saxena, “Improved fractional Fourier transform based receiver for spatially multiplexed MIMO antenna systems” Wireless Personal Communication, Springer Netherlands, vol. 50, no. 4, pp.563-574, 2009.
75. A. Shah and A. M. Haimovich, “Performance analysis of maximal ratio combining and comparison with optimum combining for mobile radio communications with co-channel interference,” IEEE Transactions on Vehicular Technology, vol. 49, pp. 1454–1463, 2000.
76. Mario Kiessling and Joachim Speidel, “Analytical performance Of MIMO zero-forcing receivers in correlated Rayleigh fading environments,” in 4th IEEE Workshop on Signal Processing Advances in Wireless Communications, SPAWC 2003, pp. 383-387, June 2003.
77. Mario Kiessling and Joachim Speidel, “Analytical performance of MIMO MMSE receivers in correlated Rayleigh fading environments,” IEEE 58th Vehicular Technology Conference (VTC 2003), vol. 3, pp. 1738-1742, Oct 2003.
78. H. Liu, Y. Song and R. C. Qiu, “The impact of fading correlation on the error performance of MIMO systems over Rayleigh fading channels,” IEEE Transactions on Wireless Communication, vol. 4, no. 5, pp. 2014-2019, Sept. 2005.
79. A. M. Tulino, A. Lozano and S. Verdu, “Impact of antenna correlation on the capacity of multiantenna channels,” IEEE Transactions on Information Theory, vol. 51, no. 7, pp. 2491-2509, July 2005.
80. S. Sampei and T. Sunaga, “Rayleigh fading compensation for QAM in land mobile radio communication,” IEEE Transactions on Vehicular Technology, vol. 42, no. 2, pp. 137–147, 1993.

81. W. T. Webb and L. Hanzo, Modern Quadrature Amplitude Modulation. IEEE Press, New York, Edition 1994.
82. J. K. Cavers, “An analysis of pilot symbol assisted modulation for Rayleigh fading channels,” IEEE Transactions on Vehicular Technology, vol. 40, no. 4, pp. 686–693, 1991.
83. J. M. Torrance and L. Hanzo, “Comparative study of pilot symbol assisted modem,” Radio Receiver and Associated Systems, Conference Publication no. 415, Sep 26-28, pp: 36-41, 1995.
84. B. Hassibi and B. M. Hochwald, “How much training is needed in multiple-antenna wireless links?” IEEE Transactions on Information Theory, vol. 49, no. 4, pp. 951-963, 2003.
85. J. G. Proakis, “Digital Communications,” McGraw-Hill, New York, 4th Edition, 2001.
86. M. Dong, L. Tong, “Optimal design and placement of pilot symbols for channel estimation,” IEEE Transactions on Signal Processing, vol. 50, pp. 3055-3069, 2002.
87. M. Martone, “A multicarrier system based on the fractional Fourier transform for time-frequency selective channels,” IEEE Transactions on Communication, vol. 49, no. 6, pp. 1011-1020, 2001.
88. R. G. Gallager, "Low-density parity-check codes", Ph.D. dissertation, Department of Electrical Engineering, M.I.T., Cambridge, Mass., Jul. 1963.
89. A. Singh and S. Srinivasan, “Digital signal processing implementations using DSP microprocessors,” Brooks/ Cole - Thompson Learning, Belmont, California, 2005.
90. D. J. C. MacKay and R. M. Neal, “Near Shannon limit performance of low density parity check codes,” Electronics Letters, vol. 32, no. 18, pp. 1645-1646, Aug. 1996.
91. J. Pearl, “Probabilistic reasoning in intelligent systems: Networks of plausible inference.” Morgan Kaufmann Publishers, Inc., Edition 1988.
92. R. M. Tanner, “A recursive approach to low complexity codes”, IEEE Transactions on Information Theory, vol. 27, no. 5, pp. 533-547, September 1981.
93. N. Wiberg, “Codes and decoding on general graphs” PhD thesis, Link¨oping University, Sweden, 1996.
94. T. J. Richardson and R. Urbanke, “The capacity of low density parity check codes under message passing decoding,” IEEE Transactions on Information Theory, vol. 47, no. 2, pp.

599-618, Feb 2001.

95. S. Y. Chung, G. David Forney, T. J. Richardson and R. Urbanke, “Analysis of sum-product decoding of low-density parity-check codes using a Gaussian approximation”, IEEE Transactions on Information theory, vol. 47, no. 2, pp. 657-670, Feb. 2001.
96. R. G. Gallager, "Low-density parity-check codes", IEEE Transactions on Information Theory, vol. 8, no. 1, pp. 21-28, Jan. 1962.